Université de Montréal

Novel, universal electrochemical DNA-based signaling mechanisms for molecular detection in a drop of blood

par Guichi Zhu

Institut de Génie Biomédical,
Département de Pharmacologie et Physiologie,
Faculté de Médecine

Thèse présentée
en vue de l'obtention du grade de Philosophiae doctor - Doctorat (Ph.D.) en génie biomédical

Octobre 2021

Faculté des études supérieures et postdoctorales

Cette thèse intitulée:

Novel, universal electrochemical DNA-based signaling mechanisms for molecular detection in a drop of blood

Présentée par:

Guichi Zhu

A été évaluée par un jury composé des personnes suivantes:

Antonella Badia
Président-rapporteur

Alexis Vallée-Bélisle
Directeur de recherche

Jonathan Perreault
Membre du jury

Yingfu Li
Examinateur externe

Résumé

Une percée majeure aura lieu dans le domaine de la santé lorsque les patients pourront surveiller les molécules indicatives de leurs conditions médicales dans le confort de leur salon. L'efficacité d'une telle stratégie a déjà été validée par des millions de patients diabétiques via l'utilisation du glucomètre. Toutefois, des technologies de détection similaires restent à être développées pour améliorer le traitement de d'autres maladies chroniques. Les capteurs électrochimiques à base d'ADN (capteurs eDNA) ont récemment attiré beaucoup d'attention grâce à leur capacité à détecter plusieurs marqueurs moléculaires dans le sang tout en utilisant un dispositif bon marché et facile d'utilisation. Dans ce type de capteurs, l'ADN est typiquement employé comme élément de reconnaissance ou pour concevoir le mécanisme de signalisation permettant de capturer des cibles moléculaires spécifiques et traduire cet événement de liaison en un signal électrochimique. Des défis particuliers, toutefois, limitent toujours la commercialisation des capteurs eDNA. Par exemple, la plupart de ces capteurs produisent encore d'importantes variations non spécifiques du courant électrique lorsque plongés dans un échantillon de sang. De plus, ces capteurs demeurent sensibles au processus de fabrication et au vieillissement, et nécessitent des modifications chimiques complexes et un long processus d'optimisation pour leur mise au point. L'objectif principal de ma thèse consiste à régler ces limitations via le développement de nouveaux mécanismes de signalisation plus performants.

Dans le chapitre 2, nous introduisons un nouveau type de capteurs eDNA basé sur l'hybridation d'ADN que nous avons nommé « essaie d'hybridation électrochimique par encombrement stérique et inhibition rédox (eSHRI) ». Ce mécanisme de signalisation potentiellement universel intègre trois niveaux d'encombrement stérique et un nouveau mécanisme d'inhibition rédox par contact. Nous avons démontré que le eSHRI peut détecter et quantifier de faibles concentrations (nanomolaire) de protéines dans une goutte de sang en moins de 3 min via une diminution de signal électrique allant jusqu'à -93.6 ± 1.36 % du signal initial. De plus, l'essai d'hybridation eSHRI demeure essentiellement indépendant de la densité

du brin de capture à la surface de l'électrode et donc insensible aux variations lors de la fabrication et du vieillissement du capteur.

Malgré ses caractéristiques impressionnantes, le eSHRI requiert généralement des modifications chimiques complexes pour attacher l'élément de reconnaissance et l'élément rédox à la même extrémité du brin d'ADN. Ainsi, dans le chapitre 3, nous avons développé un nouveau mécanisme de signalisation potentiellement universel, l'essaie de barrière moléculaire, qui nécessite uniquement une modification par brin d'ADN. Dans cet essai, l'élément de reconnaissance et l'élément rédox sont respectivement conjugués à l'ADN de capture (surface de l'électrode) et l'ADN de signalisation (libre en solution). L'essai fonctionne via la formation d'une barrière moléculaire utilisant l'analyte à détecter, une protéine. Lorsque cette dernière se lie à la surface du capteur, cela réduit l'efficacité d'hybridation entre l'ADN de signalisation et l'ADN de capture. En utilisant ce nouveau capteur, nous avons démontré la détection de deux protéines, la streptavidine et un anticorps, directement dans une goutte de sang.

Ces dernières années, les anticorps à base d'ADN, nommés aptamères, ont considérablement augmenté notre capacité à détecter des analytes cliniquement pertinents. Toutefois, les capteurs eDNA à base d'aptamères nécessitent un long processus de développement et d'optimisation, et demeurent très dépendants de la densité de surface tout en présentant d'importantes variations de signal lorsqu'ils sont déployés dans le sang. Dans le chapitre 4, nous introduisons un essai simple, hautement modulable et universel qui emploie une chimie dynamique constitutionnelle (CDC) cinétiquement programmée. Cet essai fonctionne en programmant la cinétique de trois réactions concurrentes permettant la détection moléculaire directement dans une goutte de sang. Nous avons démontré que cet essai est potentiellement universel en détectant quantitativement quatre marqueurs moléculaires : la quinine, l'ATP, la thrombine et la PDGF. Nous avons également démontré le potentiel de ce nouveau capteur en exécutant un suivi direct de la quinine dans le sang de souris vivantes.

En sommes, nous croyons que ces nouveaux mécanismes de signalisation permettent de résoudre les principales limitations des capteurs eDNA actuels et présentent toutes les

caractéristiques pour être développés en dispositifs commercialisables analogues aux glucomètres.

Mots-clés: ADN, aptamère, électrochimie, biocapteurs, diagnostic, sang, encombrement stérique, barrière moléculaire, programmation cinétique

Abstract

A breakthrough will occur in the healthcare system when patients are allowed to monitor blood molecules indicative of their condition in the comfort of their home. Such an objective has already been realized for diabetic patients through the development of the glucometer. Similar sensors urgently need to be developed to improve the monitoring and treatment of other chronic conditions. Electrochemical DNA-based sensors (eDNA sensors) have recently attracted increasing attention due to their ability to detect multiple blood markers using low-cost and easy-to-use devices. In eDNA sensors, DNA is typically employed either as a recognition element or to design a signaling mechanism that captures specific target molecules and transduces this binding event into an electrochemical signal. Specific challenges, however, limit the commercialization process of eDNA sensors. For example, most eDNA sensors exhibit strong baseline drift when employed in blood, remain sensitive to fabrication processes and aging, and require complex chemical modification and time-consuming optimization processes. The main objective of my Ph.D. project was to solve these limitations through the development of novel improved signaling mechanisms.

Chapter 2 introduces a novel hybridization-based eDNA sensing architecture called electrochemical steric hindrance and redox inhibition (eSHRI) hybridization assay. This potentially universal signaling mechanism integrates three levels of steric hindrance and a novel contact redox inhibition mechanism. We have shown that eSHRI can detect low nanomolar concentrations of protein analytes in a drop of blood in less than 3 min with up to -93.6 ± 1.36 % in signal gain. Moreover, the eSHRI hybridization assay remains primarily independent of the sensor density on the surface of the electrode and thus insensitive towards variations in fabrication or aging time.

Despite its impressive characteristics, eSHRI may see its universality limited by the complicated chemical modifications required to attach both the recognition element and the redox molecule on the same extremity of a DNA strand. In response, in chapter 3, we develop a novel, potentially universal signaling mechanism, the molecular barrier-based assay, that only

requires a single modification of its DNA strands. In this assay, the recognition element and redox molecule are conjugated to the surface-attached capturing DNA and the free-moving signaling DNA. The assay works by having the protein analytes create a molecular barrier upon binding to the sensor surface, reducing the hybridization efficiency between the capturing DNA and the signaling DNA. Using this novel sensor, we have demonstrated the detection of two proteins, streptavidin and antibody, directly in a drop of blood.

DNA-based antibodies, called aptamers, have drastically expanded our ability to detect a large proportion of clinically relevant analytes in recent years. However, the development of aptamer-based eDNA sensors still requires a long optimization process, remains highly dependent on specific surface densities, and displays significant signal drift when deployed in the blood. In response, we present in chapter 4 a simple, highly modular, universal assay that employs kinetically programmed constitutional dynamical chemistry (CDC). This assay works by programming the kinetics of three competing reactions to enable molecular detection directly in a drop of blood. We show that this assay is potentially universal by demonstrating the quantitative detection of four molecular markers: quinine, adenosine triphosphate (ATP), thrombin, and platelet-derived growth factor (PDGF). We further show the point-of-care potential of this new sensor by performing direct quinine monitoring in living mouse blood.

Overall, we believe that these new sensing mechanisms solve the main weaknesses of current eDNA sensors and display all the characteristics required for the development of commercialized devices analogous to glucose meters.

Key words: DNA, aptamer, electrochemistry, biosensor, diagnosis, blood, steric hindrance, molecular barrier, kinetic programming

Table of contents

List of tables

List of figures

List of abbreviations and symbols

A: Adenine

AI: Artificial intelligence

AIDS: Acquired immune deficiency syndrome

ATP: Adenosine triphosphate

C: Cytosine

C_0: The current in the absence of streptavidin

$C_{50\%}$: A standard 50% inhibition of precipitation

CDC: Constitutional dynamic chemistry

CE: Counter electrode

COVID-19: Coronavirus disease 2019

CV: Cyclic voltammetry

C_{strep}: The current in the presence of streptavidin

ΔG: The change of Gibbs free energy

Dig: Digoxigenin

DNA: Deoxyribonucleic acid

DNP: 2,4-dinitrophenol

dsDNA: Double-stranded DNA

E-AB sensors: Electrochemical aptamer-based sensors

eDNA sensors: Electrochemical DNA-based sensor

EIS: Electrochemical impedance spectroscopy

ELISA: Enzyme-linked immunoassay

eRCDs: Electroactive RNA-cleaving DNAzymes

eSHHA: Electrochemical steric hindrance hybridization assay

eSHRI: Electrochemical steric hindrance and redox inhibition

F: Faraday constant

G: Guanine

H: Hill factor

HDA: Helicase dependent amplification

HIV: Human immunodeficiency viruses

HPLC: High-performance liquid chromatography

HRP: Horseradish peroxidase

k: Rate constant

K_d (or K_D): Dissociation constant

LAMP: Loop-mediated isothermal amplification

MB: Methylene blue

MCH: 6-Mercaptohexanol

MW: Molecular weight

N_A: Avogadro constant

nt: Nucleotides

ODE: Ordinary differential equations

PCR: Polymerase chain reaction

PDGF: Platelet-derived growth factor

PNA: Peptide nucleic acid

POCT: Point-of-care testing

R: Ideal gas constant

RCA: Rolling circle amplification

RE: Reference electrode

RNA: Ribonucleic acid

RPC: Reverse-phase cartridge

SDA: Strand displacement amplification

SELEX: Systematic evolution of ligands by exponential enrichment

SPR: Surface plasmon resonance

ssDNA: Single-stranded DNA

SWV: Square wave voltammetry

T: Thymine

$t_{1/2}$: Half-life

TCEP: Tris (2-carboxyethyl) phosphine hydrochloride

TMB: 3,3',5,5'-tetramethylbenzidine

WE: Working electrode

WLC: Worm-like chain

To my mother and father, with love

Acknowledgements

First, I would like to thank my supervisor, Prof. Alexis Vallée-Bélisle, for his professional guidance and valuable encouragement. After a Skype interview with Alexis in Shenzhen in December 2014, I submitted a Ph.D. program application and started my adventure at the Université de Montréal. I feel fortunate that Alexis helped me a lot during the past six years of Ph.D. study, especially during the most challenging moments. The two most precious characters I see from Alexis are respecting every student and keeping endless enthusiasm for science, which will always influence and inspire me.

I would like to extend a thank you to Prof. Antonella Badia, Prof. Jonathan Perreault, and Prof. Yingfu Li for being willing to be jury members of my thesis. Special thanks to Prof. Alain Vinet for his helpful suggestions during my Ph.D. study.

I am thankful to all the Laboratory of Biosensors & Nanomachines members for their help and the pleasant working atmosphere they have created.

Special thanks to TransMedTech Institute (Polytechnique Montréal) and PROTEO (The Quebec Network for Research on Protein Function, Engineering, and Applications) for scholarship support.

I am also very grateful for the happiness and freedom that tennis brings to me, allowing me to recharge outside of the lab life. Finally, I would most like to thank my parents and girlfriend for their endless love and continued support.

Chapter 1: Introduction

1.1 Background

A vital breakthrough will take place in the healthcare system when patients are able to monitor their health condition in the comfort of their home through convenient and straightforward blood-testing technologies.[1, 2] With recent booming developments in telemedicine and artificial intelligence (AI) technology, the landscape of a future "smart" hospital is becoming clearer and promising.[3] With this technology in hand, people ought to be able to monitor their condition from home using easy-to-use blood tests and simultaneously submit their results to their doctor via cloud computing. They could then receive diagnostic or treatment suggestions from the doctor and have their prescription shipped to home from the pharmacy. Thus, the development of easy-to-use blood tests will play a determinant part in shaping the healthcare system's future.

There are two critical applications for molecular detection in patients' blood, namely clinical diagnosis and therapeutic drug monitoring. Clinical diagnosis refers to measuring specific biomarker concentrations in bodily fluids to indicate the state of human diseases.[4] Over the past few decades, polymerase chain reaction (PCR)[5] and enzyme-linked immunoassay (ELISA)[6] have been the dominant techniques to detect blood markers, including nucleic acids, small molecules, and proteins. Although PCR and ELISA are sensitive and robust, they remain cumbersome, reagent-consuming, and expensive to run since they require highly qualified technicians and expensive instrumentations. Another critical application of blood tests is monitoring the concentration of therapeutic drugs to personalize and optimize drug dosage to improve drug efficacy and reduce adverse side effects.[7] Currently, high-performance liquid chromatography (HPLC) is the gold standard assay for measuring therapeutic drug concentration,[8] but its high-cost and time-consuming procedures prevent patients from monitoring their treatment in the comfort of their home. Most importantly, the widely used techniques for molecular detection (PCR, ELISA and HPLC) typically fail when deployed in complex media, such as whole blood, and

require complicated pre-treatment procedures to simplify the sample matrix. Therefore, it has become imperative to develop more straightforward and more efficient strategies to detect various blood markers in a point-of-care setting.

1.2 Biosensors

Biosensors provide enormous opportunities for molecular detection in various fields, including biochemistry, molecular biology, immunology, diagnostic medicine, drug discovery, and environmental analysis.[9] In the early 1980s, the annual total global market for biosensors was less than US$5 million,[10] but its total yearly global market has expanded to US$25.5 billion in 2021 (the data is from *MarketsandMarkets*) and the output of approximately 5400 research papers per year (from 2017 to 2021, based on a query for "biosensor" in *Web of Science,*). The working principle of biosensors typically involves two basic functional units: a biological receptor and a physicochemical transducer (Figure 1.1).[11] Biological receptors typically employ enzymes, antibodies, nucleic acids, and cells and recognize a specific target substrate, antigen, DNA/RNA, and ligand molecules, respectively. This specific biorecognition event then needs to be detected using a specific physicochemical transducer. Typical transducers include the electrochemical, optical, thermal, and piezoelectric signal output. This transducer output will then need to be translated into a value that is easy to interpret (yes or no, or concentration value) (Figure 1.1).

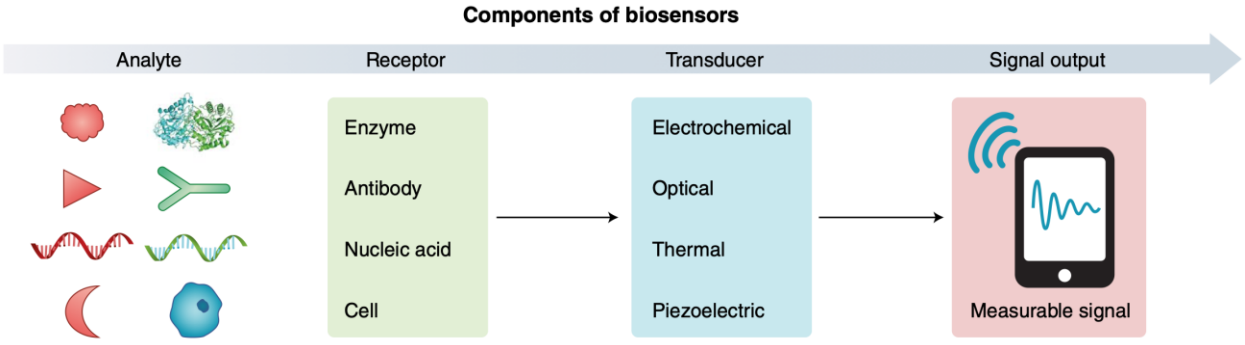

Figure 1.1 Schematic representation of biosensor components. Biosensors typically detect target analytes using a highly specific bioreceptor engineered to transduce this binding event into a specific signal readout. Reprinted with permission from ref. 11. Copyright 2019 Springer Nature.

Electrochemical biosensors have attracted increasing attention among the various transduction mechanisms due to their relative insensitivity toward the matrix effects (e.g., biological samples), their ability to provide quantitative measurements, their high sensitivity/specificity, and their low cost.[12] The glucose meter, for example, has brought considerable benefits to humanity by enabling millions of diabetic patients to monitor and treat their condition in the comfort of their home.[13] This type of biosensor typically relies on the glucose oxidase (GOx) that contains two bound flavin adenine dinucleotide (FAD) cofactors. GOx can specifically catalyze the oxidization of glucose, thereby reducing FAD to $FADH_2$. $FADH_2$ can be re-oxidized to FAD through redox mediator (such as ferrocenium/ferrocene), the electrons generated in this process will be detected by the electrode and generate an electrochemical signal. Depending on the choice of biological recognition element functionalized at the surface of the electrode, electrochemical biosensors are categorized into enzyme-based, antibody-based, and DNA-based sensors. Despite its great success, the glucose meter still faces challenges, including its short shelf-life and biofouling challenges, that limit continuous glucose monitoring applications. But more importantly, the main limitation of enzyme-based electrochemical sensors remains the low versatility of their signaling mechanism to be adapted for detecting other analytes.[14, 15] In contrast, antibody-based electrochemical sensors are widely used for molecular detection in biological samples and usually show excellent selectivity and sensitivity for a multitude of analytes due to the high specificity and sensitivity of antibodies. Their large-scale adoption, however, is still limited by their complexity of use and high cost. We believe that most of the drawbacks of enzyme- and antibody-based electrochemical sensors could be avoided by employing DNA as an alternative recognition element.

1.3 eDNA sensors

Over the past few decades, multiple electrochemical DNA-based sensors (eDNA sensors) have been developed for clinical diagnosis and therapeutic drug monitoring applications. eDNA sensors display many potential attributes such as their high sensitivity, low-cost, portability, and ability to detect directly in complex biological samples. However, one of the most distinctive

advantages of eDNA sensors is that the programmable nature of DNA chemistry facilitates the design and engineering of novel electrochemical sensors.

DNA was first isolated from white blood cells by the Swiss chemist Friedrich Miescher in 1869.[16] In the decades following DNA discovery, the main chemical components and the specific base-pairing code of DNA were determined by other scientists including Phoebus Levene and Erwin Chargaff.[17] In 1953, James Watson and Francis Crick revealed for the first time the double-helix structure of DNA.[18] DNA is a biopolymer made from four nucleobases: adenine (A), guanine (G), cytosine (C), and thymine (T). These four nucleotides can be joined together via any sequence combination (e.g., ATCGTCCAGC…, TTGCCTATA…, or GCTAGCGT…) through covalent phosphodiester bonds to form a specific DNA strand (Figure 1.2). DNA chemical synthesis can be performed simply and rapidly using an automatic DNA synthesizer or purchased at few costs (dozens of dollars) from many DNA-based companies. The most commonly used method to synthesize DNA employs solid-phase phosphoramidite chemistry, first developed by Marvin Caruthers in the 1980s.[19] This method typically involves a four-step cycle, including deprotection, base coupling, capping, and oxidation (Figure 1.3).[20] As we will see in the following sections, DNA strands can be engineered or selected to bind a wide variety of analytes with high specificity and selectivity. DNA strands can also be readily labeled and engineered into multiple signaling mechanisms with its simple labeling chemistry and highly specific A-T and G-C base pairs. We will conclude this chapter by providing a rapid overview and history of the development of eDNA sensors.

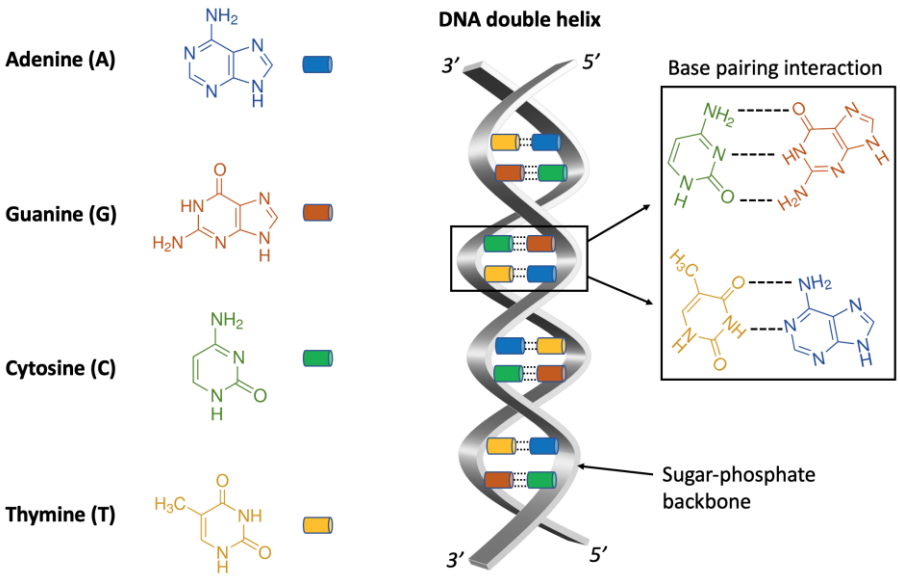

Figure 1.2 Chemical structure of the four nucleobases and DNA double helix.

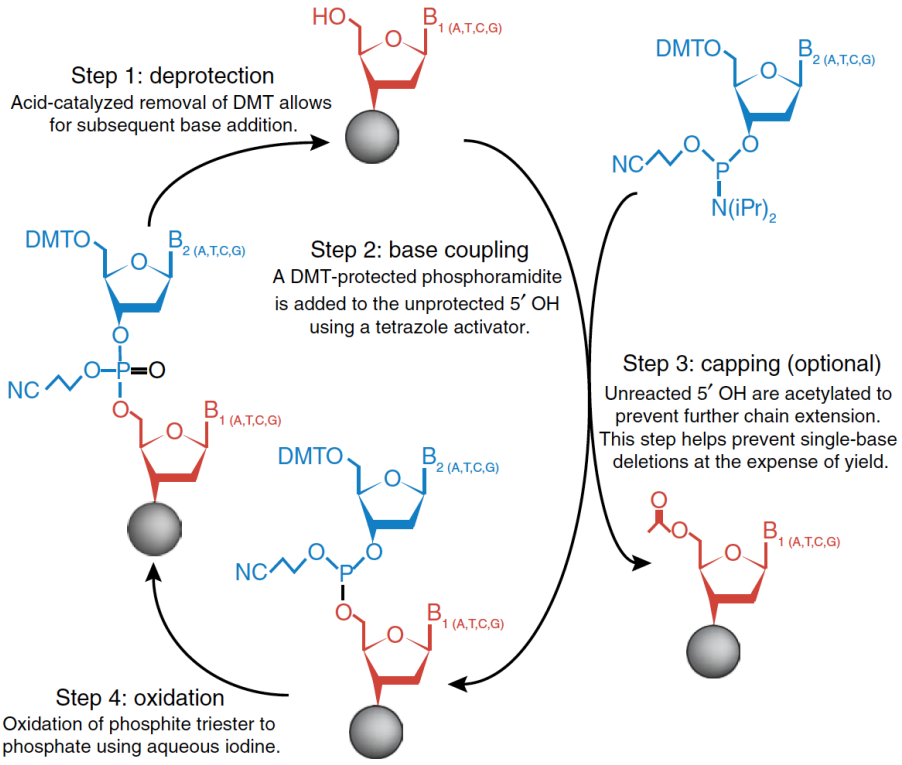

Figure 1.3 DNA chemical synthesis based on the four-step method of solid-phase phosphoramidite chemistry. Reprinted with permission from ref. 20. Copyright 2014 Springer Nature.

1.3.1 DNA: a versatile polymer to create recognition elements

The first step in any DNA sensor development is identifying a specific DNA sequence that can specifically bind the desired analyte molecules, such as nucleic acids, ions, small molecules, proteins, and cells. As it is well known, single-stranded DNA (ssDNA) can specifically bind its complementary DNA or RNA strand via its specific hydrogen-bonding interactions. Therefore, one can build a highly selective DNA or RNA sensor by simply employing a recognition DNA that displays a complementary sequence to the DNA or RNA sequence of interest (Figure 1.4a).

DNA can also be used as an effective recognition element to detect cation analytes. For example, the triplex DNA structure,[21, 22] stabilized via additional Hoogsteen base-pairing interactions, can be used to detect protons since it only assembles under acidic pH conditions following protonation (H^+) of the cytosine (Figure 1.4b). The G-quadruplex, a non-canonical DNA structure, also typically folds in the presence of potassium ions (K^+)[23] (Figure 1.4c). When located in a double helix, the mismatched base pairs of T-T and C-C also display a strong affinity and specificity for mercury ions (Hg^{2+})[24] and silver ions (Ag^{2+})[25], respectively (Figure 1.4d). DNAzymes are another widely used DNA-based recognition element for metal ions.[26] These artificially selected catalytic DNAzymes (see SELEX method below) are indeed able to cleave nucleic-acid substrates only when bound to specific cofactors (Figure 1.4e), including magnesium ion (Mg^{2+}),[27] lead ions (Pb^{2+}),[28] and uranium ion (UO_2^{2+}).[29]

By using a SELEX (systematic evolution of ligands by exponential enrichment) process, independently developed by the Szostack and Gold groups in 1990,[30, 31] short ssDNA sequences can also be selected to bind specific small molecules, proteins, viruses, cells, and even bacteria (Figure 1.4f).[32-36] These DNA sequences typically fold into various tertiary structures and interact with their analyte molecules by recognizing specific three-dimensional conformation in a manner analogous to antibody-antigen interaction. These specific binding sequences are typically called “aptamer”, “chemical antibody”, or “DNA-based antibodies”. Aptamers have shown significant advantages as a recognition element for both clinical application and industrialized production compared with antibodies.[37, 38] Firstly, the *in vitro* selection process of aptamers avoids time-consuming animal immune experiments and purification processes. Secondly, aptamers typically

display high thermal stability. For example, even if the aptamer is denatured at a high temperature (e.g., 95°C), it can still refold reversibly into its binding conformation when the temperature is decreased. In contrast, most antibodies typically lose their activity following similar treatment. Thirdly, aptamers are much less prone to aggregation, oxidation, and proteolytic degradation during storage. Fourthly, in contrast to the industrial production of antibodies, aptamer synthesis can rely on commercial DNA synthesizers with lower cost and higher chemical structure reproducibility. Finally, although the binding affinity of most aptamers (K_d =nM to µM) remains typically lower than antibodies, recent progress involving the use of modified nucleotides[39, 40] has drastically improved binding efficiencies. For example, a company called SomaLogic (Boulder, Colorado, USA) has now developed thousands of aptamers for about 7000 human proteins with binding affinity and specificity that matches the one of antibodies.[41, 42]

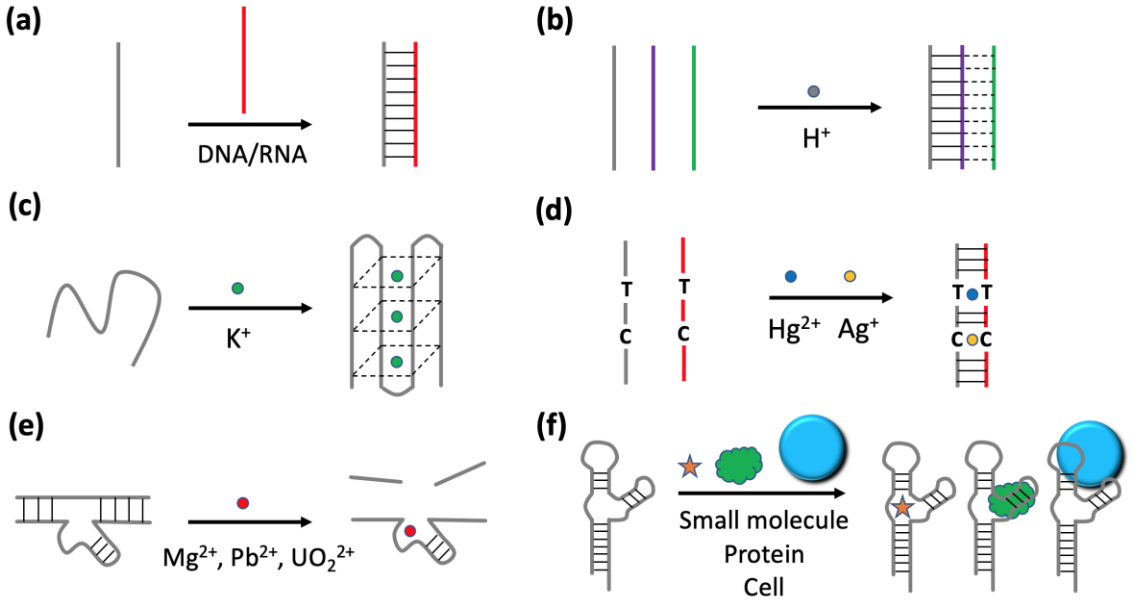

Figure 1.4 Schematic representation of DNA as a versatile recognition element for (a) nucleic acids, (b) protons, (c) potassium ions, (d) mercury and silver ions, (e) magnesium, lead, and uranium ion, and (f) small molecules, proteins, and cells.

1.3.2 DNA: a programmable polymer to engineer signaling mechanisms

In addition to its high versatility to produce efficient recognition elements, DNA also possesses the ability to be readily engineered into multiple signaling mechanisms for eDNA sensing applications. With the unique chemical properties and charge distribution of DNA strands, many electrochemically active molecules can be incorporated through electrostatic interaction, intercalation, and major/minor groove binding (Figure 1.5).[43] Those can then be used to create an efficient electrochemical signal. For example, $Ru(NH_3)_6^{3+}$, a cationic metal complex, can bind to the negatively charged phosphate groups in the DNA backbone through electrostatic interaction (Figure 1.5, left).[44-46] The number of DNA strands on the electrode surface can then be reported using the intensity of the electrochemical signal of $Ru(NH_3)_6^{3+}$. Other redox-active molecules, such as doxorubicin,[47] daunomycin,[48] ethidium bromide,[49] and $Co(phen)_3^{3+}$,[50] can specifically intercalate into double-stranded DNA (dsDNA) through hydrogen bonding, van der Waals forces, π-π stacking, and hydrophobic effect (Figure 1.5, middle).[51-53] These intercalated redox-active molecules can then distinguish ssDNA from dsDNA on the surface of the electrode. Finally, redox-active molecules such as Hoechst 33258[54] and ferrocene[55] can bind to dsDNA's grooves through hydrogen bonding, van der Waals forces, and π-π stacking to generate electrochemical signals (Figure 1.5, right).[56, 57]

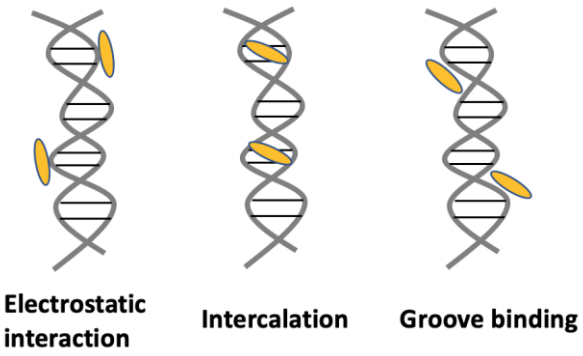

Figure 1.5 Schematic representation of three interaction modes between DNA strands and redox-active molecules.

Another advantage of DNA over the more complex protein polymer is that the chemical attachment of redox-active molecules on DNA strands remains much more straightforward and

convenient. Indeed, in recent years, the performance of eDNA sensors has been drastically improved by employing covalently bound redox molecules that typically show better stability and specificity[58] and provide higher design flexibility.[59] For example, methylene blue (Figure 1.6a), one of the most popular redox-active molecules in eDNA sensors due to its excellent electrochemical stability, high storage stability, and low potential (-0.1 to -0.4 V versus Ag/AgCl)[43, 60], is typically labeled at the extremity of the DNA sensor (Figure 1.6b).[61-63] Modifying the specific location of this redox-active molecule on the DNA strand[64] or adding multiple copies of it[65] can also significantly optimize the signaling mechanisms (Figure 1.6b).

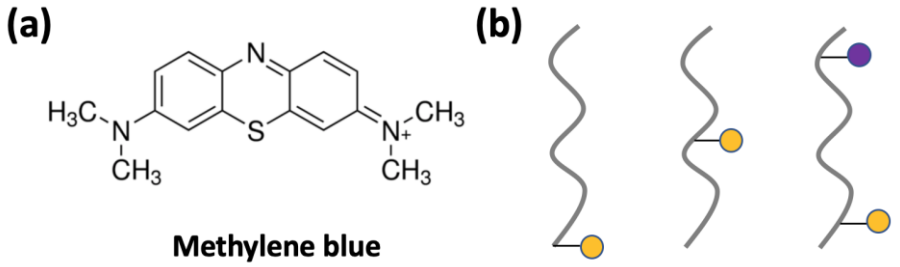

Figure 1.6 (a) Chemical structure of methylene blue. (b) Various covalently labeling strategies of redox molecules on ssDNA strands.

Another advantage of DNA in developing an efficient signaling mechanism is that most DNA recognition elements can be engineered into structure-switching molecules that can significantly enhance the specificity and signal gain of the sensor.[66] Engineering binding-induced structure-switching mechanisms can typically be realized using the population-shift model (Figure 1.7a).[67-69] For example, most DNA recognition elements can be efficiently designed via the addition of specific Watson-Crick base pair to adopt an alternative non-binding conformation. In the presence of a specific analyte, this later will prefer to bind the original binding conformation of the DNA recognition element, resulting in a structure-switching mechanism that significantly improves the specificity and signal gain of the sensor. As shown in Figure 1.7b, a ssDNA can be designed into a stem-loop structure that will be opened upon the presence and binding of a complementary nucleic acid sequence. Another advantage of switching mechanisms is that by simply changing the stability of the switch (e.g., the G-C content of the stem), one can also optimize the detection limit and dynamic range of the sensor.[67] Other advantages provided

by the programmability of DNA is that extra tail can also be added to the stem, typically "toehold" domain (Figure 1.7c),[70] to increase the rate of analyte binding. Moreover, additional complementary DNA strands can also be employed to modulate the activity of stem-loop structure, often referred to as inhibitor or activator DNA strand (Figure 1.7d-e),[71] which can help to tune the dynamic range of the sensor. Due to the great programmability of the A-T/G-C base pair, various spatial structures can also be engineered using DNA. For instance, tetrahedral-shaped DNA has been used to develop enzyme-based amplification,[72] analyte-induced structure switching,[73] and mimetic proximity ligation-based signaling mechanisms.[74] Taken together, all these features illustrate the high potential of DNA to develop efficient eDNA sensors with different sensing mechanisms.

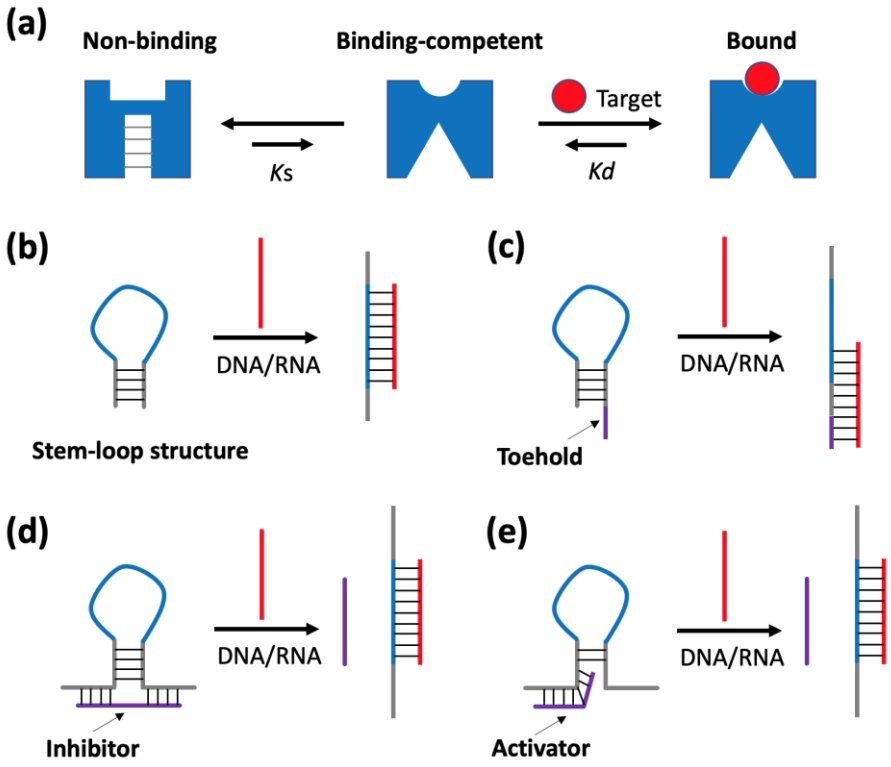

Figure 1.7 (a) Schematic representation of the population-shift model used to create DNA switches. Binding-induced structure-switching in (b) stem-loop DNA structure, (c) stem-loop DNA structure with a toehold domain, (d-e) stem-loop DNA structure with an inhibitor and an activator DNA strand.

1.3.3 A quick history of eDNA sensors

The first eDNA sensor was proposed by Emil Palecek in 1960. This pioneering technology successfully distinguished ssDNA and dsDNA based on the direct reduction of nucleotides on an electrode.[75] This was the first time that DNA, as a macromolecule, was shown to generate an apparent electrochemical signal. However, this discovery did not gain widespread attention until the development of various advanced electrochemical devices and DNA chemical synthesizers in the 1990s. It is worth noting that before the 1990s, DNA was usually obtained from biological cells extraction and enzymatic amplification.[20] With the development and commercialization of high-throughput array-based DNA synthesizers in the 1990s,[20] researchers have been able to rapidly obtain chemically synthesized DNA at low cost, which drastically contributed to the development of the field (Figure 1.8). For this reason, eDNA sensors have attracted more and more attention among the numerous biosensing technologies.[58, 76, 77] In this section, I will summarize the important developments in the field of eDNA sensors. As noted, these eDNA sensors will be classified into two main categories, label-free assays and redox-labeled assays, depending on whether they involve the covalent modification of DNA with a redox label.

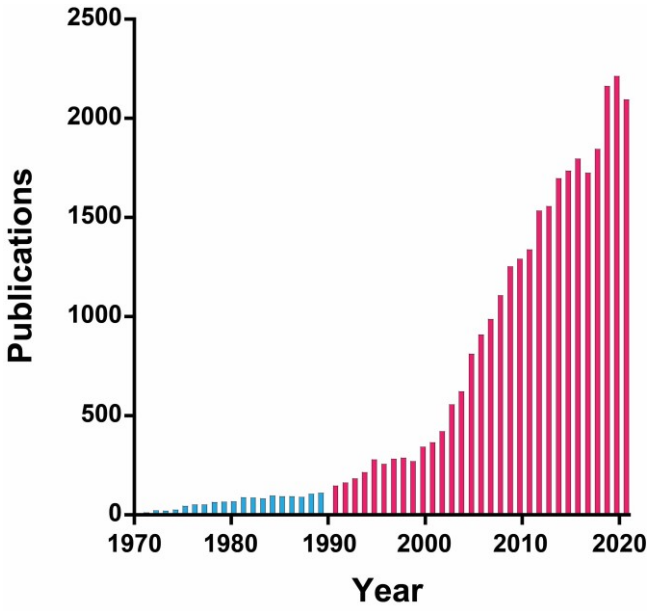

Figure 1.8 The number of publications on eDNA sensors from 1970 to 2020. The figure is based on a query of (*electrochem* AND DNA*) OR (*electrochem* AND nucleic acid**) in *Topic* in *Web of Science.*

1.3.3.1 Label-free eDNA sensors

Label-free eDNA sensors can detect an analyte without a covalently bound redox molecule attached to a DNA strand. Label-free assays are inherently simple and low-cost compared to redox-labeled assays. They can be applied directly to detect analytes without the involvement of complex and time-consuming chemical modification. Label-free assays can be typically subdivided into the following four categories: (1) Direct/electrocatalytic guanine oxidation-based assays; (2) Electrocatalytic reaction system-based assays; (3) Electrochemical impedance spectroscopy-based assays, and (4) Analyte as electrochemical indicator-based assays.

1.3.3.1.1 Direct/electrocatalytic guanine oxidation-based assays

Numerous eDNA sensors have been explored for nucleic acids detection that employs the direct oxidization of DNA nucleotides as an electrochemical signal readout.[78] Among the four standard DNA nucleotides, guanine is the most easily oxidizable electrochemically due to its low oxidation potential.[79] Wang and co-workers, for example, developed a method to detect DNA hybridization based on the direct oxidization of guanine.[80] In this strategy (Figure 1.9a), the guanine-free capturing DNA (or inosine-substituted capturing DNA) is immobilized onto the electrode, and hybridization with the target DNA brings guanine close to the electrode surface, thus generating a guanine oxidation peak. This assay can detect as low as ~13 nM of target DNA in 4 min of hybridization time. Similar assays that rely on direct guanine oxidization have also been reported.[81-84]

The electrochemical signal of guanine oxidization can be amplified through the use of electrochemical mediators, for example, an inorganic metal complex such as $[Ru(bipy)_3]^{2+}$.[85] $[Ru(bipy)_3]^{2+}$ can be oxidized to $[Ru(bipy)_3]^{3+}$ by applying an oxidation potential, then guanine in the target DNA is catalytically oxidized to guanine$^+$ via $[Ru(bipy)_3]^{3+}$, leading to an electrocatalytic cycle (Figure 1.9b). Thorp's group has explored various strategies for genetic analysis based on this catalytic oxidization of guanine.[85-89] For example, long nucleic acid targets (435-1497 base pairs) are first amplified by PCR and subsequently immobilized on the electrode surface.[86] Immobilized guanines show a strong catalytic oxidization current in the presence of $[Ru(bipy)_3]^{2+}$, and this catalytic current displays a linear function with the number of nucleic acid targets. The

detection limit of this strategy can reach as low as 550 attomol of the target strand with the assistance of PCR. Thorp and co-workers have also applied this method to detect the trinucleotide repeat expansion (5'-CTG and 5'-CGG) in unprocessed nucleic acids[88] and monitor gene expression in tumor samples.[89]

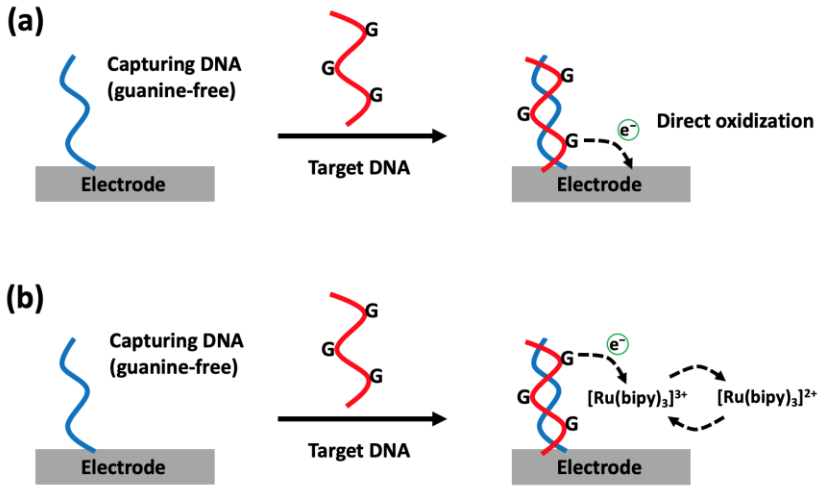

Figure 1.9 (a) Direct oxidization of guanine in target DNA. (b) Electrocatalytic oxidation of guanine using a redox mediator.

1.3.3.1.2 Electrocatalytic reaction system-based assays

Although the above mentioned label-free assays have achieved significant simplicity, a considerable background current is nevertheless generated by the relatively high potentials required for the oxidation of DNA nucleotides.[9] In addition, the feasibility of this class of assays is limited by whether the target sequence has guanine, and even if present, their sensitivity is determined by the number of guanines present in the target sequence. As shown in Figure 1.10a, the electrochemical method can be extended to a label-free assay that side-steps the necessity of guanine oxidization by using an electrocatalytic system comprised of a redox indicator ($[Ru(NH_3)_6]^{3+}$) and a redox catalyst ($[Fe(CN)_6]^{3-}$).[90, 91] Firstly, $Ru(NH_3)_6^{3+}$ is attracted to the immobilized DNA on the electrode surface through nonspecific electrostatic interaction with the negatively-charged phosphate backbone, and an electrochemical signal is generated at a reduction potential due to the reduction process of $Ru(NH_3)_6^{3+}$ to $Ru(NH_3)_6^{2+}$. Secondly, $Fe(CN)_6^{3-}$, a more easily reduced anionic electron acceptor, chemically oxidizes the $Ru(NH_3)_6^{2+}$ back to

$Ru(NH_3)_6^{3+}$, and generates an increased electrochemical signal via multiple redox cycles. This assay avoids the limitation of target sequence dependence and can analyze any random DNA sequence irrespective of whether it has guanine or not. To decrease the background of this electrocatalytic reaction system, Kelly's lab explored a new approach by using an uncharged probe consisting of peptide nucleic acid (PNA), which does not have the charged phosphate backbone in the strand.[92] More recently, a highly sensitive PNA-based method was proposed to directly detect circulating nucleic acids in lung cancer and melanoma patients.[93] The detection limit of this assay can reach as low as ~0.1 pM by virtue of an increased surface area and highly efficient strand hybridization of nanostructured microelectrodes, and also shows an impressive selectivity even for a point mutation sequence. As shown in Figure 1.10b, through introducing a neutralizer (conjugating PNA with cationic amino acids in N' and C' terminal), a universal sensor based on neutralizer displacement was developed for any type of target analytes, such as small molecules (ATP, cocaine), nucleic acids (ssDNA and RNA fragment) and proteins (thrombin).[94]

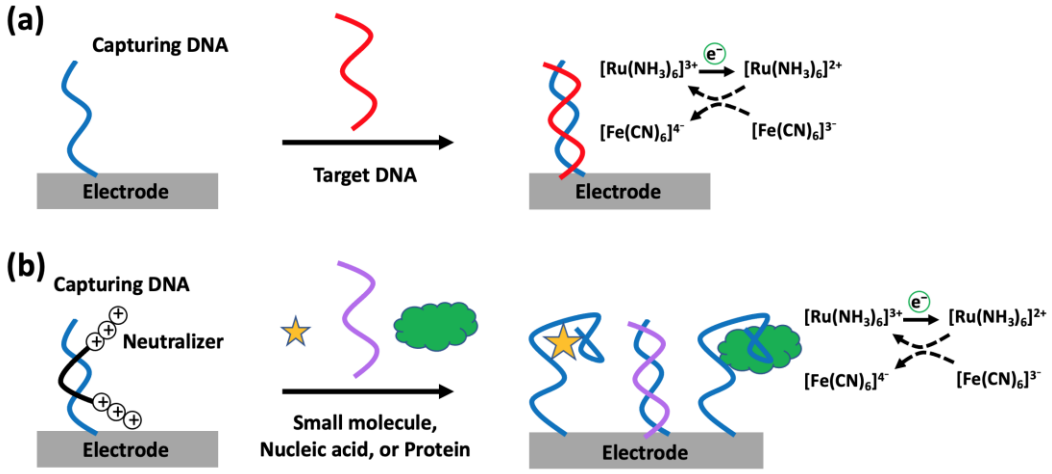

Figure 1.10 An electrocatalytic reaction system that includes a redox indicator ($[Ru(NH_3)_6]^{3+}$) and a redox catalyst ($[Fe(CN)_6]^{3-}$) is used to amplify the electrochemical signal for the detection of (a) DNA and (b) small molecules, nucleic acids, and proteins.

1.3.3.1.3 Electrochemical impedance spectroscopy-based assays

Another strategy that does not rely on guanine oxidization has been developed using electrochemical impedance spectroscopy (EIS),[95] which typically measures the electron transfer

resistance change between ssDNA and dsDNA in the presence of a redox indicator such as ferricyanide ($[Fe(CN)_6]^{3-}$) (Figure 1.11a). In this assay, an increase in the electron transfer resistance was observed upon hybridization (ssDNA to dsDNA) due to the stronger negative charge repulsion between ferricyanide and dsDNA. Willner's lab developed an EIS-based method for the analysis of gene mutants on the gold electrode.[96] This assay not only confirmed the significant difference in impedance among bare electrodes versus ssDNA- and dsDNA-functionalized electrodes, but also amplified the impedance through the use of a biotin-streptavidin complex at the electrode surface. This assay was able to detect target DNA at a concentration as low as 3.5 pM with an incubation time of 30 min. Besides detecting nucleic acids, this EIS-based method can also be applied to detect small molecules and proteins by using their respective aptamers (Figure 1.11b). By leveraging the advantages of aptamers, numerous EIS-based sensors for the detection of small molecules[97-99] and proteins[100-102] have been developed in recent years.

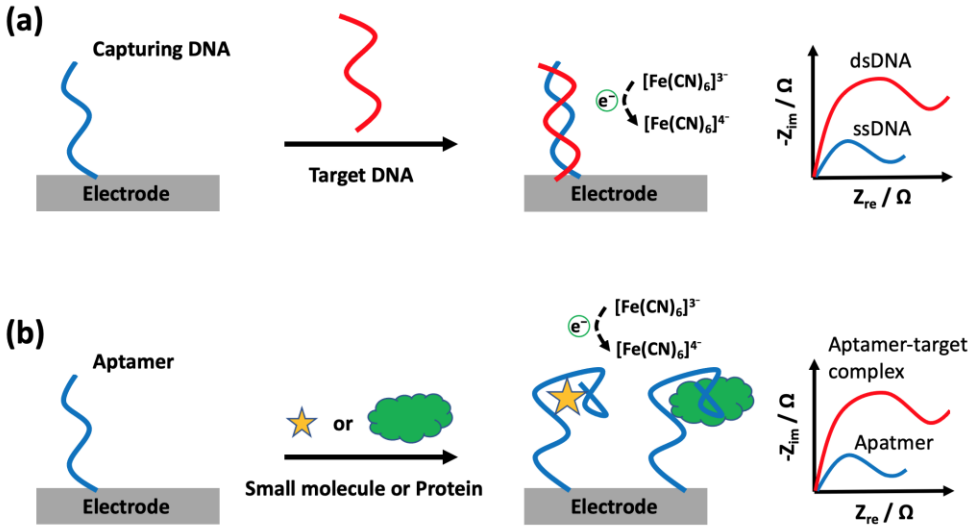

Figure 1.11 Electrochemical impedance spectroscopy (EIS)-based DNA sensor for the detection of (a) target DNA and (b) small molecules/proteins. The electron transfer resistance between redox indicator and electrode surface is increased due to the formation of DNA duplex or aptamer-target complex.

1.3.3.1.4 Analyte as electrochemical indicator-based assays

Specific approaches in label-free assays also employ the target molecules as an electrochemical indicator (e.g., drug-DNA interaction).[103] In such assay, dsDNA is immobilized at the surface of the electrode, then treated with the target molecules for interaction, which enables to concentrate the target molecules onto the electrode surface and generates an electrochemical signal (Figure 1.12). The interaction between DNA and target molecules usually includes hydrogen bonds, electrostatic attraction, intercalation, and groove binding interaction.[103] For example, Brett et al. developed a direct eDNA sensor to analyze metronidazole,[104] a widely used anti-parasitic and anti-bacterial drug for pelvic inflammatory disease, endocarditis, and bacterial vaginosis. After incubating metronidazole with a DNA-modified electrode, a potential peak from metronidazole was measured by differential pulse voltammetry. In comparison with the unmodified electrode, the DNA-modified electrode offered a lower detection limit due to the pre-concentration effect at the electrode surface. Additionally, the drugs mifepristone,[105] echinomycin,[106] and phenothiazine[107] can also be analyzed using this simple direct eDNA sensor. Of note, some drugs with excellent electrochemical activity were also employed as an indicator for DNA hybridization through the specific intercalation in dsDNA, for example, methylene blue and daunomycin.[108-110]

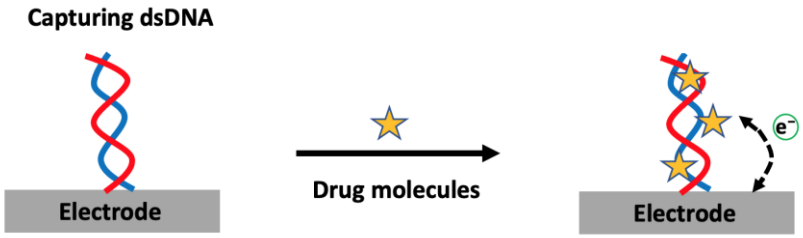

Figure 1.12 The analysis of drug-DNA interactions by eDNA sensor. The drug molecule is electrochemically active and can act as a redox indicator.

1.3.3.2. Redox-labeled eDNA sensors

Despite the simplicity of the aforementioned label-free assays, they inevitably suffer from relatively poor sensitivity and selectivity. To improve the performance of eDNA sensors, recent years have seen the development of covalently bound redox-labeled assays using an indicator

with high electrochemical activity for molecular detection. In contrast to the free-diffusing redox molecules used in label-free assays (e.g., electrochemical mediators, intercalators, and groove binders), covalently bound redox labels show better stability and specificity due to their covalent association with the DNA sensor.[58] Moreover, such redox-labeled assays enable high flexibility for researchers to explore novel ways in which signal transduction can be configured with high sensitivity and selectivity.[59] We can typically regroup the different redox-labeled assays into four classes: (1) Sandwich-based assays; (2) Structure switching-based assays, (3) Collision dynamic-based assays, and (4) Steric hindrance-based assays.

1.3.3.2.1 Sandwich-based assays

A "sandwich structure" plays an essential role in various fields, such as clinical diagnosis, food safety, and environmental monitoring.[111] The sandwich structure is highly specific due to the requirement of simultaneous binding of the capture probe and the signal probe with the target molecule. By taking advantage of the sandwich structure, Ihara et al.[112] and Umek et al.[113] have developed sandwich-based assays to detect DNA involving a redox label covalently bound to a DNA probe. Three DNA probes, including the capture DNA, target DNA, and signal DNA, are used in this system. The capture DNA is first immobilized onto the electrode surface by an S-Au bond, then hybridized with one portion of the target DNA. The non-hybridized overhang portion of target DNA then binds to the redox-labeled signal DNA, thereby forming a DNA sandwich architecture that brings the redox component close to the electrode surface (Figure 1.13a). The resulting electrochemical signal is proportional to the concentration of target DNA in the sandwich-based assay. In the absence of target DNA, the redox-labeled signal DNA is unable to attach to the electrode surface due to the lack of the complementary sequence for the capture DNA. In order to further improve the sensitivity of this sandwich-based assay, Xia et al. explored a so-called supersandwich-based assay (Figure 1.13b).[114] In this strategy, the redox-labeled signal DNA is designed to hybridize to two regions (5'- and 3'- termini) of a target DNA. When the first sandwich structure is formed at the surface, the signaling DNA is still available for binding to a second target DNA, which can hybridize to a second signal DNA, and so on. This leads to many target DNAs and signaling DNA being assembled into a long sandwich structure with multiple

repeats. This supersandwich-based assay enables the detection of target DNA at a concentration as low as 100 fM. Inspired by this idea, two similar strategies have also been developed recently.[115, 116]

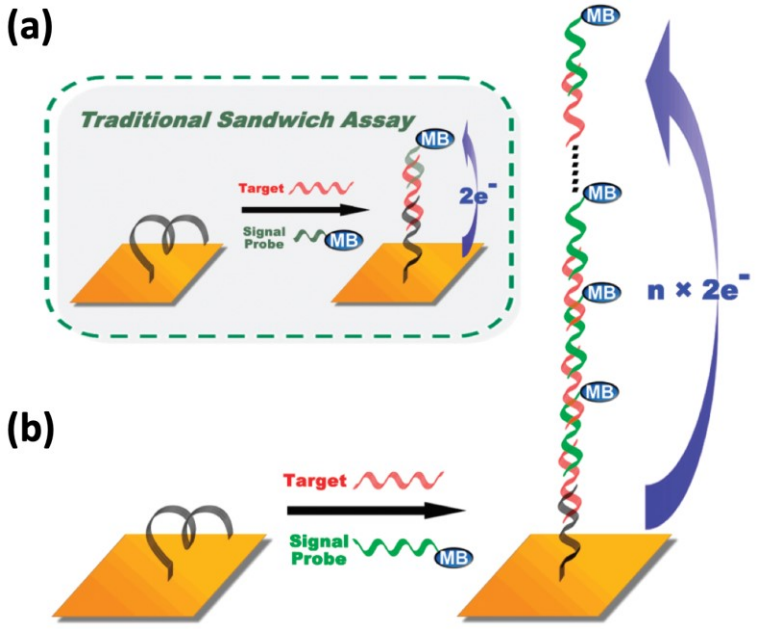

Figure 1.13 Schematic representation of (a) a traditional sandwich-based assay (inside the green dashed line) and (b) a supersandwich-based assay for the detection of target DNA. MB indicates the redox label, methylene blue. Reprinted with permission from ref. 114. Copyright 2010 American Chemical Society.

1.3.3.2.2 Structure switching-based assays

Although the sandwich-based assays are sensitive and specific, they are generally limited to the detection of nucleic acids, and thus, are not adaptable for the detection of small molecules and proteins. Structure-switching mechanisms, on the other hand, represent a universal signaling mechanism. Such mechanisms, which consist in analyte inducing a conformational change into a biomolecule (such as DNA) to trigger signaling, are employed extensively by living cells. Natural examples of such mechanisms include the calcium-triggered conformational change in the calmodulin protein,[117] and the regulation of translation by a metabolite-initiated conformational change in the leader mRNA.[118] Inspired by the efficiency and versatility of such natural mechanisms, Plaxco's[119] and Ouyang's[120] labs almost simultaneously reported the first binding-induced structure-switching eDNA sensor to detect target DNA in 2003. In this system, a redox-

labeled capturing DNA is first immobilized on an electrode surface to form a stem-loop structure (Figure 1.14a),[121] analogous to the famous fluorescent molecular beacon reported by Kramer.[122] In the absence of target DNA, the stem-loop structure of the capturing DNA brings the redox label into proximity with the electrode surface, which generates a high electrochemical current. However, in the presence of target DNA, the stem-loop structure opens due to forming a rigid double helix, which leads to a significant decrease of electrochemical current since the redox label is pulled far away from the electrode surface. This system is quite simple as it contains only one component, and it has since inspired the development of many eDNA sensors. For example, using a similar principle, Plaxco's lab also developed aptamer-based eDNA sensors for the detection of small molecules (e.g., cocaine[123]) and proteins (e.g., thrombin[124]) (Figure 1.14b-c, respectively). In these sensors, the conformation of the redox-labeled aptamer changes following the binding with cocaine or thrombin, resulting in a shift in electrochemical signal due to a change of distance between the redox label and the electrode surface.

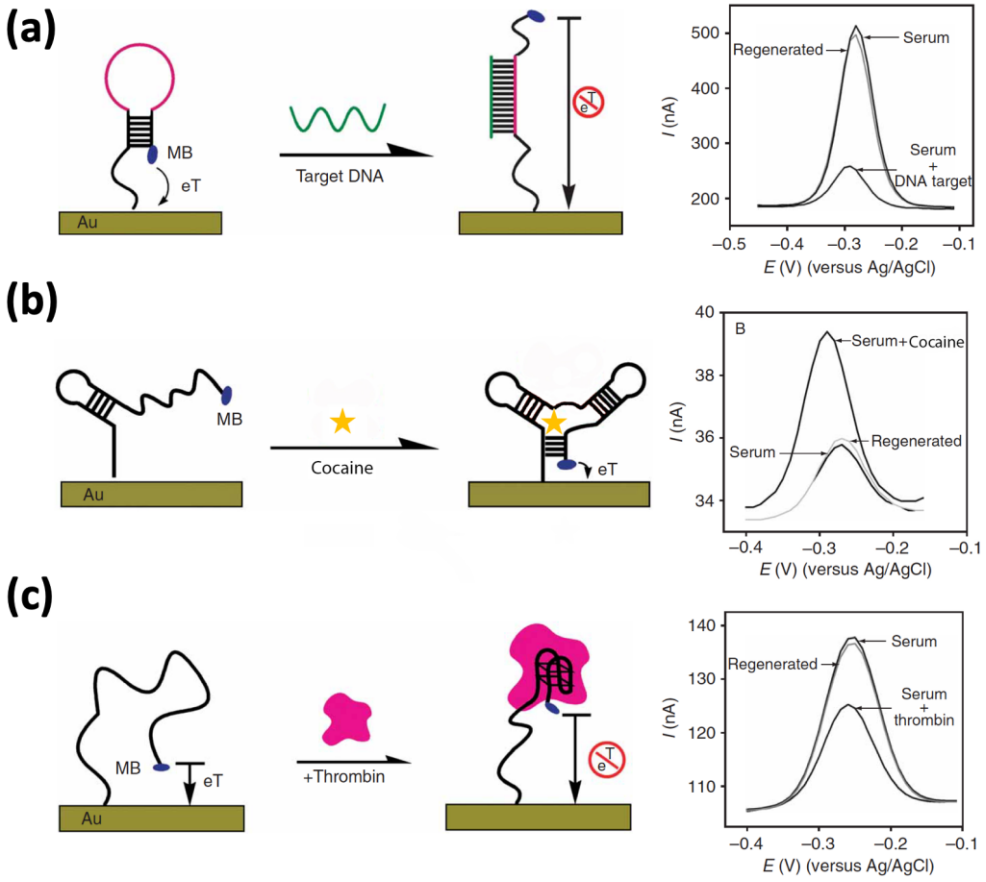

Figure 1.14 Schematic representation of switch-based assays for the detection of (a) target DNA, (b) cocaine, and (c) thrombin. MB indicates the redox label of methylene blue. Adapted with permission from ref. 121. Copyright 2007 Springer Nature.

1.3.3.2.3 Collision dynamic-based assays

Switch-based assays are versatile, but they remain limited to proteins for which we possess an aptamer with high affinity and selectivity. In order to expand the scope of the switch-based platform, Plaxco's lab further explored a new approach that employs variation in collision dynamics to detect proteins.[125] This collision dynamics-based platform comprises a dsDNA probe doubly labeled with a small recognition element and a redox molecule. As shown in Figure 1.15, the redox in the dsDNA probe is available to collide with the electrode surface and allows efficient electron transfer in the absence of target protein, thus generating a strong electrochemical signal. However, the collision efficiency of the redox element on the electrode surface is reduced following the binding of a protein to the recognition element on the dsDNA, thus decreasing the electrochemical signal. In contrast to the conformation change in the switch-based assay, the dynamics-based assay only involves the change of collision dynamics due to the use of rigid dsDNA as a stable scaffold at the surface. In recent years, this method has been applied successfully for the detection of a variety of proteins[126-128] and even small molecules by a competitive format.[129] Very recently, Kelley's lab successfully applied this collision dynamic-based assay to the detection of Covid-19 proteins and virus particles.[130, 131]

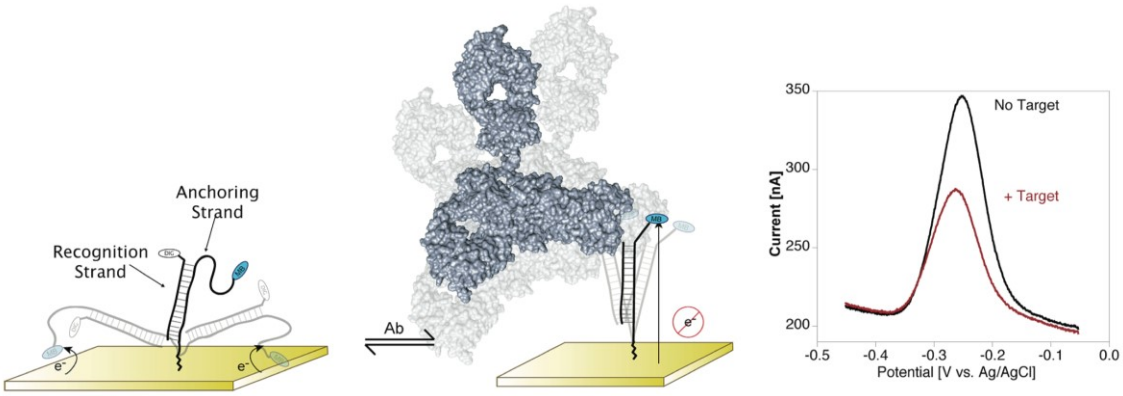

Figure 1.15 Schematic representation of collision dynamic-based assay for the detection of proteins. Reprinted with permission from ref. 125. Copyright 2009 American Chemical Society.

1.3.3.2.4 Steric hindrance-based assays

The aforementioned redox-label assays typically suffer from baseline drift when deployed in complex biological samples, such as whole blood. In order to overcome this limitation, our lab has recently developed a steric hindrance-based assay to detect proteins directly in whole blood (Figure 1.16).[132] The steric hindrance effect is one of the fundamental principles of chemical reactions and is usually observed for atoms or molecules in close proximity, which creates a high energy cost and alters their reactivity due to the mutually exclusive electron clouds between two atoms or functional groups.[133] In this assay, the hybridization efficiency between the capturing DNA and signaling DNA is changed by means of the steric hindrance effect. As shown in Figure 1.16, in the absence of the target protein, the redox-labeled signaling DNA strand quickly hybridizes to the capturing DNA strand on the electrode surface, thereby generating a high electrochemical signal because of the high hybridization efficiency. However, in the presence of the target protein, fewer redox-labeled signaling DNA strands can reach the electrode surface owing to the significant steric hindrance, thus resulting in a low electrochemical signal. To verify the steric hindrance mechanism, the relationship between the size of the target proteins and the electrochemical signal was also investigated. We found that larger target proteins, which have more steric hindrance, lead to a lower electrochemical signal. We further explored this approach for the detection of small molecules by a competition format,[134] as well as diagnosis via HIV clinical samples by using different electrodes.[135]

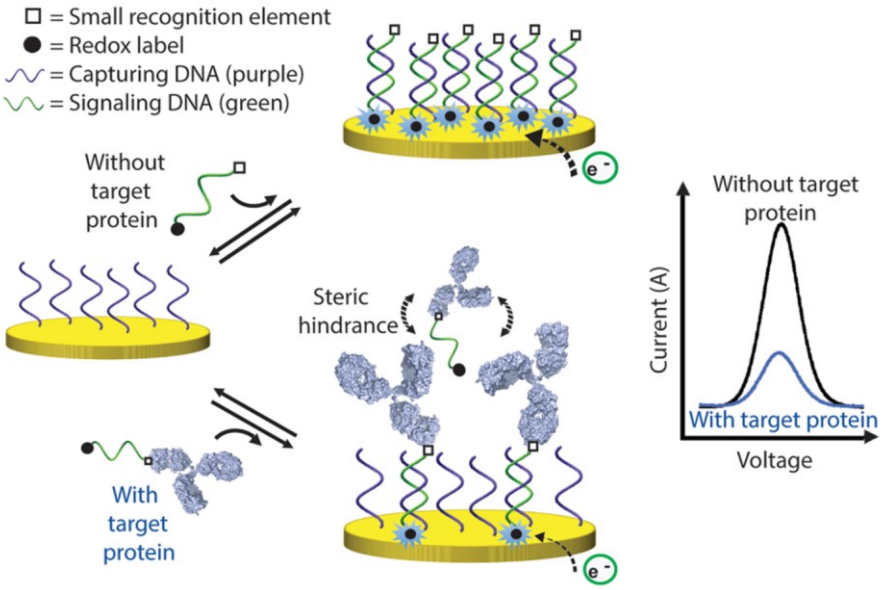

Figure 1.16 Schematic representation of our lab's steric hindrance-based assay for the detection of proteins. Reprinted with permission from ref. 132. Copyright 2015 American Chemical Society.

1.3.3.3 Other assays

Using the exact mechanisms of label-free assays or redox-labeled assays, various platforms that combine nanomaterials and protein enzymes have been developed in recent years. Nanomaterials are ideal candidates for amplified signal generation and transduction in electrochemical sensing due to their high surface area, excellent catalytic activity, and enhanced electrical conductivity.[136] To date, various nanomaterials such as gold nanoparticles, quantum dots, carbon-based nanomaterials, and nanostructured electrodes have been used for eDNA sensors.[136-138] More interestingly, DNA origami scaffold-based nanostructured electrodes have attracted attention due to improved recognition ability at the heterogeneous surface.[72, 139] For example, Fan et al. has developed a DNA tetrahedra structure-based electrochemical assay for the detection of target DNA (Figure 1.17). Typically, a "pyramidal" DNA tetrahedra structure is immobilized on the electrode surface through the self-assembly of three thiolated DNA strands and one probe-containing DNA strand. The free-standing probe DNA at the top of tetrahedra structure can bind target DNA and biotinylated reporter DNA to form a sandwich, and then this sandwich hybridization event can be transduced to electrochemical signals with the assistance of avidin-HRP (horseradish peroxidase), H_2O_2, and redox molecule (3,3',5,5'-tetramethylbenzidine,

TMB). This DNA tetrahedra structure-based eDNA sensor is also able to detect proteins, small molecules, and antigens by simply changing the free-standing probe DNA to aptamer sequence or DNA-antibody conjugate.[140, 141] In contrast to the ssDNA or dsDNA on the electrode surface, this tetrahedral DNA structure is a promising candidate to anchor biomolecules precisely on the surface due to its mechanical rigidity and structural stability. Moreover, tetrahedral DNA structures show a better sensor performance than ssDNA or dsDNA on heterogeneous electrode surfaces.

Protein enzyme-assistant amplification assays have also been widely developed to amplify the signal for molecular detection in an electrochemical format. For instance, horseradish peroxidase[142] is a widespread enzyme for electrochemical signal amplification because of its excellent catalytic activity. Moreover, through the assistance of polymerase, endonuclease, ligase, and helicase, numerous isothermal amplification-based assays such as rolling circle amplification (RCA), strand displacement amplification (SDA), helicase dependent amplification (HDA), and loop-mediated isothermal amplification (LAMP) have also been explored to improve detection sensitivity.[143-145]

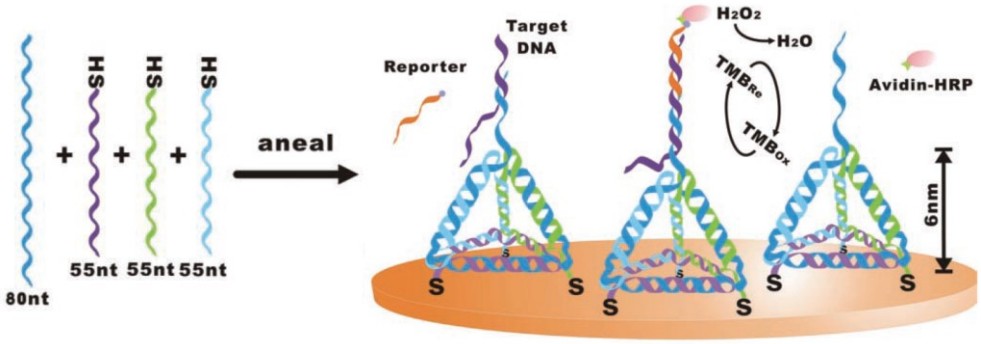

Figure 1.17 Schematic representation of tetrahedron-structured probes-based assay for the detection of target DNA. Reprinted with permission from ref. 139. Copyright 2010 John Wiley and Sons.

1.3.3.4 Summary

In summary, label-free assays have the advantages of simplicity and low cost, but typically suffer from unsatisfactory sensitivity and specificity. In contrast, redox-labeled assays enable the sensitive detection of analytes but still require time-consuming labeling reactions (for example,

dual-labeled DNA) and therefore display higher costs. eDNA sensors employing nanomaterials and protein enzymes typically allow converting a small number of target molecules into an amplified signal readout. However, these approaches usually suffer from lower reproducibility and limited stability.[136, 146] Over the past years, Plaxco's lab has invested significant efforts in the development of various eDNA sensing systems for *in vivo* drug monitoring,[147-150] but their signaling mechanisms typically display significant baseline drift when deployed in whole blood and remain stable only for a couple of hours. To the best of my knowledge, only two companies have successfully commercialized eDNA sensor technologies so far. For example, GenMark Diagnostics (USA) has developed an electrochemical sensing platform that employs the hybridization between a capture probe and a ferrocene-labeled signal probe to detect viral DNA. CombiMatrix Diagnostics (USA) has also developed an electrochemical-based DNA microarray platform for genotyping and gene expression assays. This latter method uses a capture probe attached to the surface of an electrode and a biotinylated target DNA complementary to the capture probe. The bound biotinylated target DNA can bind to the streptavidin-HRP (horseradish peroxidase) complex and subsequently catalyzes the oxidation of tetramethylbenzidine (TMB). Unfortunately, these two technologies still rely on complex sample pre-treatment procedures that include nucleic acid extraction, PCR amplification, exonuclease digestion, or target DNA labeling, which undoubtedly limit their point-of-care application. Up to date, the total global market of biosensors is still primarily dominated by glucose monitoring (85%-90%),[77] and despite their promise eDNA sensors have not yet delivered on their potential. In the next section, I will present a summary of the main challenges that must be addressed for eDNA sensors to be successfully developed and deployed in all biosensing fields.

1.4 Current challenges in eDNA sensors

Although eDNA sensors have shown an outstanding potential to achieve a highly sensitive, specific, and reagent-less detection for various molecules in different biological samples, many challenges remain to be solved to see their large-scale adoption. After working many years in this field, hours of discussions with players in the industry, and hundreds of papers and reviews digested, I discuss below what I believe to be the four main challenges to move forward.

1) *Baseline drift in blood*: eDNA sensors, such as the popular structure switching-based assays,[76] typically contain a redox molecule attached to the capture probe. This DNA sequence, often the recognition element, is immobilized on the surface of the electrode. Upon binding to its specific analyte, the conformation of the capture probe is changed, which in turn causes a variation in distance between the redox molecule and the electrode surface, leading to a change of electrochemical signal. This strategy typically works well in simple buffers, but this mechanism creates significant baseline drift in the first few minutes when deployed in a complex biological sample, such as whole blood. This is because blood contains thousands of different cells, proteins, and other molecules, many of which display sufficient affinity to the sensor surface to bind and affect the chemistry or location of the redox molecule. Different strategies have been developed to account for this signal drift[151, 152], but these complicate the signal analysis and reproducibility of the sensors. Furthermore, the nonspecific adsorption of molecules at the surface of a sensor significantly reduces its half-life (no more than 10 hours) when deployed in a continuous monitoring setting (personal communication with Prof. Kevin Plaxco, *University of California Santa Barbara*). Thus, the development of novel signaling mechanisms that prevent non-specific adsorption at the surface of the sensor would represent a substantial advance.

2) *Limited reproducibility and stability*: The performance of eDNA sensors is entirely dependent on the reproducibility and stability of the electrodes. Since electrochemistry is a highly sensitive and heterogeneous technology, a small change on the electrode surface may cause a significant signal variation. For example, typically commercialized electrodes display significant batch-to-batch variation. In 2019-2020, our lab ordered the same type of electrode from the same company twice, and the electrodes for these two orders came from two different production batches. Quality control experiments on these lots found that the electrode showed a signal difference up to about 50% (data not shown). Also, current electrode functionalization processes generate variability in the density of the DNA on the surface, which in turn affects the signaling process.[153] In addition, eDNA electrodes do not display sufficient stability during storage. Latest studies have shown that ~50% of the DNA on the electrode surface will be degraded after 2-3 weeks of storage,[154, 155] which causes significant errors for signaling mechanisms sensitive to

probe density. Since commercialized sensors typically aim for reproducibility that accounts for less than 5% error (personal communication with Anasens Inc.), we believe that novel signaling mechanisms insensitive to probe density on the surface should extensively address this issue.

3) *Complex synthesis*: eDNA sensors often require dual labeling on one DNA strand. For example, the signaling DNA shown in Figure 1.16 involves the attachment of both a redox molecule and a recognition element, which remains challenging and expensive to achieve. Our lab recently obtained a quote from the industry for a dual labeled DNA containing a methylene blue and a DBCO at >USD$ 5000 for 300 nanomole with no guaranty of product and yield. Moreover, this dual-labeled DNA is not the final product: DBCO is required to conjugate the desired recognition element (such as peptides), which will undoubtedly increase the cost and time of synthesis. One of my colleagues has spent the last three years exploring novel chemical strategies for simplifying these dual-labeled syntheses. Another way to streamline sensor synthesis could be to develop novel signaling mechanisms that only require single labeling on DNA strand.

4) *Long and tedious development time*: Aptamers have been widely used in eDNA sensors development,[37, 38] however, designing efficient aptamer-based signaling mechanisms requires tedious, semi-rational optimization processes. For example, selecting an optimal position for the redox molecules on aptamer is time-consuming because different label positions will obviously affect the performance of the sensor, including its signal gain, whether it is signal-on or signal-off reading out. Additionally, the direct addition of redox molecules on the aptamer may also affect its binding affinity and specificity for the analyte. Aptamer-based eDNA sensors also often work best at low surface coverage because aptamers need a certain space on the electrode surface to fold into a specific conformation before binding to the analyte. A low surface coverage sensor, however, typically yields weak raw currents, thereby requiring more expensive instrumentation to read the electrochemical signal. Moreover, electrodes using low surface coverage were also found more susceptible to degradation over time.[156] Overall, these limitations definitely slow down the commercialization process of sensors and make them very dependent on many conditions (fabrication, storage…).

1.5 Objective and overview of this thesis

Over the last 15 years, numerous publications on eDNA sensor development and maturation have tried to address the challenges presented in section 1.4. For example researchers have tried to introduce novel calibration-free mechanism,[152, 157] electrodes with different monolayers,[158-160] double redox molecules labeling strategies,[65, 161-163] various nanomaterials,[136] and enzymes based eDNA sensors.[164-166] We believe that a real step towards commercialization may only be achieved by developing novel sensing and signaling mechanisms that do not display the limitations and challenges described in section 1.4.

Chapter 2 addresses the challenge of fabrication variability, limited shelf life, and limited signal gain by conceiving a signaling mechanism that is independent of the DNA density on the electrode surface. This novel sensing mechanism employs various steric hindrance mechanisms and introduces a binding-induced redox inhibition mechanism for the first time. In contrast to other classic eDNA sensors, we show that this novel signaling mechanism produces high signal gains that are relatively insensitive to variation in the DNA density on the sensor surface. This important mechanistic feature ensures minimizing signal variation arising from electrode fabrication or sensor degradation taking place during storage. Moreover, the signal gain achieved by this new method (up to -93.6 ± 1.36 % at 3 min) is close to the theoretical maximum value, i.e., -100%. It is important that this hybridization assay also eliminates the baseline drift challenge in whole blood samples since methylene blue is not fixed on the electrode surface but is instead attached to the free diffusing signaling DNA.

Chapter 3 focuses on addressing the challenges linked to synthesizing complex dual-labeled DNA strands. We and others[167] have found that synthesizing a dual-labeled DNA molecule remains time-consuming and expensive, especially when the recognition element is complex (e.g., peptide, sugar…). In response, we asked ourselves whether it is possible to design a novel signaling mechanism that does not require dual-labeled DNA? Based on this idea, we designed a sensing mechanism that employs a single labeled redox molecule-signaling DNA conjugate and a single-labeled recognition element-capturing DNA fixed on the electrode surface. In this novel

sensing mechanism, the target protein present in the sample can bind the recognition elements on the sensor surface and form a barrier that prevents the hybridization of the signaling DNA, thereby reducing the electrochemical signal. We found that by changing the length of the capturing DNA on the surface, we can create a molecular barrier that produces up to -90% signal gain. This novel method also performs well directly in whole blood without baseline drift.

Chapter 4 addresses the challenges inherent to aptamer-based eDNA sensors that typically require careful optimization steps while displaying low current densities and signal drift in the blood sample. We propose a novel sensing mechanism by employing a kinetically programmed constitutional dynamic chemistry (CDC) assay. With the programmability of DNA hybridization, three reactions with different binding kinetics are designed in a one-step format, and the target molecule can be detected through various competing reactions. We demonstrate the universality of this method by detecting small molecules such as quinine and adenosine triphosphate (ATP), as well as proteins such as thrombin and platelet-derived growth factor (PDGF). This sensing mechanism was further tested to monitor the pharmacokinetics of an antimalaria drug, quinine, in living mice, which demonstrates that this new class of sensor could be applied for real-time drug monitoring.

Chapter 2: Density-independent electrochemical DNA sensors that use steric hindrance and redox inhibition mechanisms

Guichi Zhu[1,2], Alexis Vallée-Bélisle[1,2,3,4]*

[1]Institut de Génie Biomédical, Département de Pharmacologie et Physiologie, Université de Montréal, Montréal, Québec H3T 1J4, Canada.
[2]Laboratoire de Biosenseurs & Nanomachines, [3]Département de Chimie, and [4]Département de Biochimie et Médecine Moléculaire, Université de Montréal, Montréal, Québec H3T 1J4, Canada.

Author contributions: G.Z. and A.V.-B. conceived and designed the study. G.Z. performed all experiments. G.Z. and A.V.-B. created the figures and wrote the manuscript.

This manuscript will be submitted in 2022.

2.1 Abstract

Remote monitoring of chronic diseases in patients by telemedical devices requires inexpensive user-friendly sensors for molecular analysis in blood. Electrochemical DNA-based sensors (eDNA sensors) have shown great promise for the rapid detection of multiple classes of blood markers due to their high sensitivity, low cost, and relative insensitivity toward the matrix effects of biological samples. However, several challenges have been slowing down the commercialization of eDNA sensors. Among them, the performance of eDNA sensing mechanisms remains strongly affected by the variation of the DNA probe density on the electrode surface. Here we designed a novel electrochemical hybridization-based assay for detecting proteins that integrates four distinct signaling mechanisms to create a highly sensitive, density-independent sensing mechanism that performs reproducibly well even with fabrication variation

or aging. This signaling mechanism uses protein analyte binding on a recognition element attached to a redox-active signaling DNA to inhibit its hybridization and redox activity on an electrode containing its complementary strand. Protein analyte binding in close proximity to the redox molecule further limits electroactivity through a contact inhibition mechanism. We show that this novel sensing mechanism allows the detection of a low nanomolar concentration of protein analytes in a drop of blood in less than 3 min, with nearly optimal signal gain (up to -95.2 ± 0.61 %). Given its attributes, we believe that this electrochemical steric hindrance and redox inhibition (eSHRI) hybridization assay holds excellent promise for commercialization into point-of-care sensors.

2.2 Introduction

Over the past few decades, electrochemical DNA-based sensors (eDNA sensors) have attracted increasing attention due to their high sensitivity, specificity, low cost, and ability to detect broad classes of biomarkers.[77] The remarkable universality of eDNA sensors relies on their ability to employ any type of recognition elements and signaling mechanism. For example, eDNA sensors have been designed to utilize nucleic acids, small molecules, peptides, proteins and even enzymes as their recognition elements. eDNA sensors have also been engineered using numerous signaling mechanisms, including structure-switching,[76, 119, 123, 124] diffusion-collision,[125, 129] enzyme catalysis,[168-170] and steric-hindrance.[132, 134, 135, 171, 172] These sensing mechanisms display specific advantages depending on the class of biorecognition element employed, but most of them also display important limitations. Their performance, for example, enormously varies with factors affecting their surface density such as fabrication variation or sensor aging and their electrochemical baseline typical drifts when deployed in the complex sample such as blood.[147, 151]

Few studies have focused on the reproducibility of sensor fabrication and the optimization of their stability over time. While these challenges trigger less academic interest, on the other hand, they continue to significantly limit the commercialization process of eDNA sensors even 20 years after their first development.[9, 119] Various strategies have been proposed to reduce the

impact of these limitations. Plaxco et al.[151] and Ellington et al.[65], for example, have recently proposed using an additional control sensor employing an additional control redox probe that does not respond to the analyte and therefore only reports the electrochemical component linked to signal drift. Plaxco et al.[152] have also recently proposed a similar ratio-metric strategy that employs multiple frequencies to remove the electrochemical element related to the non-specific signal drift. Although these methods have improved the accuracy and precision of eDNA sensors, they remain complex and of limited use to account for all factors affecting sensor reproducibility, such as variation in sensor density linked to fabrication and aging. To address such limitation, we believe that developing a novel signaling mechanism that remains unaffected by the sensor density on its electrode surface would drastically simplify calibration strategies and the commercialization process of eDNA sensors.

Among the different signaling mechanisms developed for eDNA sensors, the recently developed steric hindrance hybridization assays have shown many advantages.[132, 134, 135, 171-175] Since the redox molecule is not located on the surface of the sensor when the sensor is first immersed in the biological sample, and DNA hybridization can take place in biological sample without interference, this specific eDNA sensing architecture works efficiently in whole blood without signal drift.[132] Even though appearing relatively universal, this sensing mechanism, however, requires high sensor density on its surface to achieve optimal performance.[132, 134, 135, 171, 172] To solve this limitation, here we propose to explore a novel sensing mechanism that employs electrochemical steric hindrance and redox inhibition hybridization assay, which displays less dependence on the sensor density.

2.3 Results and discussions

In the classic version of electrochemical steric hindrance hybridization assay (eSHHA, Figure 2.1a), a signaling DNA containing a redox molecule and a recognition element at opposite extremity diffuses in the sample and hybridizes to a complementary capturing DNA located at the surface of the electrode. Upon protein analyte binding to the signaling DNA, fewer signaling DNA reach the electrode surface due to the steric hindrance produced between the large protein

analytes (Figure 2.1a). Unfortunately, eSHHA can only generate a high signal gain on electrodes with high surface densities because the steric hindrance is dependent on the distance between the capturing DNAs on the surface. To create a density-independent sensing mechanism, a novel electrochemical steric hindrance and redox inhibition (eSHRI) hybridization assay is presented in Figure 2.1b. We hypothesized that analyte binding may produce more or less steric hindrance depending on where it binds on the signaling DNA. For example, analyte binding close to the redox molecule may likely result in additional steric hindrance between the protein analyte and the capturing DNA layer and even between the analyte and the gold surface. Alternatively, having the protein analyte binding in the vicinity of the redox molecule could also lead to inhibition, a mechanism that could significantly reduce the electron transfer rate and improve the signaling mechanism of eDNA sensors.

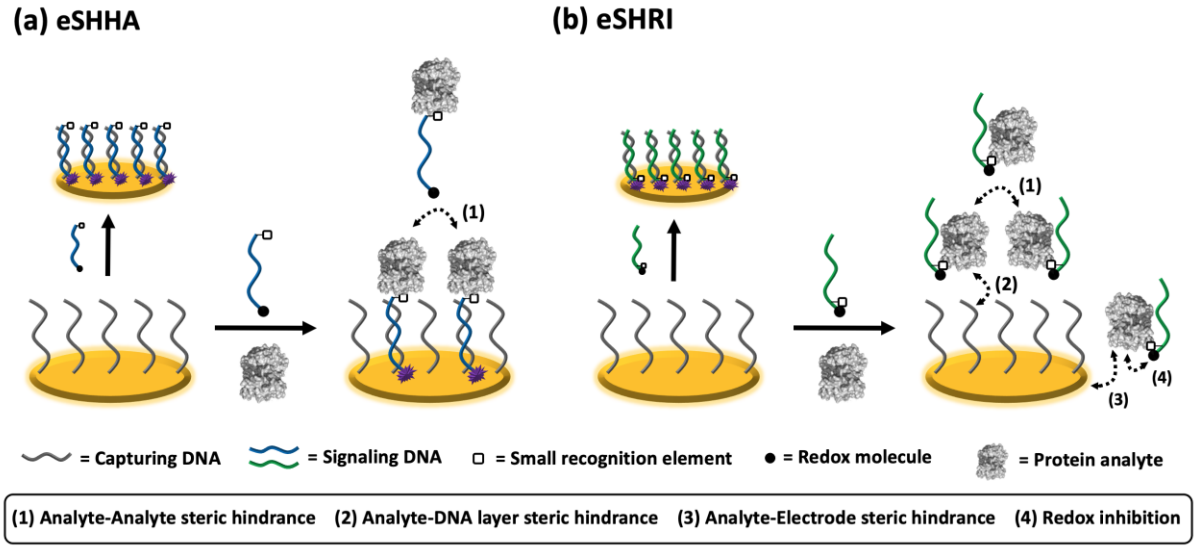

Figure 2.1 Creating a density-independent signaling mechanism through electrochemical steric hindrance and redox inhibition (eSHRI) hybridization assay. (a) In the classic electrochemical steric hindrance hybridization assay (eSHHA), the hybridization efficiency of a redox-labeled signaling DNA is reduced through steric hindrance between the large analyte proteins.[132] (b) By strategically positioning the location of the recognition element closer to the gold surface and the redox molecule, we hypothesized that a new sensing mechanism could take place between the analyte and capturing DNA layer or the analyte and the gold surface. Additionally, protein analyte binding in the vicinity of the redox molecule may lead to a redox inhibition mechanism.

We assumed that the hybridization efficiencies between a signaling DNA and a capturing DNA would vary with the position of the recognition element on the signaling DNA strand (Figure 2.2a). To explore these novel steric hindrances and redox inhibition mechanisms, we designed six signaling DNAs that vary the location of the recognition element, here biotin, from the most distal location to the redox molecule (signaling DNA-16, Figure 2.2b) to its most proximal location (signaling DNA-01, Figure 2.2b). These 16 nucleotides long signaling DNAs display the same sequence and are all labeled with methylene blue at their 5' extremity to generate an electrochemical readout signal upon hybridizing to their complementary DNA attached on the gold surface. We synthesized these DNAs in-house using a DNA/RNA Synthesizer (K&A Laborgeraete, Germany), a methylene blue phosphoramidite to label the 5' extremity and a modified thymine-biotin (see 2.6 supporting information). In the absence of protein analyte, all signaling DNAs can hybridize on the electrode surface with similar efficiencies: all showed very similar electrochemical current at -0.3 V after 5 min (Figure 2.2b, gray curves). These results indicate that the location of the small biotin group does not affect the hybridization efficiency. In contrast, upon binding of the protein analyte (here streptavidin) to the signaling DNA, the hybridization efficiency is primarily affected by the location of the recognition element. For example, the most distal location of biotin (signaling DNA-16) only reduced the hybridization efficiency by 50%, but the most proximal location reduced the hybridization efficiency by up to 93% after only 5 min.

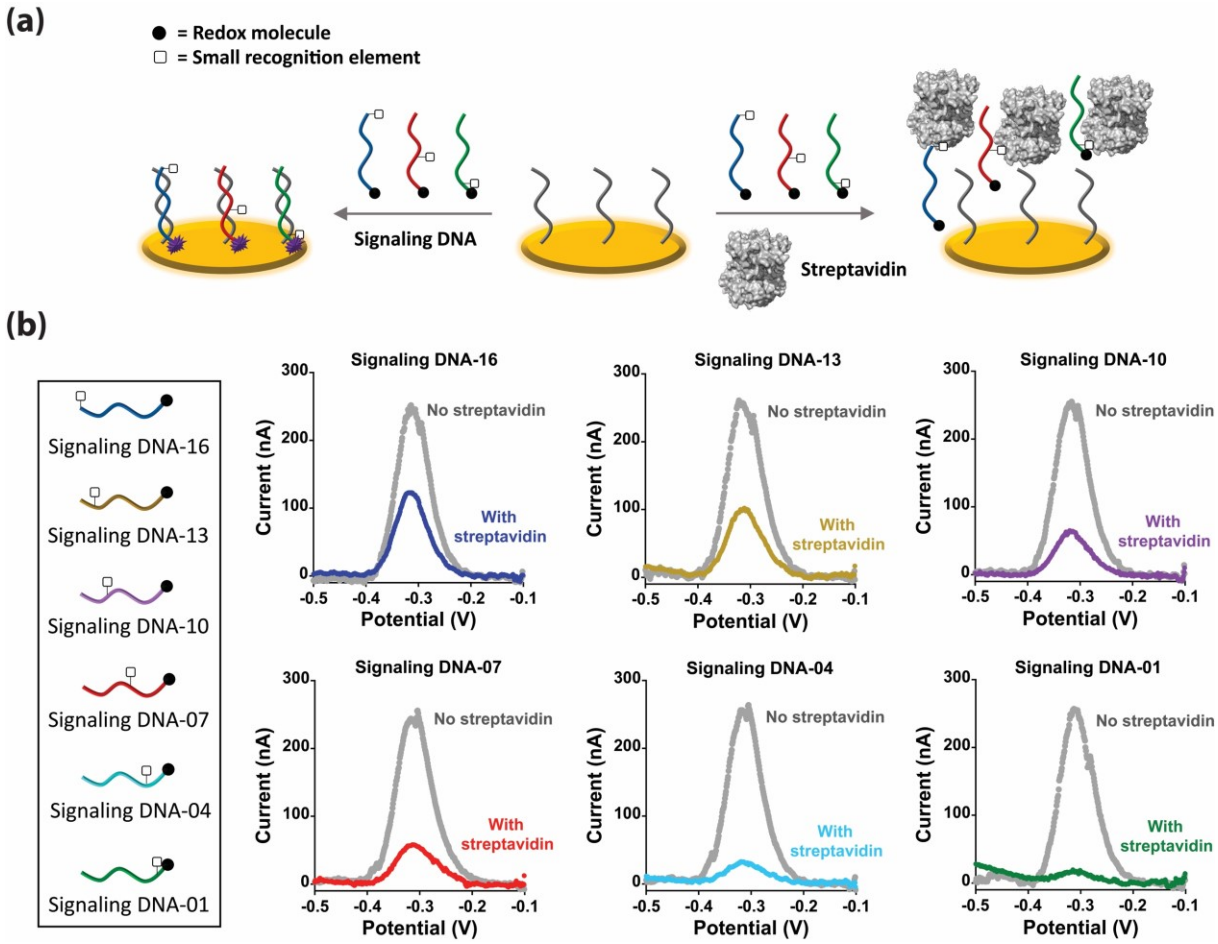

Figure 2.2 (a) Hybridization efficiencies between a signaling DNA and a complementary capturing DNA attached to an electrode surface drastically decrease when the analyte binds near the electrode surface and the redox molecule. (b) All signaling DNAs are labeled with methylene blue (●, at 5' end) and biotin (□) at different positions in the strand. The signaling DNA is named according to the distance between the biotin and methylene blue. For example, signaling DNA-16 indicates that there are 16 nucleotides between the biotin and methylene blue. Square wave voltammograms (SWV) after 5 min of hybridization in the absence (grey) and presence (color) of streptavidin. In the absence of streptavidin, all signaling DNAs display similar peak currents (242 ± 9 nA) while the peak current decreases significantly in the presence of 100 nM streptavidin as the biotin moves closer to the gold surface and methylene blue. The concentrations of capturing DNA and signaling DNAs used in this assay were 300 nM and 100 nM, respectively.

We further characterized the impact of protein binding location of the signaling DNA on the hybridization kinetics. In the absence of streptavidin, all six signaling DNAs displayed very

similar kinetic traces (Figure 2.3a, grey curves), i.e., the currents after 5 min (Figure 2.3b, grey curve), and the hybridization rates (Figure 2.3d, grey curve). In contrast, upon streptavidin binding, all six signaling DNAs showed a decrease in the hybridization efficiency that is inversely proportional to the distance between the biotin and the methylene blue (Figure 2.3a, color curves). Moving the location of the biotin from the most distal location (signaling DNA-16) to the most proximal location next to the gold surface (signaling DNA-01) reduces the hybridization by 86% after 5 min (Figure 2.3b) and the rate of hybridization by four-fold (Figure 2.3d). Interestingly, the signal gain of these streptavidin sensors increases linearly from -49% (signaling DNA-16) to -93% (signaling DNA-01) as the location of the biotin is moved closer to the gold surface or methylene blue (Figure 2.3c). In addition to significantly improving the signal gain of the sensor, our new assay is also very rapid with the maximal signal gain being reached after only two minutes (Figure 2.3e).

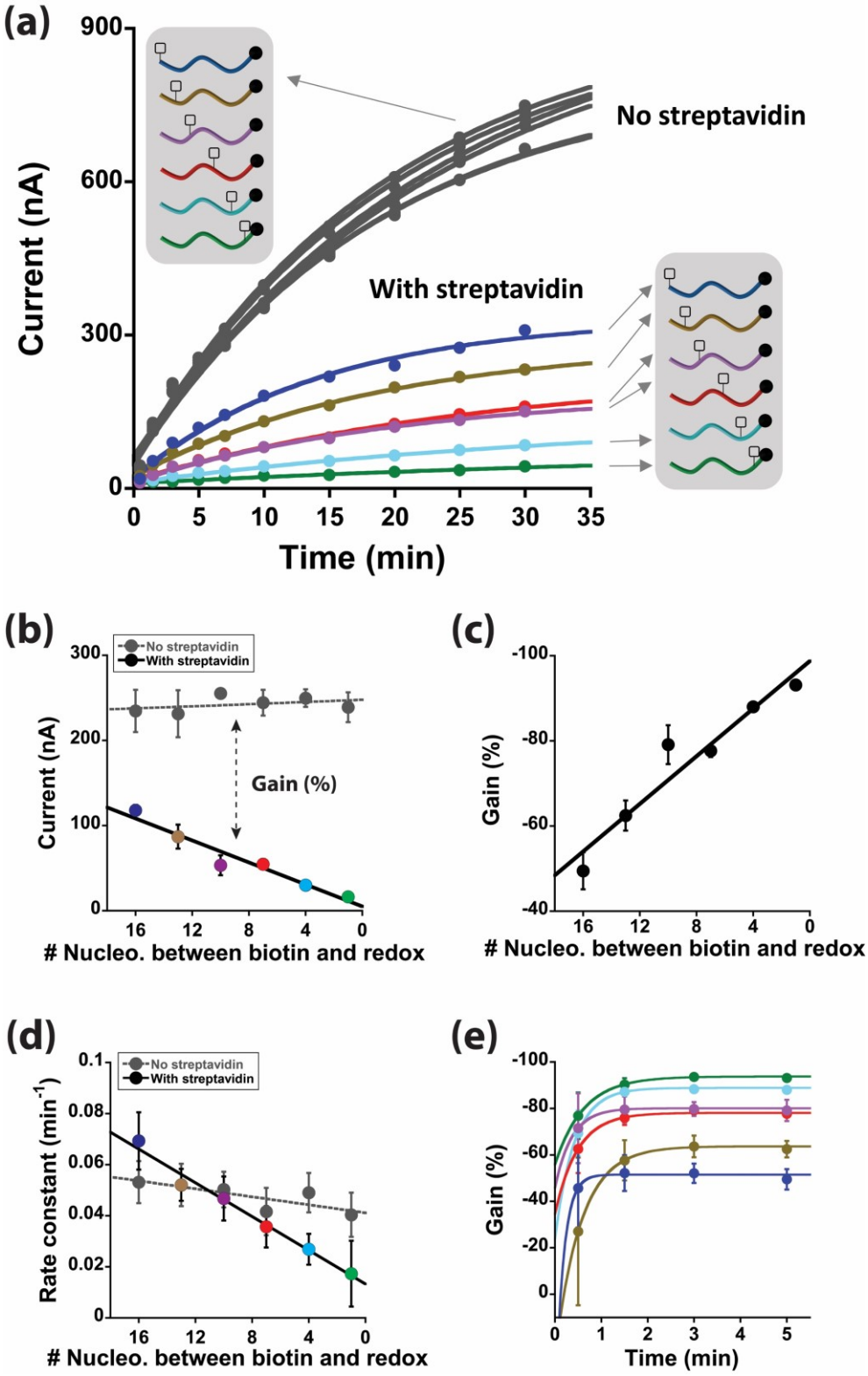

Figure 2.3 Hybridization efficiency and kinetics of a signaling DNA to a complementary capturing DNA located on the surface of the sensor decrease linearly with decreasing distance between the analyte

binding site and the electrode surface or the redox molecule. (a) The kinetic profile of the surface hybridization of six signaling DNAs and capturing DNA in the absence and presence of 100 nM streptavidin; (b) Raw current after 5 min; (c) Signal gain after 5 min, the signal gain is calculated by the percentage of current decrease with streptavidin versus no streptavidin (gain: C_{strep}-C_0/C_0); (d) Rate constant with or without streptavidin; (e) Signal gain of the sensor versus time. The concentrations of capturing DNA and signaling DNAs used in this assay were 300 nM and 100 nM, respectively. The error bars represent the standard deviation of the current and signal gain obtained from three electrodes. The error bars of the rate constant come from the errors of kinetic fitting.

A primary advantage of the eSHRI is that its performance should, in principle, be less dependent on the variation of the capturing DNA density on the electrode surface. We have previously shown that the classic eSHHA mechanism is drastically affected by the variation in the capturing DNA densities: when the average distance between two capturing DNAs becomes wider than the size of the protein analyte, there is no or few steric-hindrance.[132] eSHHA, therefore, requires a high surface density to perform optimally. In the eSHRI mechanism, we also expect the analyte to create steric hindrance with the DNA layer (which is also density-dependent) and with the electrode surface. As the protein analyte gets closer to the methylene blue, we may also expect redox inhibition, a potentially novel signaling mechanism in eDNA sensors. Analyte-electrode steric hindrance and redox inhibition should remain relatively insensitive to the variation in the capturing DNA densities.

To verify this hypothesis, we investigated the streptavidin assay at different capturing DNA densities. As expected, the electrochemical currents were significantly reduced when decreasing the capturing DNA densities (Figure S2.2). We then assessed the efficiency of the steric hindrance assay by testing these different sensors in the presence or absence of streptavidin. As expected, the signal gain for the classic eSHHA assay (signaling DNA-16) decreased from -53% to -7% upon decreasing the capturing DNA density (Figure 2.4a). Moving the location of the biotin three nucleotides within the DNA layer (signaling DNA-13) created enhanced steric hindrance at a high surface density (-65% signal gain, Figure 2.4b). This enhanced steric hindrance is likely occurring between the streptavidin and the DNA layer since this effect remains primarily dependent on the

density of the capturing DNA. Deepening, even more, the location of biotin into the DNA layer (e.g., signaling DNA-10 and -07) further improved steric hindrance at a high surface density (-80% and -78% signal gain, Figure 2.4c-d) but less steric hindrance is also observed when decreasing the density of the DNA layer (-8% and -21% at low surface coverage, respectively, Figure 2.4c-d). In contrast, when moving the analyte binding site even closer to the electrode surface, for example signaling DNA-04 and -01, a large signal gain (-76% and -83%, Figure 2.4e-f) is also observed at a low density. These results suggest that the enhanced steric hindrance effect observed is no longer only due to *(1) analyte-analyte steric hindrance* or *(2) analyte-DNA layer steric hindrance*. We suggest that the enhanced signal gain may be attributed to either a *(3) analyte-electrode steric hindrance* mechanism or due to a *(4) redox inhibition* mechanism between methylene blue and streptavidin. This novel sensing mechanism that remains independent of the capturing DNA density offers a considerable advantage in terms of reproducibility since fabrication procedure and sensor aging typically modify DNA density and thus sensor performance.

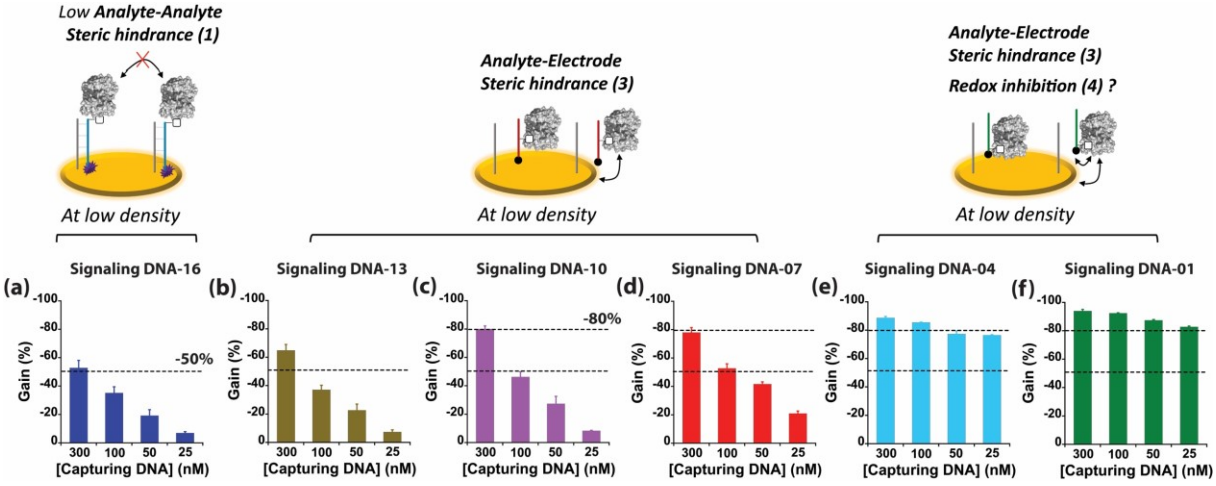

Figure 2.4 Decreasing the distance between the analyte binding site on the signaling DNA and the electrode surface, and the redox molecule renders the assay insensitive to capturing DNA density. Here, we used 300 nM, 100 nM, 50 nM, and 25 nM of capturing DNA concentration (in 200 uL) to create electrodes with different surface densities (a 300 nM capturing DNA concentration saturates the electrode surface - see Figure S2.1). The raw currents obtained at different densities are shown in Figure S2.2. The signal gain is calculated by the percentage of current decrease with streptavidin versus no streptavidin at 30 min. The length of capturing DNA used in this assay was 16 nucleotides (nt). The

concentrations of signaling DNAs and streptavidin used in this assay were 100 nM and 100 nM, respectively. The error bars represent the standard deviation obtained from three electrodes.

To further explore the nature of the eSHRI mechanism, we then varied the length of the capturing DNA to confirm the involvement of this later in creating the "analyte-DNA layer" steric hindrance. We hypothesized that reducing the length of the capturing DNA (while keeping a 16-nt signaling DNA length) should display two effects: a) reduction of the "analyte-analyte" steric hindrance since less signaling DNA can hybridize on the surface due to the lower affinity of the capturing DNA; b) reduction of the "analyte-DNA layer" steric hindrance since the average distance between the analyte and the DNA layer is increased. Indeed, the distance between the analyte and the DNA layer will increase when employing shorter capturing DNA with the original 16-nt signaling DNA. Additional non hybridized nucleotides on the signaling DNA should act as a flexible linker that will weaken steric hindrance between the analyte and the DNA layer.

To investigate these effects, we tested capturing DNAs with decreasing length from 16, 13, to 10 nucleotides (nt). As expected, we observed that the 10-nt capturing DNA greatly reduced the affinity for the signaling DNA (Figure S2.3). Less signaling DNA can hybridize to the surface modified with 10-nt capturing DNA, therefore it drastically reduced analyte-analyte steric hindrance resulting in little signal gain upon adding streptavidin for signaling DNA-16 and -13 (Figure 2.5a-b). Of note, when the biotin penetrates the DNA layer even farther with signaling DNA-10 and -07, the assay becomes less dependent on the number of signaling DNA on the surface: the low-affinity 10-nt capturing DNA still produces -50% (signaling DNA-10, Figure 2.5c) and -75% (signaling DNA-07, Figure 2.5d) signal gain upon adding streptavidin. These results confirm that when the analyte binds in the middle of the capturing DNA layer, the dominant steric hindrance effect is no longer the *(1) analyte-analyte steric hindrance* but rather either the *(2) analyte-DNA layer steric hindrance* or the *(3) analyte-electrode steric hindrance*. Finally, when inserting the biotin closer to the electrode with signaling DNA-04 and -01, the signal gain is further increased and remains constant with all capturing DNA lengths (Figure 2.5e-f). These results suggest that additional steric hindrance with the gold electrode or a potential redox inhibition mechanism is obtained upon methylene blue binding to the surface of the protein

analyte.

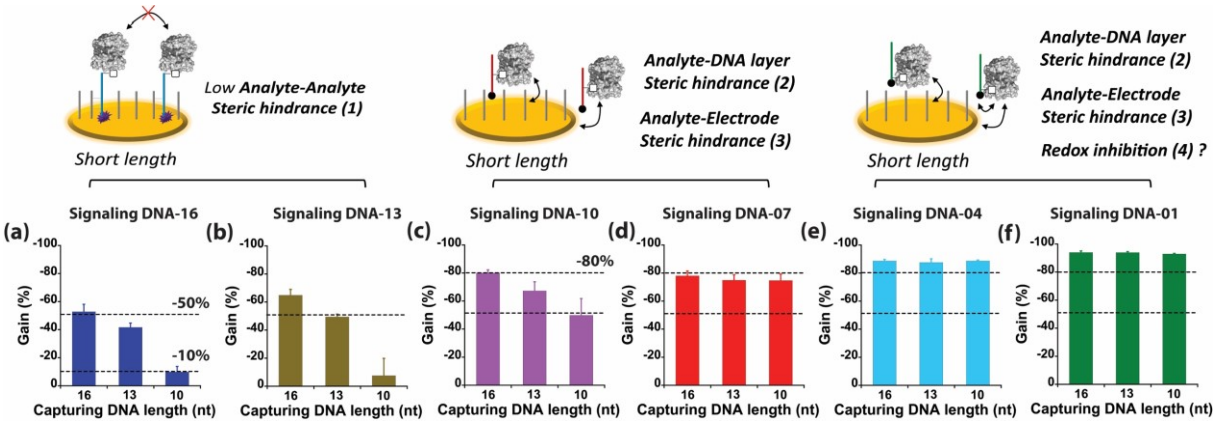

Figure 2.5 Decreasing the distance between the analyte binding site on the signaling DNA and the electrode surface, and the redox molecule renders the assay insensitive to variation in hybridization affinity between the DNA strands. Capturing DNA with the length of 16, 13, and 10 nucleotides (nt) are employed to vary the hybridization affinity on the surface. The signal gain is calculated by the percentage of current decrease with streptavidin versus no streptavidin at 30 min. The concentrations of capturing DNAs, signaling DNAs, and streptavidin used in this assay were 300 nM, 100 nM, and 100 nM, respectively. The error bars represent the standard deviation obtained from three electrodes.

eSHRI displays higher signal gain and is drastically less sensitive to sensor fabrication parameters (e.g., surface density, length of capturing DNA) or to sensor degradation than classic eSHHA. Next, we wanted to determine whether eSHRI also reduces the detection limit and improves the sensitivity. To demonstrate this, we compared the dose-response curve obtained using the signaling DNA-16 (classic eSHHA) and signaling DNA-01 (eSHRI). At optimal conditions (i.e., at high surface density and long capturing DNA), both assays exhibit a sigmoid curve centered around the K_D of 19 nM and 15 nM (Figure 2.6a), respectively. It is noted that classic eSHHA displays a 22% change of signal gain between 10 nM and 30 nM streptavidin concentration, while eSHRI reduces its signal gain by 66%, thus significantly improving sensitivity by 3-folds (Figure 2.6a). As demonstrated above, the performance of eSHRI is also independent of various sensor fabrication parameters. For example, when surface density is reduced due to fabrication variation or sensor aging, classical eSHHA drastically reduces its performance, but eSHRI remains unchanged (Figure 2.6b). Similarly, when hybridization efficiency is affected by

factors reducing affinity between the signaling and capturing DNA (e.g., high temperature, destabilizing matrix/buffers), the performance of eSHRI remains unaffected while classic eSHHA is drastically affected (Figure 2.6c). Overall, these results demonstrate that in addition to displaying an enhanced sensitivity, eSHRI also remains insensitive to sensor degradation and various exterior factors affecting sensor performance (batch to batch fabrication, temperature, and matrix).

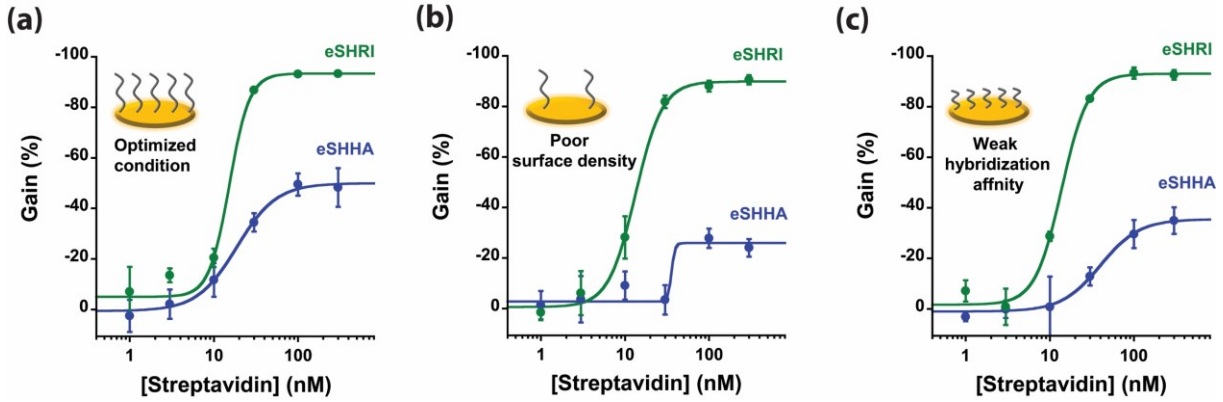

Figure 2.6 The highly sensitive eSHRI remains unaffected by variation in sensor fabrication and factors affecting DNA hybridization (e.g., temperature, matrix buffer). (a) Optimal conditions were realized at maximum surface density (when employing 300 nM capturing DNA to fabricate the sensor-see also Figure S2.1) using 1 mL of 100 nM of signaling DNA-16 (observed K_D= 19 nM) and signaling DNA-01 (observed K_D= 15 nM), for classic eSHHA and eSHRI, respectively. (b) Poor surface density employed 25 nM capturing DNA; (c) Weak hybridization affinity employed 10-nt capturing DNA at high density. The error bars represent the standard deviation obtained from three electrodes. In all condition, signaling DNA strands are in excess compared to the amount of capturing DNA strands.

To demonstrate that eSHRI enables the selective detection of protein analyte directly in complex biological samples, we performed streptavidin detection directly in a drop of blood using a small integrated electrode. All results showed so far have been obtained using a classic three electrodes system including a rod gold working electrode, a glass tubing Ag/AgCl reference electrode, and a platinum wire counter electrode, which typically requires large sample volumes of 1000 µL (Figure 2.7a). To test our sensor for point-of-care applications in a drop of blood, we adapted our assay on a small disposable electrode made using photolithography methods from

Micrux Technologies. This Micrux electrode includes a gold working electrode (WE), a platinum reference electrode (RE), and a platinum counter electrode (CE) on a small glass chip (6 *10 mm) (Figure 2.7b). The smaller surface area of the electrode (0.785 mm^2) only requires 5 µL sample volume (a small drop of blood) to perform the assay. We first detected streptavidin in the buffer to compare the performance of both the Micrux and rod electrodes. We found that both electrodes display similar high signal gain (Micrux= -96% at 5 min, Figure 2.7c inset; rod= -93% at 5 min, Figure 2.3c) and kinetics (Micrux= 0.035 min^{-1}, Figure 2.7c; rod= 0.04 min^{-1}, Figure 2.3d). We then explored the performance of these small streptavidin sensors directly in a drop of blood (Figure 2.7d). We found that the results in blood display comparable high signal gain (-95% at 5 min) as in buffer but show slightly faster kinetics (0.1 min^{-1}). It is worth noting that the raw current in the blood is about 25% lower than that in buffer, which may be caused by the decrease of electron transfer rate in blood. These results demonstrate the high specificity and selectivity of eSHRI's signaling mechanism that remains insensitive to any nonspecific absorption of proteins on the surface of the sensor.

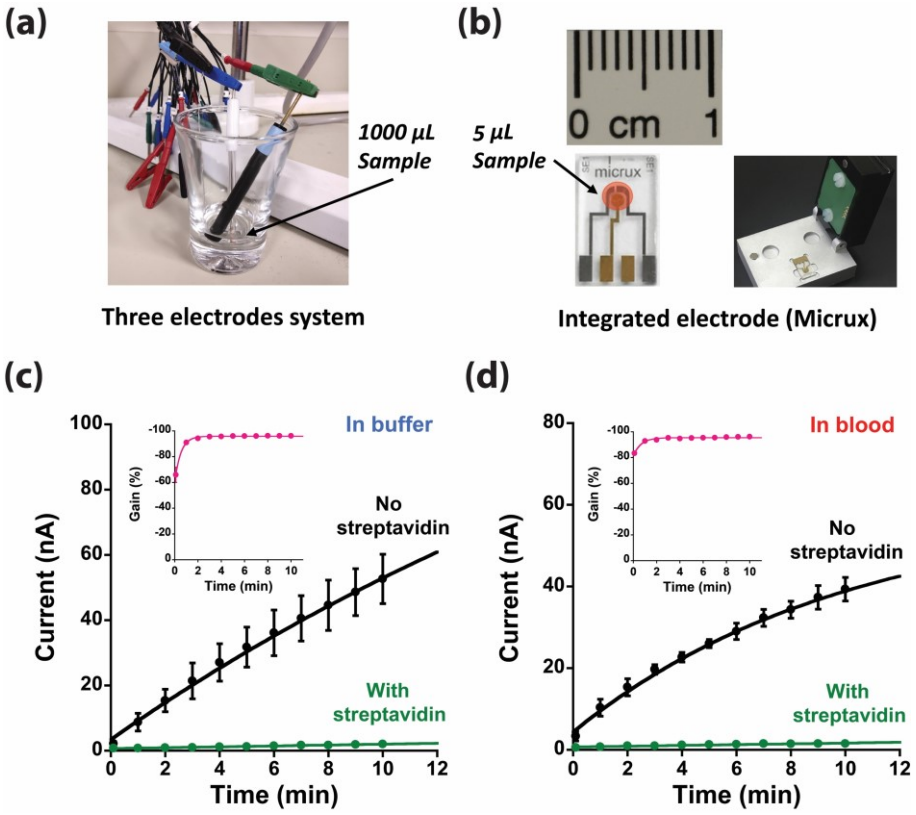

Figure 2.7 Adaptation of eSHRI in a point-of-care format for rapid detection in a drop of blood. (a) The classical three electrodes system employed so far (Figure 2.2 to 2.6) uses a rod gold electrode (diameter=2 mm), a glass tubing Ag/AgCl reference electrode, and a platinum wire counter electrode. (b) A small integrated electrode from Micrux Technologies contains a small gold working electrode (WE: 1 mm), a platinum reference electrode (RE), and a platinum counter electrode (CE). (c) The kinetic profile (0.1-10 min) of streptavidin assay in buffer using Micrux electrodes. (d) The kinetic profile (0.1-10 min) of streptavidin assay directly in 5 µL blood using Micrux electrodes. The concentrations of capturing DNA, signaling DNA, and streptavidin used in this assay were 300 nM, 100 nM, and 100 nM, respectively. The error bars represent the standard deviation obtained from three electrodes.

2.4 Conclusions

We have developed a density-independent electrochemical eDNA sensing mechanism that employs novel electrochemical steric hindrance and redox inhibition mechanisms (eSHRI). This new strategy aimed to solve many limitations of current eDNA sensors, including limited signal gain and high dependence on sensor fabrication and aging. We first found that novel steric hindrance and redox inhibition mechanisms are created by decreasing the distance between the analyte binding site and the electrode. These mechanisms enhanced the signal gain up to -93% (close to the highest theoretical value of -100%) and rendered the signaling mechanism independent of sensor density on the surface of the electrode. Importantly, this new method achieves rapid (<3 min) and one-step detection of protein analyte at low nanomolar range directly in a drop of blood.

Compared to the classical eSHHA that only uses one steric hindrance mechanism,[132] eSHRI employs three different steric hindrance mechanisms: *(1) analyte-analyte*, *(2) analyte-DNA layer*, and *(3) analyte-electrode surface*. Furthermore, we also described for the first-time a *(4) redox inhibition* mechanism that takes place when the protein analyte contacts and binds the redox molecule (methylene blue). eSHRI is a potentially universal signaling mechanism and maybe be adapted for the detection of other proteins analytes, such as clinically relevant antibodies (Covid-19 and HIV antibodies), by simply replacing the biotin with the specific antigen or epitope molecule. It will be interesting to see whether protein analytes that display different spatial

structures, charge distributions, and hydrophobic or hydrophilic properties may also produce this mechanism and render this novel signaling mechanism universal. Alternatively, employing structural analogues of methylene blue or other redox molecules that display higher affinities for a given analyte surface may also further enhanced the universality of this signaling mechanism. We believe that with its ability to perform equally well in unoptimized conditions (fabrication variation and sensor aging), eSHRI displays all the advantages to be readily adapted and commercialized into various point-of-care sensing applications.

2.5 Acknowledgments

A.V.-B. is Canada Research Chair in Bioengineering and Bionanotechnology, Tier II, G.Z. acknowledges a TransMedTech Excellence Scholarship as well as a PROTEO fellowship. The authors also thank Prof. William D. Lubell and Xiaomeng Wang for useful comments on the manuscript and the members of the Laboratory of Biosensors & Nanomachines (LBN).

2.6 Supporting information

2.6.1 Materials

Tris (2-carboxyethyl) phosphine hydrochloride (TCEP) and 6-Mercaptohexanol (MCH) were purchased from Sigma Aldrich. Streptavidin was obtained from New England BioLabs. Whole blood (newborn calf) was purchased from Innovative Research. Methylene Blue II phosphoramidite (Catalog # is 10-5961-95) was purchased from Glen Research. 3'-Thiol modified column (Catalog # is CG1-5003-1) and biotin modified thymine amidite (Catalog # is BNS-5022-50) were purchased from Biosearch Technologies. The standard adenine, guanine, cytosine, and thymine columns and reagents for DNA synthesis were purchased from Biosearch Technologies and ChemGenes Corporation, respectively. The buffer is 50 mM NaH_2PO_4, 150 mM NaCl, pH 7.0.

2.6.2 DNA sequences

The DNAs were synthesized in our laboratory using a DNA/RNA synthesizer (K&A Laborgeraete, Germany). Unlabeled DNAs were purified by reverse-phase cartridge (RPC) while labeled DNAs (methylene blue-labeled or biotin-labeled) were purified using high-performance liquid chromatography (HPLC) equipped with a XBridge Oligonucleotide BEH C18 column (130 Å, 2.5 μm, 4.6 mm×50 mm, 1/pkg). The sequences of DNAs are listed in Table S2.1.

Table S2.1 Sequences of signaling DNA and capturing DNA

Notes	Sequence (5'-3')
Signaling DNA-16	*MB**-TCCT GCT CAT TCT CGT[#]
Signaling DNA-13	*MB*-TCCT GCT CAT TCT CGT
Signaling DNA-10	*MB*-TCCT GCT CAT TCT CGT
Signaling DNA-07	*MB*-TCCT GCT CAT TCT CGT
Signaling DNA-04	*MB*-TCCT GCT CAT TCT CGT
Signaling DNA-01	*MB*-TCCT GCT CAT TCT CGT
16-nt Capturing DNA	ACG AGA ATG AGC AGGA-*SH*
13-nt Capturing DNA	AGA ATG AGC AGGA-*SH*
10-nt Capturing DNA	ATG AGC AGGA-*SH*

**MB= Methylene blue.* [#]The underlined T in signaling DNA indicates the biotin labeling.

2.6.3 Electrode fabrication and electrochemical measurement

We cleaned the gold working electrodes (rod) (0.2 cm diameter, 0.0314 cm^2 surface area, West Lafayette, IN) based on the literature.[121] The capturing DNA was immobilized on the clean gold electrode by the following procedures. Firstly, 1 μL of 100 μM capturing DNA and 2 μL of 10 mM TCEP was mixed for 1 hour at room temperature to reduce disulfide bond. Secondly, the reduced capturing DNA was diluted to the final concentration of 300 nM (unless otherwise stated) by buffer (50 mM NaH_2PO_4, 150 mM NaCl, pH 7.0), and then the gold electrode was incubated with the diluted capturing DNA solution (300 nM) for 2 hours at room temperature. Thirdly, the

gold electrode was rinsed by deionized water to remove the non-immobilized capturing DNA on the surface, followed by further incubation with 2 mM MCH solution for 2 hours at room temperature to remove physically adsorbed capturing DNA and to passivate the gold electrode. Lastly, the functionalized gold electrodes were rinsed with deionized water for subsequent measurement or stored in buffer at 4 °C until use.

The electrochemical measurements were started immediately after putting capturing DNA functionalized gold electrode into the sample solution containing 100 nM signaling DNA and 100 nM streptavidin, unless otherwise stated. We recorded the electrochemical data by using square wave voltammetry (SWV) between -0.1 to -0.5 V. The peak currents were collected by using the manual fitting mode in the PSTrace 5.4 (2018) software. The kinetic profile of current versus time, signal gain versus time, and binding curves were fitted using Kaleidagraph, version 4.1 (2009). A EmStatMUX potentiostat multiplexer (Palmsens Instruments, Netherland) equipped with a standard three-electrodes cell containing a working electrode (gold rod electrode), a counter electrode (platinum, Sigma-Aldrich), and a reference electrode (Ag/AgCl (1 M KCl), CH Instruments) was employed to perform the electrochemical measurements at room temperature.

The Micrux electrodes (ED-SE1-AuPt, MicruX Technologies, Asturias, Spain) was fabricated by the following procedures. Firstly, the Micrux electrode was cleaned by 0.05 M H_2SO_4 with cyclic voltammetry (-1.5 to +1.5 V with scan rate of 0.1 V/s, and the number of scans is 10). Secondly, the Micrux electrode was functionalized with the capturing DNA using the same procedure as the rod gold working electrode. The electrochemical measurement on Micrux electrode was performed by adding 5 μL blood containing 100 nM signaling DNA and 100 nM streptavidin to Micrux electrode surface. The experimental data was recorded by using square wave voltammetry (SWV) between -0.2 to -0.65 V. The peak currents were collected by using the manual fitting mode in the PSTrace 5.4 (2018) software.

2.6.4 Determination of the surface density of the capturing DNA

To obtain the surface density of capturing DNA on the rode electrode, we determined two parameters, i.e., the electrochemical surface area and the number of capturing DNA on the

electrode surface. The electrochemical surface area can be estimated by cyclic voltammetry (CV) based on the previously published literature.[176] The cleaned rod electrode was inserted into 0.05 M H_2SO_4 for CV measurement, where the scanning potential range was 0 V to 1.5 V (versus Ag/AgCl) and the scan rate was 0.1 V/s. The obtained reduction peak of the CV was integrated to calculate the electrochemical surface density using the following formula:[177]

$$S_e = \frac{C}{v\alpha}$$

where S_e is the electrochemical surface area (cm^2), C is the integration value of reduction peak (μAV), v is the scan rate (V/s), α is a theoretical value (400 $\mu C/cm^2$) for polycrystalline gold based on the assumption that oxygen is chemisorbed on gold in a 1:1 ratio.[177]

The number of capturing DNA strands on the electrode can also be estimated by CV measurement. For this procedure, we assumed that each capturing DNA strand could hybridize to a signaling DNA strand, and each signaling DNA contains one methylene blue molecule, in which electron transfer only occurs between the methylene blue and the electrode surface upon binding of the signaling DNA. Based on this assumption, the number of methylene blue molecules on the electrode surface measured by CV is equal to the number of signaling DNA hybridized on the electrode surface, which is equal to the number of capturing DNA on the electrode surface. Before CV measurement, the 16-nt capturing DNA-modified electrode was inserted into a buffer containing 500 nM signaling DNA-01 for a 3 h incubation to achieve saturation. Then, the CV measurement was carried out between -0.1 V to 0.45 V (versus Ag/AgCl) with a scan rate of 0.1 V/s. The reduction peak of methylene blue was integrated to calculate the number of capturing DNA by the following formula:[148]

$$N = \frac{10^{-6} C' N_A}{nvF}$$

where N is the number of capturing DNA strands, C' is the integration value of reduction peak of methylene blue (μAV), N_A is the Avogadro constant (mol^{-1}), n is the number of electrons transferred per redox molecule (here is methylene blue, i.e., n = 2), v is the scan rate (V/s), F is the Faraday constant (C/mol).

Finally, the surface density of capturing DNA was determined through dividing the number of methylene blue by the electrochemical surface area:

$$\rho = \frac{N}{S_e}$$

where ρ is the surface density of capturing DNA (strands/cm^2), N is the number of capturing DNA strands on the electrode, S_e is the electrochemical surface area (cm^2).

2.6.5 Supporting figures

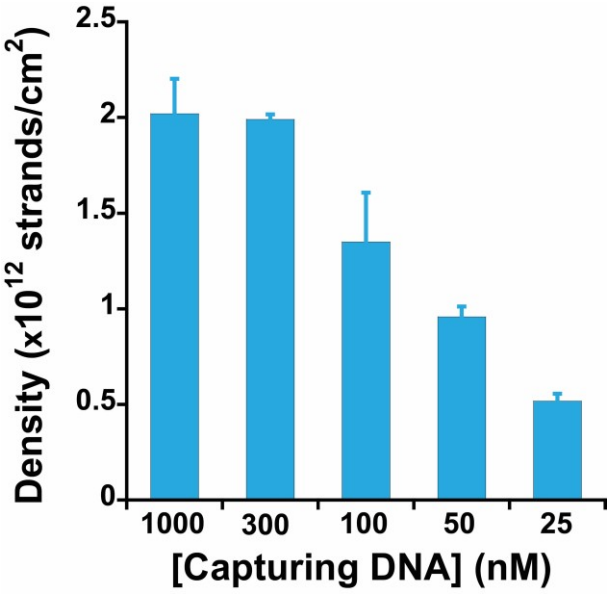

Figure S2.1 Surface densities at different concentrations of capturing DNA. The error bars represent the standard deviation obtained from three electrodes.

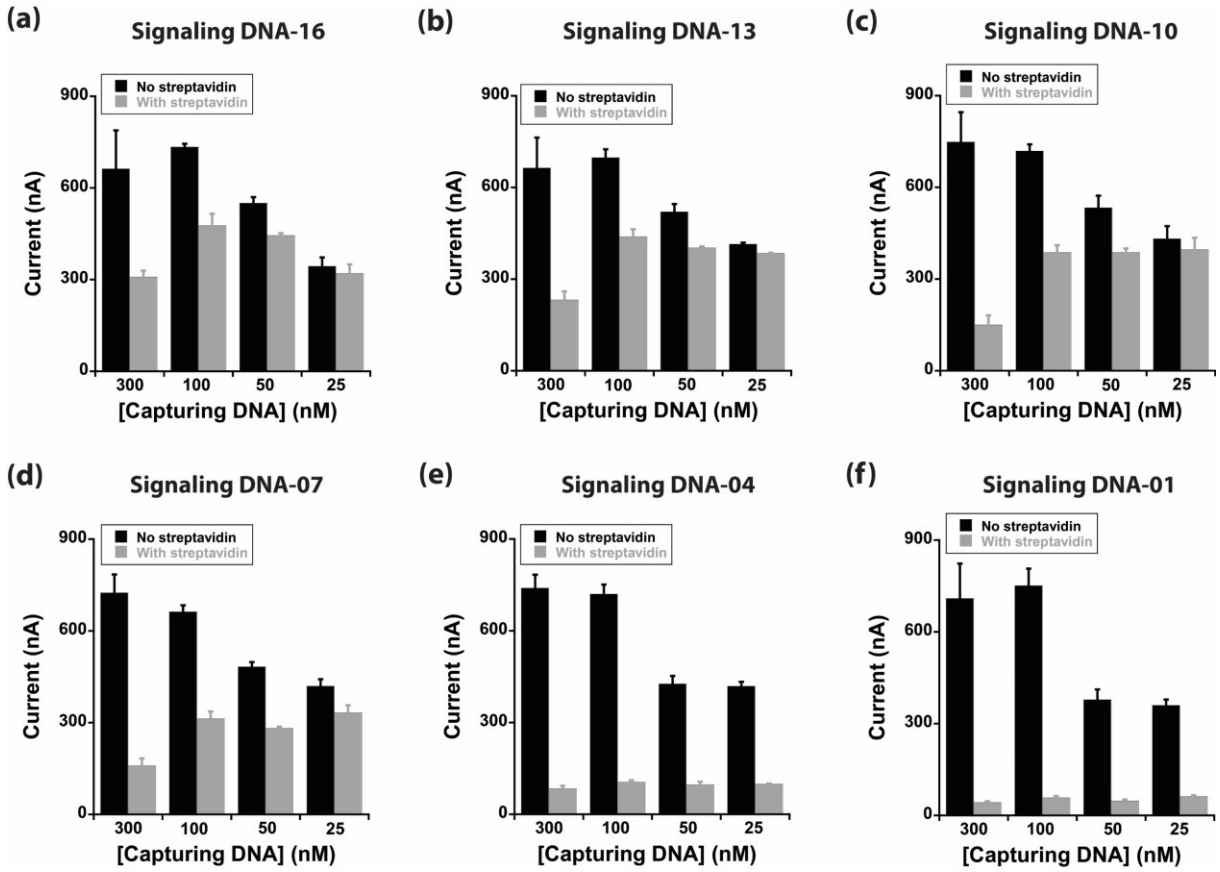

Figure S2.2 The raw current of different surface densities at 30 min. Here we used 300 nM, 100 nM, 50 nM, and 25 nM of capturing DNA concentration to create electrodes with different surface densities. The length of capturing DNA used in this assay was 16 nt. The concentrations of signaling DNAs and streptavidin used in this assay were 100 nM and 100 nM, respectively. The error bars represent the standard deviation obtained from three electrodes.

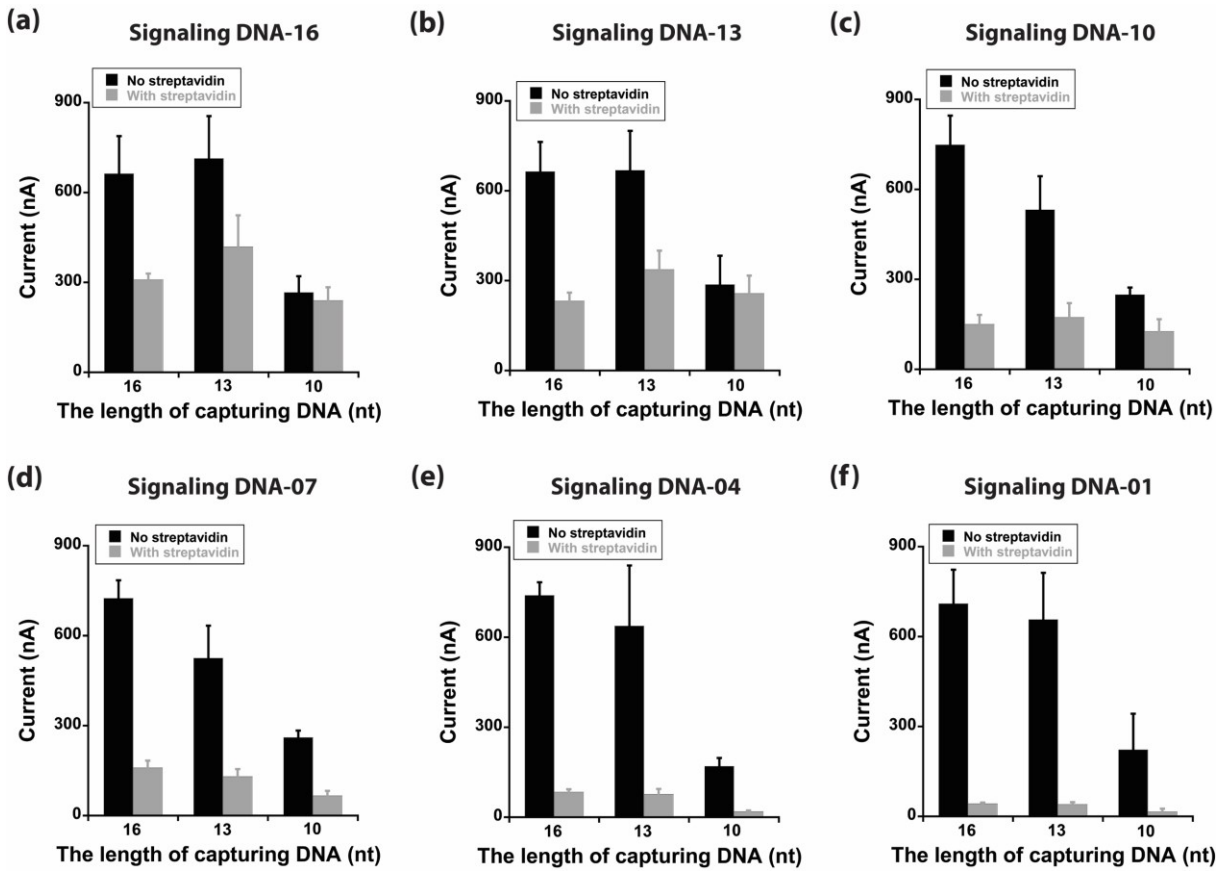

Figure S2.3 The raw current of different capturing DNA length at 30 min. Capturing DNA with the length of 16, 13, and 10 nt were employed to vary the hybridization affinity on the surface. The concentrations of capturing DNAs, signaling DNAs, and streptavidin used in this assay were 300 nM, 100 nM, and 100 nM, respectively. The error bars represent the standard deviation obtained from three electrodes.

Chapter 3: An electrochemical molecular barrier assay for the detection of proteins directly in whole blood

Guichi Zhu[1,2], Alexis Vallée-Bélisle[1,2,3,4]*

[1]Institut de Génie Biomédical, Département de Pharmacologie et Physiologie, Université de Montréal, Montréal, Québec H3T 1J4, Canada.
[2]Laboratoire de Biosenseurs & Nanomachines, [3]Département de Chimie, and [4]Département de Biochimie et Médecine Moléculaire, Université de Montréal, Montréal, Québec H3T 1J4, Canada.

Author contributions: G.Z. and A.V.-B. conceived and designed the study. G.Z. performed all experiments. G.Z. and A.V.-B. created the figures and wrote the manuscript.

This manuscript will be submitted in 2022.

3.1 Abstract

With the increasing demand for rapid, point-of-care, inexpensive blood analysis, it is crucial to develop simple, reliable point-of-care sensors that can allow the detection of various protein biomarkers directly in whole blood. Unfortunately, conventional detection strategies for protein detection, such as ELISA, remain too complex and expensive to redesign as simple, affordable devices that can be used by patients at home. In response, we report here an electrochemical hybridization assay for the detection of protein biomarkers in a drop of blood through the formation of a nanoscale molecular barrier on the surface of the electrode. We surprisingly found that short capturing DNAs can create more efficient molecular barriers and produce a higher signal gain (*e.g.,* -89% for an 8 nucleotides DNA *versus* -40% for a 16 nucleotides DNA). Using this strategy, we demonstrate the rapid detection of streptavidin and anti-DNP antibody in whole blood through a simple and one-step procedure, while outlining its high potential for adaptation into a rapid, inexpensive, easy-to-use point-of-care testing platform.

3.2 Introduction

Nowadays, with the popularization of telemedicine and remote monitoring, combined with the need to better assist patients with chronic diseases, much effort has been invested into the development of inexpensive, easy-to-use sensors for molecular analysis in blood. As such, proteins represent an important class of biomarkers that one would like to detect in the comfort of their home. Indeed, protein detection has already proven to be a powerful approach for the diagnosis and management of numerous diseases, including cancer[178-184], cardiovascular[185, 186] and autoimmune diseases[187-190], as well as neurological disorders such as Alzheimer's[191, 192]. Protein detection, especially of antibodies, is also widely used to test the presence of infectious agents, such as Covid-19,[193, 194] acquired immune deficiency syndrome (AIDS),[195, 196] and Hepatitis B[197, 198], to name a few. In central laboratories, the widely used method for the detection of proteins typically employs enzyme-linked immunosorbent assay (ELISA), but these require expensive instrumentation and well-trained technicians[6, 199]. A "home" version of the ELISA test does exist in the form of a lateral flow assay, but it remains largely a qualitative "yes or no" test that is not readily multiplexable. Other alternatives would be lab-on-chips and microfluidics-based assays, both of which have shown promise for point-of-care applications[200-203], however, the downsides of these are their high cost and complex handling by untrained patients. Therefore, the development of a simple and inexpensive universal approach for the quantitative detection of proteins in a drop of whole blood remains very challenging.

Over the past decades, various electrochemical assays have been developed for the rapid detection of proteins.[77] Among them, electrochemical DNA-based sensors (eDNA sensors) have shown much promise for adaptation into the inexpensive point-of-care format.[9, 76] For example, work by Plaxco et al. on eDNA sensors that employ binding-induced structure-switching mechanisms has demonstrated great applications for continuous blood monitoring. Structure-switching-based eDNA sensors have also been developed for the detection of specific proteins, such as antibodies.[124, 204] Although these display attractive potential, they also typically suffer from significant baseline drift when immersed in whole blood and require complex chemistry for

their synthesis.[147, 151] To circumvent these limitations, we recently developed an electrochemical steric hindrance hybridization assay (eSHHA) for the detection of proteins that does not suffer from signal drift upon addition of blood on its surface.[132, 135, 171] Although this eSHHA strategy was successfully adapted to detect various antibodies, the maximum signal gain (%) of such sensors remains limited to -50% to -60%. In order to further improve the signal gain, we previously developed an improved electrochemical steric hindrance and redox inhibition (eSHRI) hybridization assay (see Chapter 2). eSHRI employs a variety of steric hindrance effects, including analyte-analyte, analyte-DNA layer, and analyte-electrode. Surprisingly, the maximum signal gain reached by eSHRI was -93.6%, which is very close to the theoretical maximum value of -100%. However, eSHHA and eSHRI still require complex and expensive DNA chemistry in order to attach both the recognition element and the redox molecule to the same DNA strand, which undoubtedly increases the complexity and the cost of the assay. In response, we report a novel, robust and selective electrochemical sensing mechanism that enables the sensitive, high gain (-90%) detection of low nanomolar concentrations of specific protein markers directly in whole blood using simple DNA chemistry.

Our novel sensing mechanism employs a simple hybridization assay in which a soluble signaling DNA strand containing methylene blue (MB) as a redox molecule at its 5' end, can hybridize with a capturing DNA strand attached on the surface of a gold electrode. A small recognition element, specific to the target protein (or analyte of interest), is located at the 5' end of the capturing DNA. In the presence of the target protein, binding to the recognition element allows the target protein to create a nanoscale molecular barrier between the electrode surface and the signaling DNA, therefore preventing the signaling DNA from reaching the electrode surface, yielding low current (Figure 3.1). On the other hand, in the absence of target protein, the molecular barrier cannot be formed, and the redox-labeled signaling DNA is free to reach the surface of the electrode and hybridize efficiently with the capturing DNA, bringing the methylene blue into proximity with the electrode surface to produce a strong electrochemical signal.

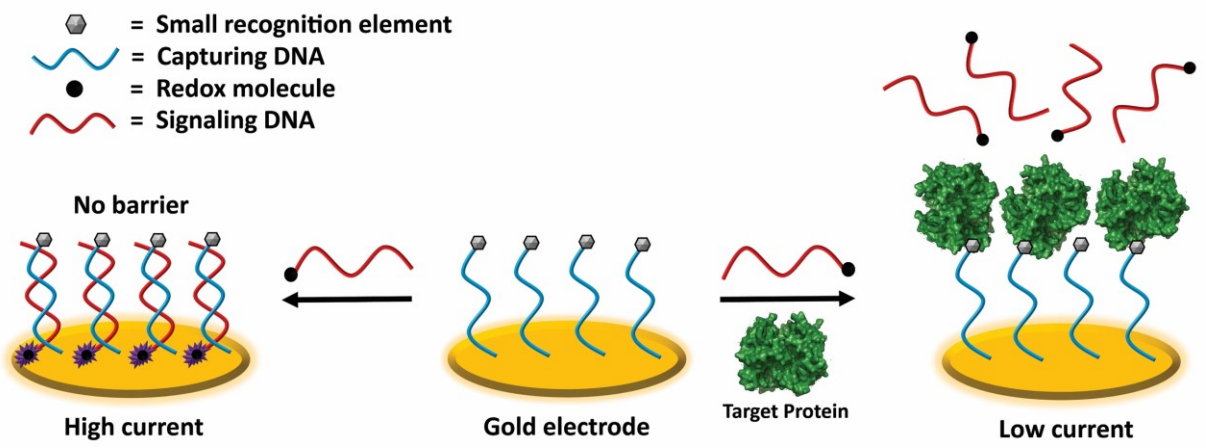

Figure 3.1 Principle of the electrochemical molecular barrier hybridization assay for the detection of protein. In this assay, a large target protein binds a recognition element attached at one end of an electrode-bound capturing DNA (blue). In the absence of target protein, a signaling DNA containing a redox molecule can efficiently hybridize to its complementary capturing DNA attached to the electrode, leading to a strong electrochemical signal. In the presence of target protein, however, a protein barrier is expected to form on the surface of the sensor, reducing the ability of the signaling DNA to reach its complementary capturing DNA, resulting in a low electrochemical signal.

3.3 Results and discussions

As a proof of concept to validate our strategy, we turned to the streptavidin-biotin model. Streptavidin, a non-glycosylated protein purified from *Streptomyces avidinii*,[205] has been widely used in biochemistry and molecular biology due to its high affinity (Kd=56 fM)[206] and specificity with biotin. Streptavidin possesses four binding sites for biotin and has a molecular weight of 52.8 kDa (5.0 x 4.5 × 4.5 nm),[207] which is about ten times larger than the typical 16 nucleotides (nt) signaling DNA (MW: ~5 kDa) used in our set up. As expected from most small molecule-protein interactions, the association rate constant of streptavidin-biotin (10^7-10^8 M^{-1} s^{-1})[206, 208] is four orders of magnitude faster than that of hybridization between two complementary DNA strands located on the electrode surface (10^3-10^4 M^{-1} s^{-1}).[209, 210] In theory, this significant difference in association rate constants should be sufficient to ensure that streptavidin creates a molecular barrier with biotin before the signaling DNA has time to reach the electrode surface to bind to its complementary strand. Of note, the sensor architecture of our proposed molecular

barrier assay can be achieved through simple chemistry with the help of a wide variety of commercially available reagents. For instance, the 5' end methylene blue-labeled signaling DNA can be directly synthesized on an automated DNA synthesizer using Glen Research's Methylene Blue II phosphoramidite reagent.[211] As for the thiolated capturing DNA, synthesis can be achieved using a 3' modified thiol column (Biosearch Technologies) to which the recognition element is then attached on its 5' end via standard chemistry. In contrast, other hybridization assays, like eSHHA,[132, 134, 171] require complex dual-labeling strategies to attach both the recognition element and the redox molecule on the same signaling DNA strand.

For the preliminary validation of our molecular-barrier mechanism, we first tested our sensor by employing 16-nt strands for capturing and signaling DNA (Figure 3.2a). When monitoring the hybridization of the signaling DNA in the absence of streptavidin using buffer only, the electrochemical current increased rapidly in a Langmuir-like kinetic,[212] reaching 1145 nA after 30 min (Figure 3.2a, black curve). In the presence of 100 nM streptavidin, however, the observed current was reduced by -40 % (Figure 3.2a, green curve and right panel), likely due to the molecular barrier created by the attachment of streptavidin to the biotin located on the surface of the electrode. In contrast, when employing a capturing DNA devoid of any biotin label, no change in hybridization efficiency is observed in the presence of streptavidin (see Figure S3.1), confirming that the molecular barrier is formed through the specific interaction between streptavidin and biotin and not due to non-specific adsorption of streptavidin on the sensor surface.

It is well established that varying the length of a DNA-based monolayer can drastically affect its flexibility and conformation.[213] We have therefore hypothesized that this parameter may well affect the structure of the molecular barrier. The worm-like chain (WLC) model,[214, 215] for example, predicts that DNA increases its flexibility with its number of nucleotides. This effect is likely to affect the physical feature of the streptavidin layer formed over the electrode. To explore the impact of modifying the DNA monolayer on the performance of the molecular barrier assay, we synthesized capturing DNA strands with different lengths, namely from 16- to 8-nt capturing DNA, and immobilized them on the electrode surface (Figure 3.2). Following testing of

the different DNA monolayers using our standard 16-nt signaling DNA, we found that reducing the length of the capturing DNA significantly increased the performance of the assay. For example, the signal gain increased from -40% (16-nt capturing DNA) to -89% (8-nt capturing DNA) (Figure 3.2a-c). However, reducing the length of the capturing DNA below a certain threshold also yielded some expected drawbacks, such as reducing hybridization efficiency due to lower duplex stability. For example, after 30 min in the absence of streptavidin, the 8-nt capturing DNA, only yielded 192 nA of raw current *versus* 1145 nA for 16-nt capturing DNA. One could argue that the enhanced signal gain (%) observed with sensors built using shorter capturing DNA could also be due to increased surface density obtained when functionalizing the electrode with shorter DNA. This hypothesis, however, is not supported by the fact that DNA length variation from 16 to 8 nt does not significantly affect surface density.[213] Overall, we found that a 10-nt capturing DNA length represents an ideal trade-off between high raw current and signal gain (663 nA and -90% after 30 min, respectively, Figure S3.2). These results also suggest that the streptavidin molecular barrier is more compact when employing shorter capturing DNA. We believe that this is due to the fact that shorter capturing DNA will expose more biotin molecules on the top of the DNA layer, therefore forming a more compact streptavidin molecular barrier that prevent signaling DNA from reaching its complementary capturing DNA.

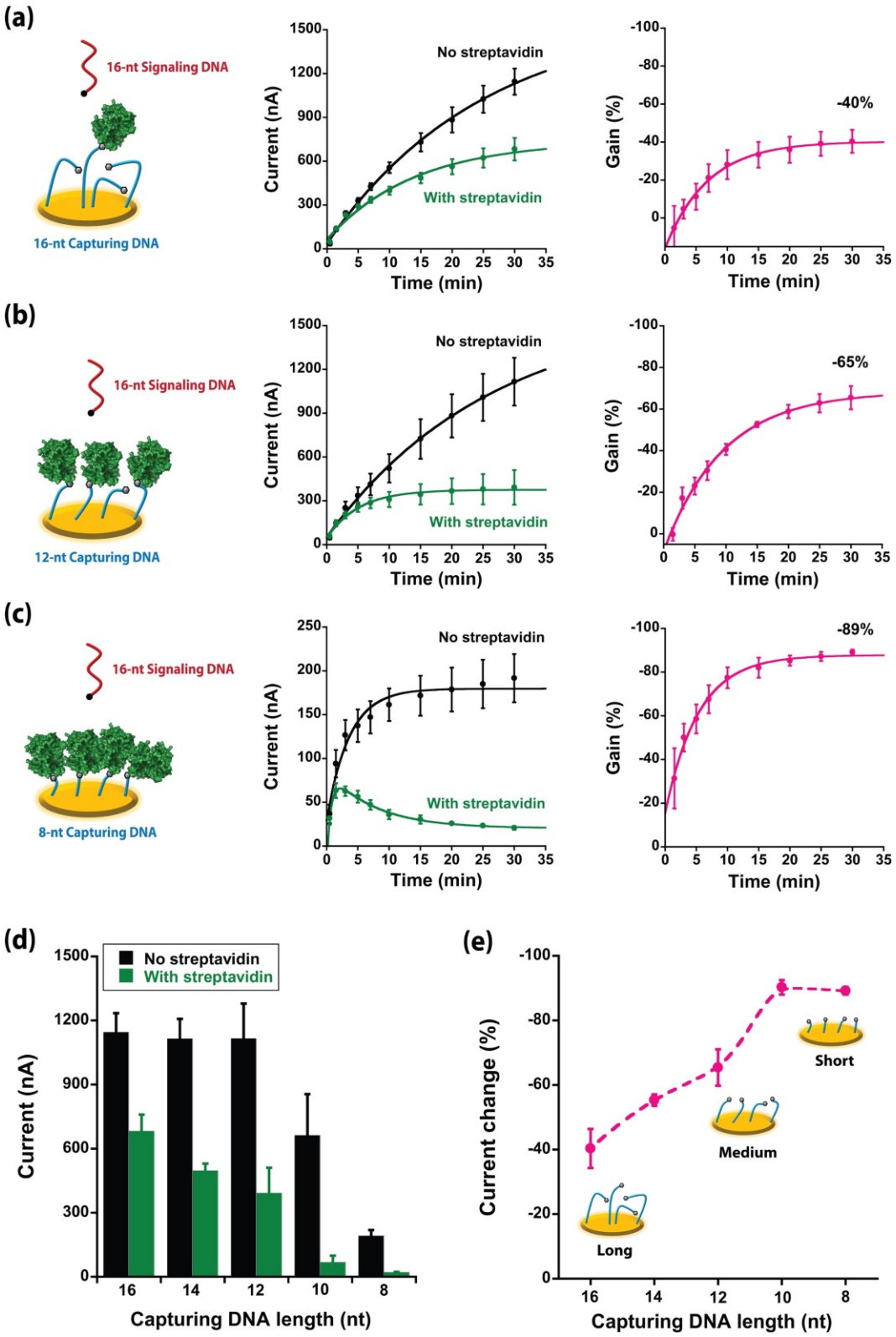

Figure 3.2 Reducing the length of capturing DNA improves both the kinetic and signal gain of the molecular barrier assay. (a) Using a 16-nucleotide (nt) capturing DNA; (b) Using a 12-nt capturing DNA; (c) Using an

8-nt capturing DNA. All results were carried out with a 16-nt signaling DNA. Hybridization was monitored using square wave voltammetry (SWV) in the absence (C_0) and presence of 100 nM streptavidin (C_{strep}) (center panel). The signal gain (right panel) was determined using the formula $(C_{strep}-C_0)/C_0$. Assessing the impact of decreasing the length of the capturing DNA on the hybridization efficiency in terms of (d) raw current and (e) signal gain for the 30 min time point, while keeping the 16-nt length of the signaling DNA constant. The concentrations of capturing DNAs and signaling DNA used in this assay were 300 nM and 100 nM, respectively. The error bars represent the standard deviation obtained from three electrodes.

Interestingly, small capturing DNA, such as 8-nt capturing DNA, also displayed rather complex hybridization kinetics in the presence of the streptavidin barrier, as illustrated by the gradual current decrease observed after 1.5 min of assay time in the presence of streptavidin (Figure 3.2c, green curve, center panel). This pattern suggests that a previously bound 16-nt signaling DNA can dissociate or be "kicked out" from the 8-nt capturing DNA following streptavidin binding. A potential explanation for this "kicking out" mechanism may be that in order to bind to the biotin on the short capturing DNA, streptavidin needs to physically penetrate within the structural layer formed by the 8 unbound nucleotides overhanging above the capturing DNA monolayer. These results could also suggest that the steric hindrance created through this event destabilizes the weak double helix formed between the long signaling DNA and the shorter capturing DNA. To verify the latter hypothesis, we investigated the dissociation kinetics of the DNA double helix occurring between the capturing and signaling DNA by spiking streptavidin after 30 min of hybridization time. As expected, less stable capturing-signaling DNA complexes, resulting from shorter 8-nt and 10-nt capturing DNA, led to proportionally more and faster dissociation of the signaling DNA upon adding streptavidin (Figure 3.3). This confirms that a less stable double helix formed by short capturing DNA is destabilized more easily by streptavidin, or in other words, our target protein trying to reach its recognition element, than their longer, more stable counterparts, likely through a steric hindrance effect.

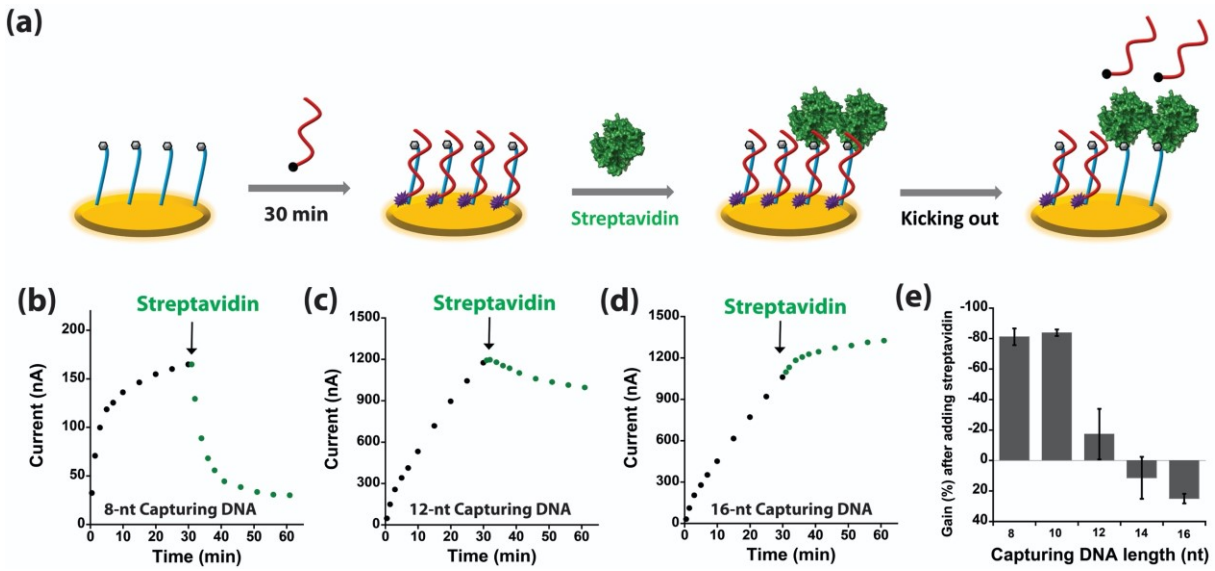

Figure 3.3 Streptavidin triggers dissociation of the signaling DNA when employing short, less stable, biotin labeling capturing DNA. (a) Signaling DNA is left to hybridize with the capturing DNA for 30 min to form the duplex conformation, prior to adding streptavidin to initiate the kick out of the signaling DNA from the duplex. (b-d) Hybridization kinetic between 16-nt signaling DNA and 8-nt, 12-nt, and 16-nt capturing DNA (black points), and kicking out kinetic upon addition of streptavidin (green points). (e) Signal gain after adding streptavidin for 8-nt, 10-nt, 12-nt, 14-nt and 16-nt capturing DNA. All results were carried out with a 16-nt signaling DNA. The concentrations of capturing DNAs, signaling DNA, and streptavidin used in this assay were 300 nM, 100 nM, and 100 nM, respectively. The error bars represent the standard deviation obtained from three electrodes.

So far, all results were obtained using varying lengths of capturing DNA, all bearing the biotin at the 5' end of the strand. To further investigate the molecular basis behind the reduced efficiency of longer capturing DNA on the performance of the assay, we explored the effect of shifting the position of the biotin within the capturing DNA (towards its 3' end). To do so, we synthesized five variants of 16-nt capturing DNA, ranging from original 16-nt capturing DNA bearing its biotin the farthest from the electrode surface to variant 16-nt-i3 capturing DNA ("i3" indicates the internal biotin labeling and the distance between biotin and electrode) bearing the biotin closest to the electrode (Figure 3.4a-e). Our results clearly demonstrate that an optimal molecular barrier is created with the biotin positioned in the middle of the strand. For example, the signal gain obtained with the original 16-nt capturing DNA was -40% compared to -66% when

biotin is located at the 16-nt-i7 position (Figure 3.4g). Moving the biotin closer to the electrode surface (e.g., 16-nt-i3), however, results in more signaling DNA being able to hybridize to the surface (gain: -41%, Figure 3.4g), most likely because the biotin becomes less accessible to streptavidin, therefore creating a more permeable surface barrier. Of note, while the location of the biotin on the capturing DNA influences the tightness of the molecular barrier and the resulting signal gain, it does not affect the rate of hybridization (Figure S3.3). We believe that this optimal "middle" location for the biotin represents a fair trade-off between the ability to create an efficient, compact molecular barrier (closer to the surface) while enabling sufficient accessibility of the biotin to the streptavidin (closer to the sample).

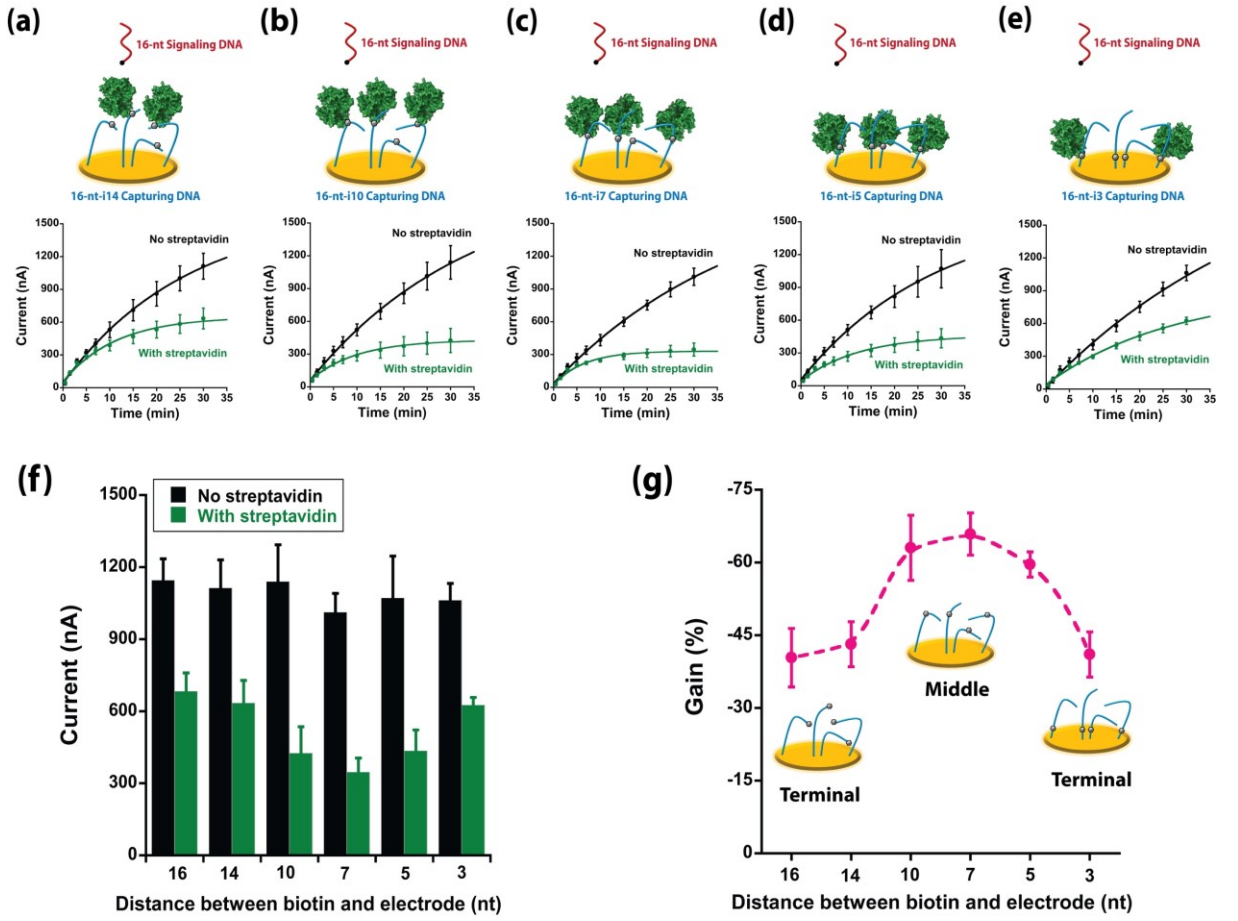

Figure 3.4 Optimal surface barrier is obtained when attaching the biotin in the middle of the 16-nt capturing DNA. Assessing sensor performance using a 16-nt capturing DNA with the biotin located internally at different positions: (a) 16-nt-i14, (b) 16-nt-i10, (c) 16-nt-i7, (d) 16-nt-i5, and (e) 16-nt-i3. For example, "i10" indicates the internal biotin labeling and the distance between biotin and electrode. (f)

Raw current obtained after 30 min hybridization time for original and five variants 16-nt capturing DNA in the presence and absence of 100 nM streptavidin. (g) The relationship between signal gain and biotin labeling position in the capturing DNA. All results were carried out with a 16-nt signaling DNA. The concentrations of capturing DNAs and signaling DNA used in this assay were 300 nM and 100 nM, respectively. The error bars represent the standard deviation obtained from three electrodes.

As we have already discussed, more efficient molecular barriers are created by employing shorter capturing DNA, but could sensor performance also be improved if longer, less permeable signaling DNA were used? To answer this question, we tested the molecular barrier assay using signaling DNA whose length varied from 16- to 8-nt while the length of capturing DNA remains constant with 8-nt (Figure 3.5). Three statements were verified and confirmed. First, employing shorter signaling DNA was expected to increase the affinity between the 8-nt capturing DNA and the "long" overhang signaling DNA. This was confirmed experimentally with 8-nt signaling DNA producing a current that is 4-folds higher than with the 16-nt signaling DNA (755 nA versus 192 nA, respectively) after 30 min in the absence of streptavidin (Figure 3.5d). The second hypothesis would be that longer signaling DNA increases the signal gain by making it harder for the signaling DNA to cross the molecular barrier. Indeed, we found that the signal gain of the assay varied from -79% to -89% when increasing the signaling DNA length from 8-nt to 16-nt (Figure 3.5e). Finally, we had also expected that longer signaling DNA should be more likely to be kicked out following the formation of the molecular barrier due to steric hindrance and charge repulsion between the overhanging tail and the streptavidin. This presumed predisposition of longer DNA to be kicked out was also validated experimentally using 8-nt signaling DNA and 16-nt signaling DNA, displaying respectively 36% and 67% of dissociation from the 8-nt capturing DNA (Figure 3.5a and c). Overall, the optimal length of signaling DNA represents a trade-off between higher hybridization current obtained with shorter signaling DNA (and a short capturing DNA) and higher signal gain obtained with longer signaling DNA.

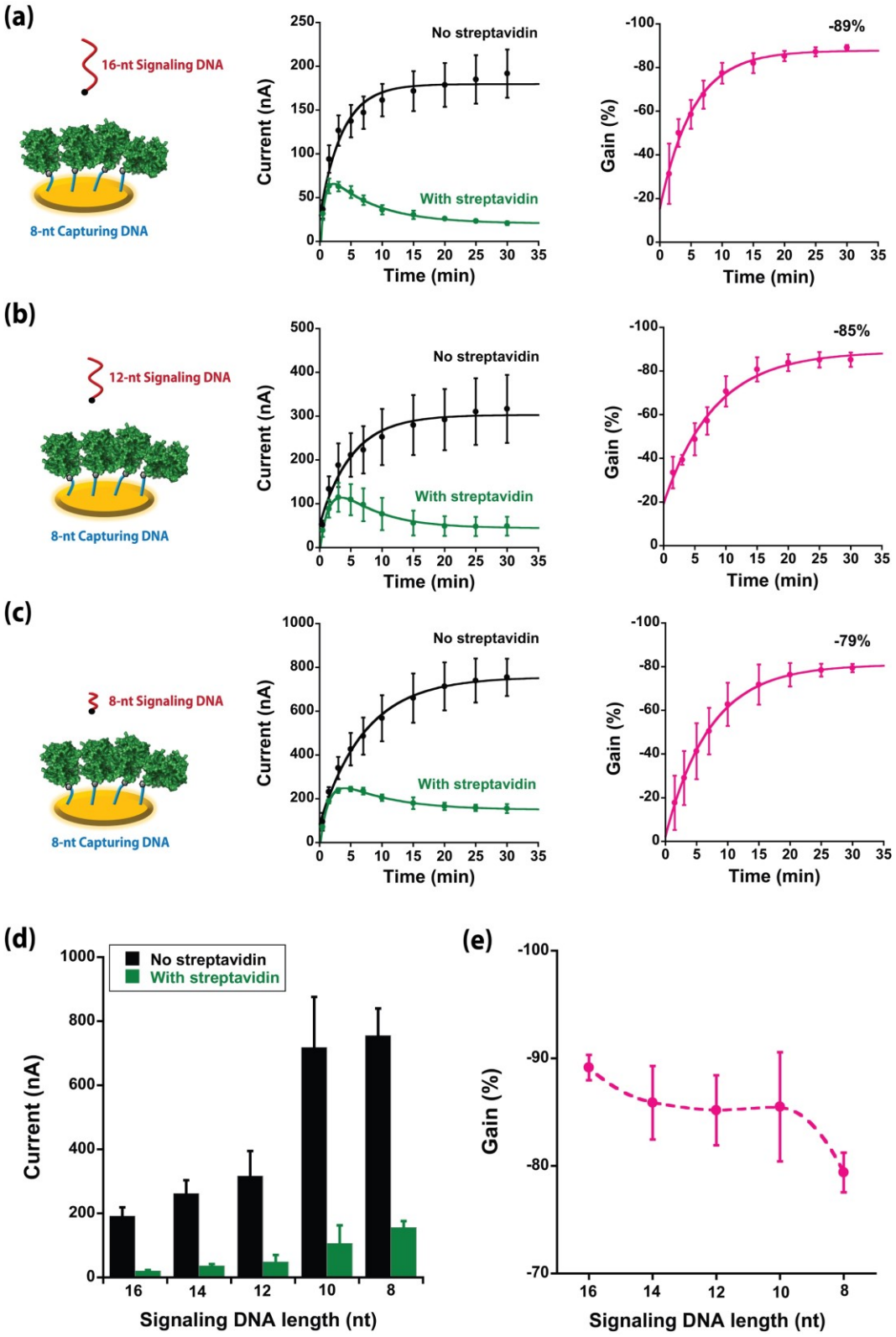

Figure 3.5 Reducing the length of signaling DNA enhances hybridization current but decreases the signal gain (%) of the molecular barrier assay. Assessing assay performance by employing signaling DNA of

varying lengths (a, b, c: 16, 12, 8-nt, respectively) using the shorter 8-nt capturing DNA. (d-e) Effect on raw current and signal gain for different signaling DNA lengths at the 30 min time point. The concentrations of capturing DNA, signaling DNAs, and streptavidin used in this assay were 300 nM, 100 nM, and 100 nM, respectively. The error bars represent the standard deviation obtained from three electrodes.

We then performed titration curves to explore the dynamic range and detection limit of the molecular barrier assay. To trigger signaling, the molecular barrier assay requires the formation of a large molecular barrier that covers the entire surface of the electrode and the capturing DNA. Based on an estimated surface coverage of ~20 nm^2 for one molecule of streptavidin, we evaluate, for example, that our 3 mm^2 electrode requires at least $1.5x10^{11}$ streptavidin molecules to fully cover its surface, which corresponds to a concentration of 0.25 nM for a 1 mL sample. Surprisingly, we found instead that 21 nM of streptavidin (in a 1 mL sample) was required to reach 50% of the molecular barrier capacity (Figure 3.6). This $C_{50\%}$ value is six orders of magnitude larger than the expected K_D for the biotin-streptavidin pair (Kd=56 fM),[206] but it is also 100-folds higher than the theoretically determined 0.25 nM of streptavidin required to saturate the electrode. Two explanations may help explain this larger $C_{50\%}$ value: 1) *Kinetics*: lower protein concentrations are expected to lead to slower barrier formation, therefore allowing more signaling DNA to reach the surface; 2) *Reduced affinity between streptavidin-biotin*: optimal formation of the molecular barrier (optimized packing) may involve steric hindrance constraints, which reduce the strength of the analyte-recognition element system. Also, the sensor response fitted well with a ligand-depletion regime model[216, 217] that is not dependent on the true affinity of the biotin-streptavidin system but rather on the effective number of biotins on the sensor surface. As expected from ligand-depletion systems, the dynamic range of the sensor is slightly narrower (here between 3 nM and 100 nM of streptavidin) than the 81-fold change in analyte concentration typically observed for typical biosensors.[218]

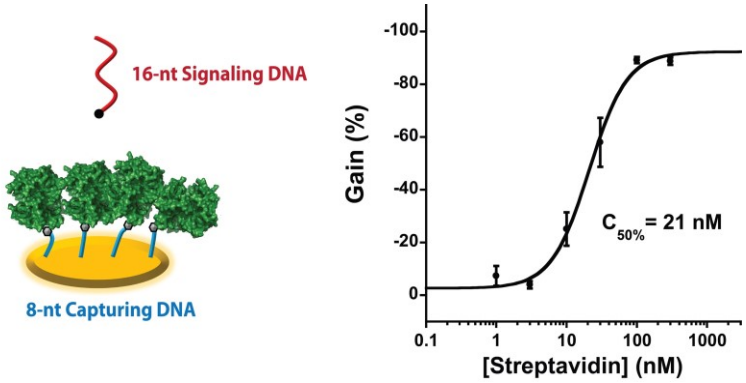

Figure 3.6 The dynamic range of the molecular barrier assay built with 8-nt capturing DNA fits well with a ligand-depletion regime model.[216, 217] The length of signaling DNA used in this assay was 16-nt. The concentrations of capturing DNA and signaling DNA used in this assay were 300 nM and 100 nM, respectively. The error bars represent the standard deviation obtained from three electrodes.

To explore the universality of the molecular barrier assay, we adapted this assay to detect antibodies, an important class of disease markers. To do so, we employed the well-characterized 2,4-dinitrophenol (DNP) as our model antigen to specifically detect its corresponding antibody.[217, 219] For this assay, we employed the 16-nt signaling DNA together with the 10-nt capturing DNA. As shown in Figure 3.7, the molecular barrier assay yielded a -49% signal gain when employing an antibody barrier and was able to detect a 1/400 dilution of anti-DNP antibody. In contrast to the streptavidin assay, however, no "kicking out" behavior was observed. This may be explained by the fact that the binding affinity between the antibody and DNP antigen (K_D= 0.8-200 nM[220, 221]) is typically six orders of magnitude weaker than the streptavidin-biotin complex (K_D=56 fM[206]), therefore preventing the antibody-antigen interaction from outcompeting the 16-nt signaling DNA and 10-nt capturing DNA interaction. Moreover, we tested a sensor whose capturing DNA did not bear DNP to confirm the assay specificity. Results show that no signal gain is observed in the presence of anti-DNP antibody, confirming that the formation of a molecular barrier requires the specific interaction between the anti-DNP-antibody and the surface-bound DNP antigen (Figure S3.4).

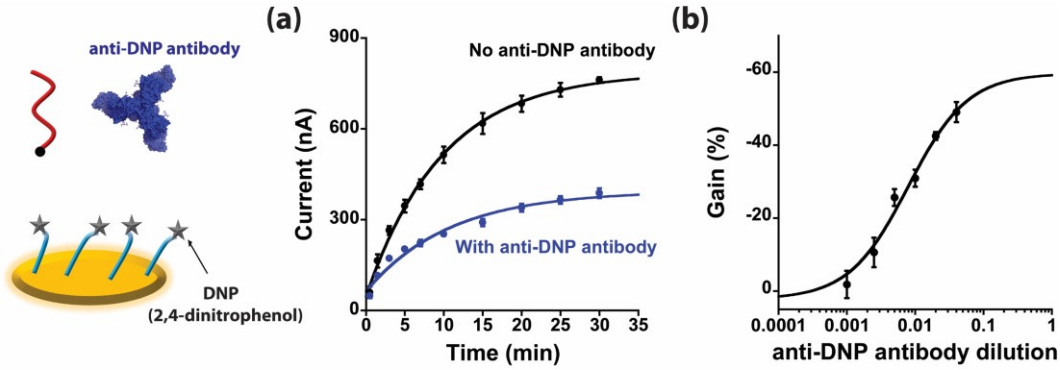

Figure 3.7 The molecular barrier assay can also be adapted to detect other proteins, such as antibodies. Here we show the detection of anti-DNP antibodies using 2,4-dinitrophenol (DNP) as a recognition element. (a) Kinetics of DNA hybridization in the presence (blue) or absence (black) of anti-DNP antibody. Since the concentration of anti-DNP antibody in sample (serum polyclonal antibody) is unknown, 40 µL anti-DNP antibody was added into 960 µL buffer (i.e., 1:25 dilution) in this assay. (b) The binding curve for the anti-DNP antibody assay at 30 min. Different dilutions (e.g., 1:1000, 1:400, 1:200, 1:100, 1:50, and 1:25) of anti-DNP antibody were assayed. The length of capturing DNA and signaling DNA used in this assay was 10-nt and 16-nt, respectively. The concentrations of capturing DNA and signaling DNA used in this assay were 300 nM and 100 nM, respectively. The error bars represent the standard deviation obtained from three electrodes.

To demonstrate the potential of our molecular barrier assay for point-of-care application, we adapted our assay into an inexpensive disposable electrode that could enable clinical diagnosis directly in a single drop of blood. We selected the Micrux electrode that only requires 5 µL of sample volume thanks to its small 0.785 mm^2 gold working electrode (WE) and its platinum reference (RE) and counter (CE) electrodes (Figure 3.8a). We first tested the streptavidin and anti-DNP-antibody assay on Micrux electrodes in buffer and obtained similar kinetics and signal gain (%) compared to the much larger rod electrodes (Figure S3.5). For instance, the streptavidin sensor (using 100 nM streptavidin) displayed a signal gain of -90% (rod) and -86% (Micrux), while the antibody sensor (using a 1/25 dilution) displayed a signal of -49% (rod) and -61% (Micrux). We then tested the ability of the molecular barrier assay to perform directly in whole blood (Figure 3.8b). We found that the streptavidin sensor at 100 nM streptavidin displayed a signal gain of -70% at 30 min, while the antibody sensor displayed a signal gain of -51% at 30 min (Figure 3.8b). Of note, each assay performed on the Micrux electrode was also

found to be specific to its relevant analyte, with the streptavidin assay being unresponsive to the presence of the antibody and vice versa (data not shown). The high specificity of this platform combines with its ability to work directly in whole blood without signal drift or non-specific response from other blood proteins, suggest that our molecular barrier assay holds great potential for further applications in clinical diagnosis.

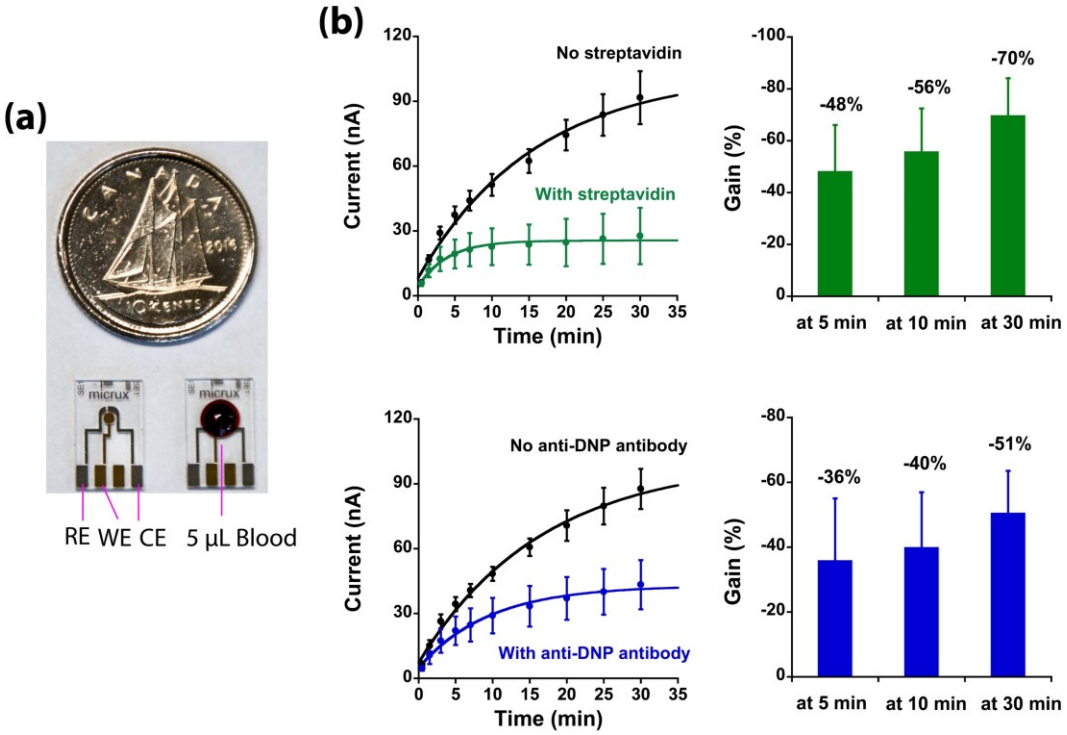

Figure 3.8 Adaptation of the molecular barrier assay into a rapid point-of-care format. (a) Sample volumes as small as a drop of blood of 5 µL can be assayed on the small Micrux electrode (size compared to a 10 cents Canadian coin of 1.8 cm diameter). RE=reference electrode, WE=working electrode, and CE=counter electrode. (b) Hybridization kinetics with and without analyte directly in whole blood (top panel: streptavidin; bottom panel: anti-DNP antibody). To prevent the blood from drying out during long-time measurement (30 min), a blood sample volume of 20 µL was used in this assay. 10-nt capturing DNA and 16-nt signaling DNA were used in this assay. The concentration of capturing DNAs, signaling DNA, and streptavidin used in this assay was 300 nM, 100 nM, and 100 nM, respectively. The dilution of anti-DNP antibody used in this assay was 1:25. The error bars represent the standard deviation obtained from three electrodes.

3.4 Conclusions

Here we report a novel electrochemical signaling mechanism for the one-step detection of proteins directly in whole blood based on creating a nanoscale molecular barrier. We show that this molecular barrier mechanism can be optimized by employing short capturing DNA (8- to 10-nt) that has less flexibility and creates a more compact molecular barrier. We also identified that optimal performance is achieved with longer signaling DNA (16-nt) due to the overhanging tail with negative charge repulsion that minimizes barrier crossing through the analyte-barrier. This longer signaling DNA can also be kicked out efficiently from the electrode surface by dissociating from the capturing DNA upon binding the large target protein to its recognition element, providing further thermodynamics information about the strength of the target protein-recognition element interaction. We have also demonstrated that this molecular barrier strategy can also be adapted to detect and quantify important classes of protein markers, such as antibodies. This suggests that our new assay could be adapted, in principle, for the detection of any protein for which a small recognition element can be attached to the capturing DNA. More importantly, this novel molecular barrier mechanism, combined with the hybridization signaling mechanism, is selective and specific enough to work directly in whole blood without signal drift produced by the non-specific adsorption of proteins on the sensor surface.

A primary advantage of this molecular barrier assay over other hybridization-based assays such as eSHHA [132] is that it does not require the more complex dual modification of the signaling DNA with both the recognition element and redox molecule. More importantly, the signal gain of molecular barrier assay has been dramatically improved compared to eSHHA, specifically from -50% of eSHHA to -90% of the molecular barrier assay. The molecular barrier assay also deploys well directly in whole blood without any signaling drift that typically plagues other eDNA sensors. This ability to work directly in the blood through a simple, one-step procedure without the requirement of time-consuming separation, washing, or additional purification steps distinguishes this method from other classic protein detection methods, such as ELISA, which requires well-trained technicians and expensive centralized laboratories. Furthermore, the molecular barrier assay can be adapted on commercially available, inexpensive, disposable

electrodes (e.g., Micrux) using inexpensive portable potentiostats. We believe that this novel signaling mechanism could be readily adapted for the detection of important disease markers (e.g., HIV and Covid-19 antibodies) detection by simply changing the recognition element located on the capturing DNA. These sensors could be deployed in physician offices or in the patient home to enable efficient and rapid monitoring of their health conditions and treatment.

3.5 Acknowledgments

A.V.-B. is Canada Research Chair in Bioengineering and Bionanotechnology, Tier II, G.Z. acknowledges a TransMedTech Excellence Scholarship as well as a PROTEO fellowship. The authors also thank Liliana Pedro for valuable comments on the manuscript and the Laboratory of Biosensors & Nanomachines (LBN) members.

3.6 Supporting information

3.6.1 Materials

Tris (2-carboxyethyl) phosphine hydrochloride (TCEP) and 6-mercaptohexanol (MCH) were purchased from Sigma Aldrich. Streptavidin was obtained from New England BioLabs. Anti-DNP antibody produced in rabbits was purchased from Sigma Aldrich. Whole blood (newborn calf) was purchased from Innovative Research. Methylene Blue II phosphoramidite (Catalog # is 10-5961-95) and DNP phosphoramidite (Catalog # is 10-1985-95) were purchased from Glen Research. 3’-Thiol modified column (Catalog # is CG1-5003-1) and 5'-Biotin amidite (Catalog # is BNS-5021-50) were purchased from Biosearch Technologies. The standard adenine, guanine, cytosine, and thymine columns and reagents for DNA synthesis were purchased from Biosearch Technologies and ChemGenes Corporation, respectively. The buffer used for the streptavidin and anti-DNP antibody assay is 50 mM NaH_2PO_4, 150 mM NaCl, pH 7.0.

3.6.2 DNA sequences

DNA oligonucleotides were synthesized in-house on a DNA/RNA synthesizer (K&A Laborgeraete, Germany) using standard phosphoramidite chemistry. Unlabeled DNA was purified

by reverse-phase cartridge (RPC) while labeled DNA (using methylene blue or a fluorophore) was purified using high-performance liquid chromatography (HPLC) equipped with a XBridge Oligonucleotide BEH C18 column (130 Å, 2.5 µm, 4.6 mm×50 mm). DNA sequences are listed in Table S3.1.

Table S3.1. Sequences of capturing DNA and signaling DNA

Notes	Sequence (5'-3')
16-nt Capturing DNA	*Biotin*-AGT CCG TGG TCT CTG G-*SH*
14-nt Capturing DNA	*Biotin*-TCC GTG GTC TCT GG-*SH*
12-nt Capturing DNA	*Biotin*-CGT GGT CTC TGG-*SH*
10-nt Capturing DNA	*Biotin*-TGG TCT CTG G-*SH*
8-nt Capturing DNA	*Biotin*-GTC TCT GG-*SH*
16-nt-i14 Capturing DNA	AG<u>T</u> CCG TGG TCT CTG G-*SH*
16-nt-i10 Capturing DNA	AGT CCG <u>T</u>GG TCT CTG G-*SH*
16-nt-i7 Capturing DNA	AGT CCG TGG <u>T</u>CT CTG G-*SH*
16-nt-i5 Capturing DNA	AGT CCG TGG TC<u>T</u> CTG G-*SH*
16-nt-i3 Capturing DNA	AGT CCG TGG TCT C<u>T</u>G G-*SH*
16-nt Signaling DNA	*MB**-CCA GAG ACC ACG GACT
14-nt Signaling DNA	*MB*-CCA GAG ACC ACG GA
12-nt Signaling DNA	*MB*-CCA GAG ACC ACG
10-nt Signaling DNA	*MB*-CCA GAG ACC A
8-nt Signaling DNA	*MB*-CCA GAG AC
10-nt Capturing DNA-DNP	DNP-TGG TCT CTG G-*SH*

**MB= Methylene blue,* the underlined T in 16-nt-i14 to 16-nt-i3 capturing DNA indicates the position of the biotin label.

3.6.3 Electrode fabrication and electrochemical measurement

Experiments were carried out on rod gold working electrodes (0.2 cm diameter, 0.0314 cm^2 surface area, West Lafayette, IN) that had been previously cleaned following standard

procedures.[121] The capturing DNA was then immobilized on a clean gold electrode using the following steps (all performed at room temperature). First, 1 μL of 100 μM capturing DNA and 2 μL of 10 mM TCEP were mixed for 1 hour to reduce disulfide bonds. Covalent attachment of the capturing DNA to the gold surface was then carried out by diluting the previously reduced capturing DNA to a final concentration of 300 nM (unless otherwise stated) using assay buffer (50 mM NaH_2PO_4, 150 mM NaCl, pH 7.0), and adding it to the gold electrode for 2 hours. After thoroughly rinsing with deionized water to remove any unbound capturing DNA off its surface, the gold electrode was then further incubated with 2 mM MCH solution for 2 hours to remove any physically adsorbed DNA and passivate the electrode surface. Lastly, the functionalized gold electrode was rinsed with deionized water for subsequent measurements or stored in the buffer at 4 °C until use.

The electrochemical measurements were started immediately upon complete immersion of the functionalized gold electrode surface with the sample solution containing 100 nM of signaling DNA and 100 nM streptavidin (or 1:25 dilution anti-DNP antibody), unless otherwise stated. We recorded the electrochemical data using square wave voltammetry (SWV) between -0.1 and -0.5 V. Peak currents were collected using the manual fitting mode in the PSTrace 5.4 (2018) software. The kinetic profile of current versus time, signal gain versus time, and binding curves were fitted using Kaleidagraph, version 4.1 (2009). A EmStatMUX potentiostat multiplexer (Palmsens Instruments, Netherland) equipped with a standard three-electrodes cell containing a working electrode (gold rod electrode), a counter electrode (platinum, Sigma-Aldrich), and a reference electrode (Ag/AgCl (1 M KCl), CH Instruments) was employed to perform the electrochemical measurements at room temperature.

The Micrux electrode sensor (ED-SE1-AuPt, MicruX Technologies, Spain) was fabricated according to the following procedures. First, the Micrux electrode was cleaned by 0.05 M H_2SO_4 using cyclic voltammetry (10 cycles between -1.5 to +1.5 V with a scan rate of 0.1 V/s). The Micrux electrode was then functionalized with the capturing DNA using the same procedure described previously for the rod gold working electrode. Electrochemical measurements were started upon adding 20 μL of blood containing 100 nM signaling DNA and target protein to Micrux electrode

surface. Experimental data was recorded using square wave voltammetry (SWV) between -0.2 and -0.65 V. Peak currents were collected using the manual fitting mode in the PSTrace 5.4 (2018) software.

3.6.4 Supporting figures

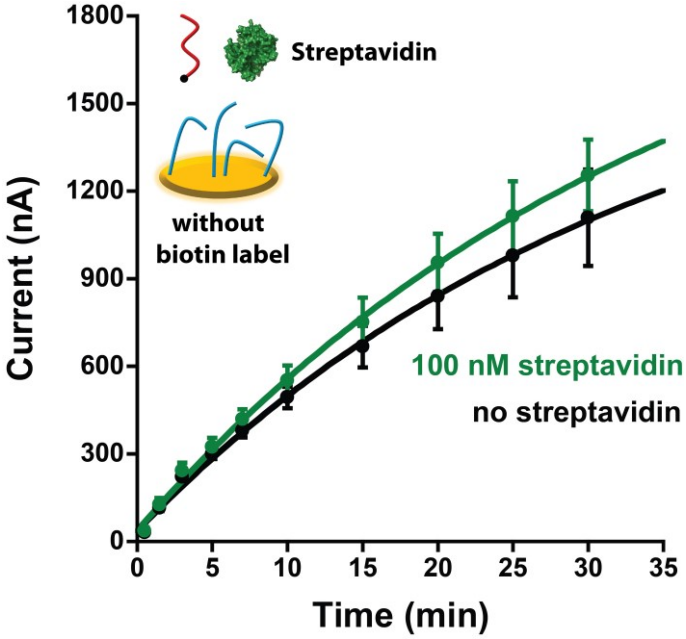

Figure S3.1 A negative control of the molecular barrier assay for streptavidin detection. In this assay, the 16-nt capturing DNA does not contain a recognition element (i.e., biotin), and no significant difference in hybridization efficiency is observed in the presence or absence of streptavidin (unpaired *t-test*, p = 0.724), which indicates that the molecular barrier is formed through the specific interaction between streptavidin and biotin and not because of non-specific adsorption of streptavidin on the sensor surface. The length of signaling DNA used in this assay was 16-nt. The concentrations of capturing DNA and signaling DNA used in this assay were 300 nM and 100 nM, respectively. The error bars represent the standard deviation obtained from three electrodes.

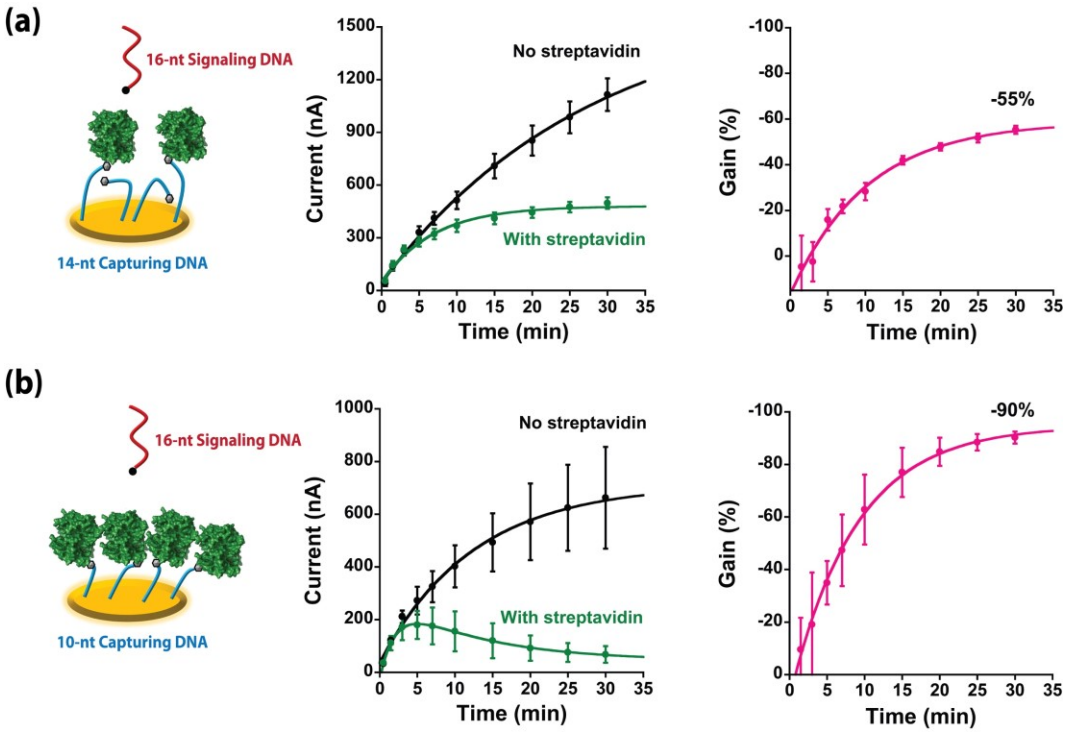

Figure S3.2 The kinetic and signal gain of the molecular barrier assay by using (a) 14-nt capturing DNA and (b) 10-nt capturing DNA. All results were carried out with a 16-nt signaling DNA. The concentrations of capturing DNAs, signaling DNA, and streptavidin used in this assay were 300 nM, 100 nM, and 100 nM, respectively. The error bars represent the standard deviation obtained from three electrodes.

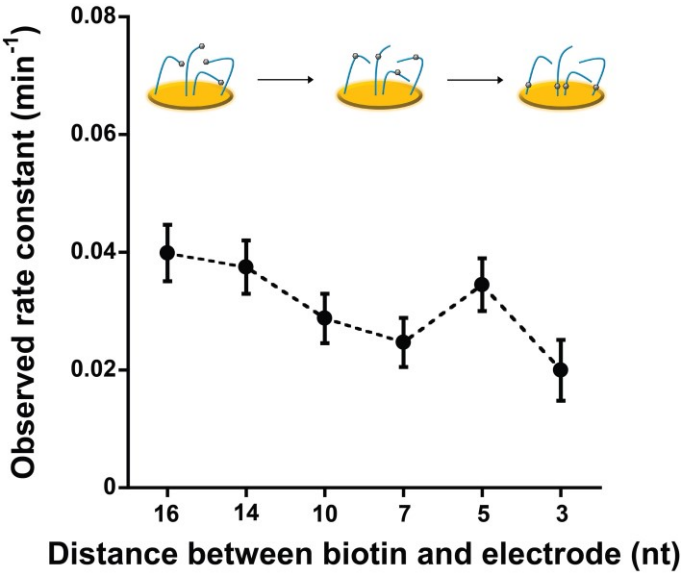

Figure S3.3 The labeling position of biotin in the capturing DNA does not affect the hybridization rate of the capturing DNA and the signaling DNA. The range of observed rate constant is typically located from 0.02 min^{-1} to 0.04 min^{-1}. The observed rate constants were obtained from the hybridization between the 16-nt signaling DNA and different capturing DNA variants in the absence of streptavidin. The error bars of the rate constant come from the errors of kinetic fitting.

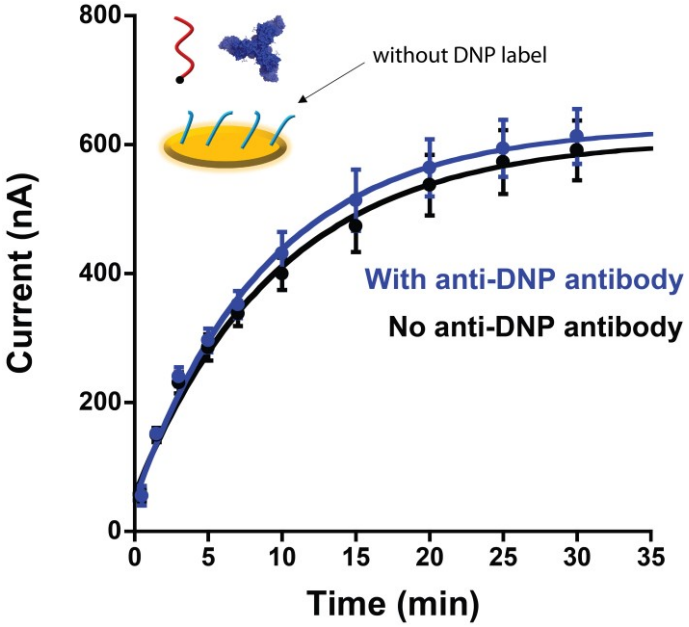

Figure S3.4 A negative control of the molecular barrier assay for anti-DNP antibody detection. In this assay, the 10-nt capturing DNA does not contain the recognition element (i.e., DNP molecule), and no significant difference in hybridization efficiency is observed in the presence or absence of anti-DNP antibody (unpaired *t-test*, p = 0.836). The length of signaling DNA used in this assay was 16-nt. The concentrations of capturing DNA and signaling DNA used in this assay were 300 nM and 100 nM, respectively. The dilution of anti-DNP antibody used in this assay was 1:25. The error bars represent the standard deviation obtained from three electrodes.

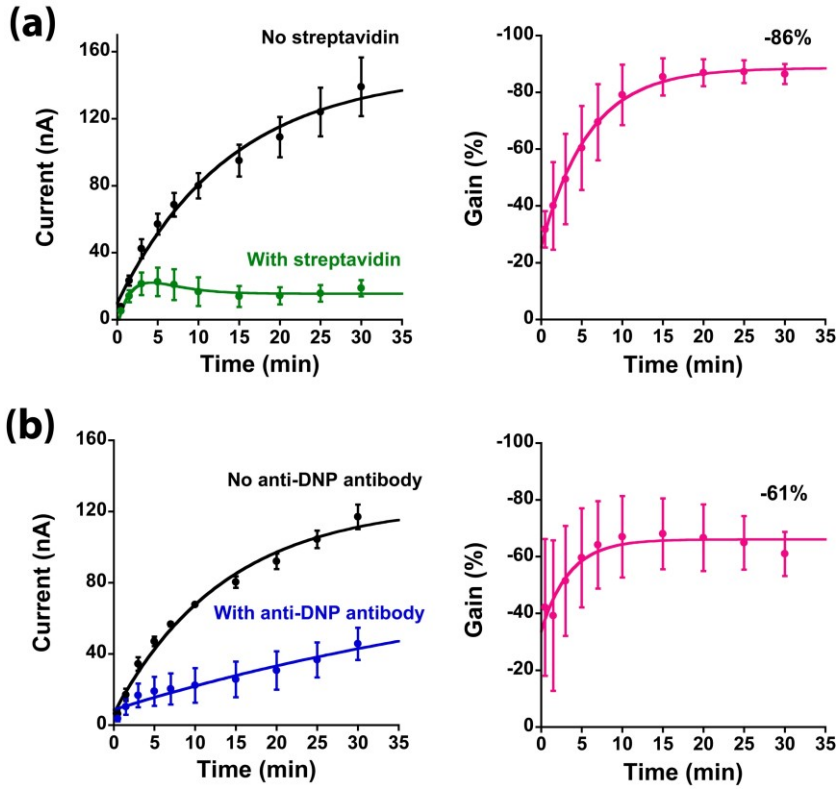

Figure S3.5 The kinetics and signal gain of (a) streptavidin and (b) anti-DNP antibody detection in the buffer using the Micrux electrode. The length of capturing DNA and signaling DNA used in this assay was 10-nt and 16-nt, respectively. The concentration of capturing DNAs, signaling DNA, and streptavidin used in this assay was 300 nM, 100 nM, and 100 nM, respectively. The dilution of anti-DNP antibody used in this assay was 1:25. The error bars represent the standard deviation obtained from three electrodes.

Chapter 4: Rapid, one-step molecular detection in a drop of blood using kinetically programmed constitutional dynamic chemistry

Guichi Zhu[1,2], Dominic Lauzon[2,3], Carl Prévost-Tremblay[2,4], Arnaud Desrosiers[2,4], Bal-Ram Adhikari[2,3], Alexis Vallée-Bélisle[1,2,3,4]*

[1]Institut de Génie Biomédical, Département de Pharmacologie et Physiologie, Université de Montréal, Montréal, Québec H3T 1J4, Canada.
[2]Laboratoire de Biosenseurs & Nanomachines, [3]Département de Chimie, and [4]Département de Biochimie et Médecine Moléculaire, Université de Montréal, Montréal, Québec H3T 1J4, Canada.

Author contributions: G.Z. and A.V.-B. conceived and designed the study. D.L. and C.P.-T. wrote the equations for kinetic mechanism. D.L. wrote the MATLAB script for the kinetic simulations. A.D. performed the HPLC measurement of quinine in mouse blood. B.-R.A. optimized the cleaning and functionalization of Micrux electrode. G.Z. performed all other experiments and kinetic simulations. G.Z. and A.V.-B. created the figures and wrote the manuscript.

This manuscript is under review by "*Nature Chemistry*"

4.1 Abstract

A drastic breakthrough in health care will take place when patients are able to monitor blood molecules indicative of their health status regularly in the comfort of their home.[1, 2, 222, 223] Unfortunately, most technologies for molecular detection in blood employ chemical systems that are still too complex and expensive to develop efficient, easy-to-use home devices. Here we report a simple, versatile, one-step, DNA-based constitutional dynamic chemistry (CDC) assay composed of three kinetically programmed competing reactions (recognition, inhibition and

signaling reactions) that enable quantitative detection of any specific molecules directly in a drop of blood. Using this strategy in an inexpensive electrochemical format, we demonstrate therapeutic drug monitoring of an antimalarial drug in living mice in a simple, one-step, five-minutes procedure that only requires 5 µL of unprocessed blood. We discuss the potential applications of kinetically programmed CDC assays for point-of-care diagnostic/monitoring applications and their implication for the development of more simple and efficient chemistries.

4.2 Introduction

Human-designed chemistry typically relies on complex multiple-step reactions necessitating various purification steps and experimental conditions. In contrast, nature has developed a wide variety of dynamic chemistries where multiple reactions are sequentially programmed to achieve a complex synthesis, regulation, or functional mechanism. For example, typical chemical assays developed for molecular diagnostic applications require complicated, multi-step, wash- and reagent-intensive chemistries that require precise temperature control and complex optical detection (e.g., enzyme-linked immunosorbent assay,[6] polymerase chain reaction,[5] high-performance liquid chromatography,[224] and fluorescence polarization assay[225]). Current point-of-care devices for molecular diagnostic applications typically automate these chemical processes using complex microfluidics,[226-229] but these systems remain too complicated, expensive, and unreliable for home use (e.g., i-STAT and Piccolo).

Living organisms have developed various finely controlled dynamic chemistries (e.g., receptors, enzymes, and riboswitches) that can selectively and quantitatively detect the presence of any specific molecule in complex biological surroundings.[230-233] Given their outstanding performance, many efforts are currently invested into developing more simple and efficient "nature-inspired" chemistries.[69, 234-237] To this end, the field of constitutional dynamic chemistry (CDC) is currently exploring and developing chemical systems capable of responding to chemical inputs by modifying their constitution through the reorganization of non-covalent bonds or component exchange.[238-241] In recent years, for example, CDC systems have been developed and exploited for applications ranging from drug screening,[242, 243] to smart functional materials,[244-247]

and DNA nanomachines.[248-250] We believe that similar systems could drastically enhance our ability to rapidly and efficiently detect specific molecules directly in complex biological fluids such as whole blood.

In the last 30 years, various biosensing strategies have been developed for the quantitative detection of specific molecules in a one-step procedure. Still, few of them, besides perhaps enzyme-based glucometers, have shown mass scale adoption by industry. Typical biosensing strategies, for example, consist of engineering a bio-recognition element in such a way that it transduces a specific binding event into a measurable output, such as fluorescence,[217, 251] colorimetry,[252, 253] Raman,[254, 255] electrochemistry,[76, 77] and surface plasmon resonance (SPR).[256, 257] Although these strategies have had some success, they often display the following two limitations. First, their performance is strongly dependent on the nature of the markers detected (e.g., ions, small molecules, nucleic acids, and proteins).[153, 258] But most importantly, they typically fail when deployed in complex media, such as whole blood, and require elaborate drift correction strategies to control non-specific adsorption of blood proteins on the sensor surface.[151, 259] To circumvent these limitations, here we have developed a simple, versatile CDC assay that employs three competing reactions: a recognition (k_1), an inhibition (k_2), and a signaling (k_3) reaction to detect any specific ligand (or target) molecule in a one simple step (Figure 4.1a).

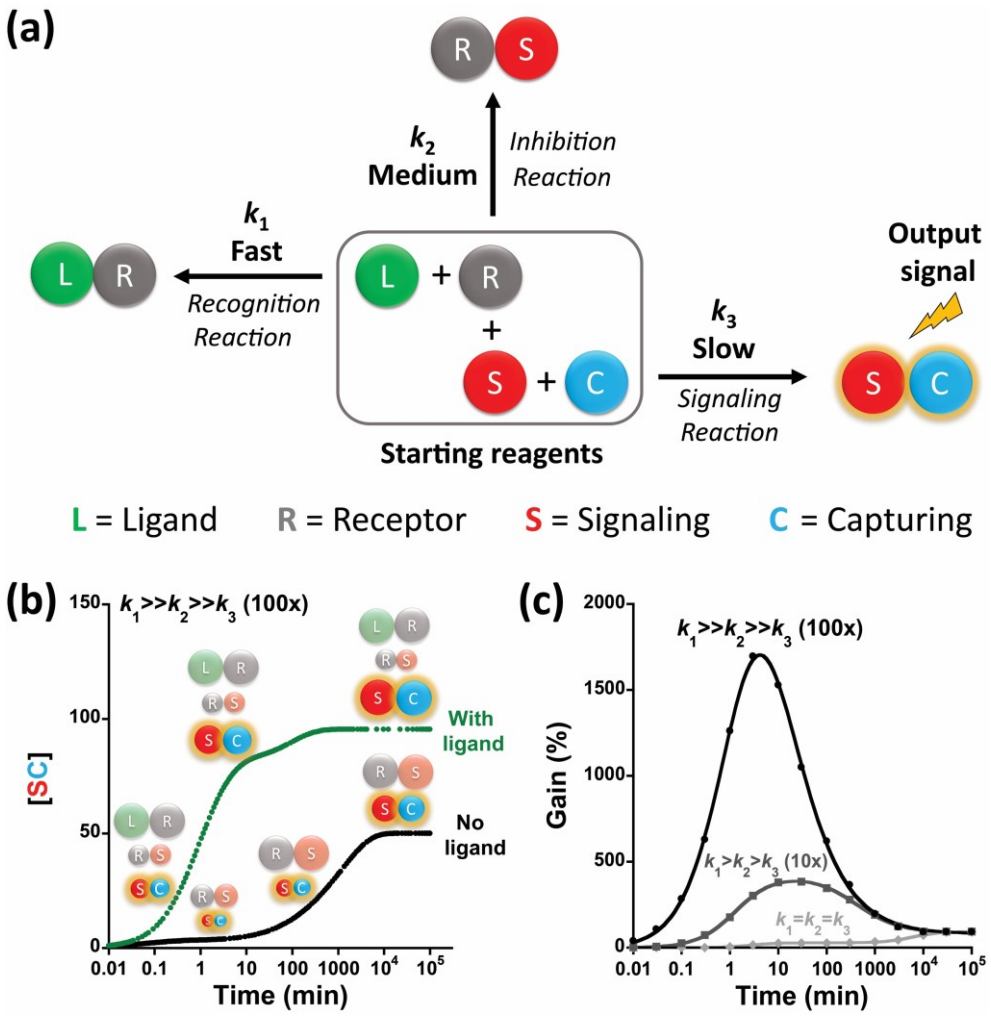

Figure 4.1 A one-step, kinetically programmed CDC assay for molecular detection. (a) This one-step three reactions system (k_1>k_2>k_3) quantitatively detects the concentration of ligand molecule L through specific binding to receptor molecule R. The receptor molecule R can competitively bind to either ligand molecule L or signaling molecule S. in the presence of ligand molecule L, the ligand molecule L binds to the receptor molecule R (formation of the L-R complex) preventing the latter from binding to the signaling molecule S. The signaling molecule S is now free to bind to the capturing molecule C, thus generating an output signal (formation of the S-C complex). In the absence of ligand molecule L, the receptor molecule R is available to bind the signaling molecule S (formation of the R-S complex), therefore preventing the signaling molecule S from interacting with the capturing molecule C. (b) Simulated kinetics of complex formation (L-R, R-S and S-C) in our CDC system in the presence (green) or absence (black) of ligand molecule L (k_1 = 100*k_2 = 10000*k_3). (c) Simulations demonstrate that when k_1>>k_2>>k_3, this CDC system produces much better gain before reaching equilibrium (see Figure S4.1 for all details on this simulation).

This one-step CDC assay starts with a *recognition reaction* performed by a specific ligand-binding receptor molecule (R). In the presence of the specific ligand molecule (L), L binds R in such a way that it precludes R from binding and inhibiting signaling molecule (S) (*inhibition reaction)*. The signaling molecule S, therefore, remains free and can bind to the capturing molecule (C), thus generating a signal proportional to L, the ligand concentration (*signaling reaction*). This strategy possesses two main advantages: 1) the recognition, inhibition and signaling reactions are highly modular and can be easily adapted, with few optimizations, for the detection of any ligand molecules for which a simple nucleotide-based receptor exists; 2) the signaling reaction, based on the hybridization between signaling and capturing DNA molecule, is always "signal-on" and can be monitored directly in whole blood without any signal drift.[132] More importantly, this assay can be kinetically programmed to generate high signal gains rapidly, well before reaching equilibrium (Figure 4.1b-c). For example, simulations show that when increasing the kinetic difference between all three competing reactions from 1 to 100-times, the gain of the assay is improved by order of magnitude, and the maximal gain is reached orders of magnitude faster than the rate of equilibrium (see also Figure S4.1).

4.3 Results and discussions

We have engineered and tested this one-step, modular CDC assay using DNA chemistry since DNA molecules can be: *1)* selected to recognize a wide range of molecules specifically;[260, 261] *2)* readily re-engineered into molecular switches;[66, 262] and *3)* adapted in multicomponent binding reactions.[263-265] The main advantage of DNA chemistry is that one can typically select DNA sequences to specifically and selectively bind any specific non-nucleic acid ligand. In addition to binding these ligands, these DNA sequences will also competitively bind to their complementary DNA sequences through sequence-specific hybridization to form DNA duplexes, thus giving rise to multiple simple and universal allosteric mechanisms.[71, 266] Multiple hybridization reactions can also proceed simultaneously, in the same sample, without cross reactivity. An often-overlooked aspect of multicomponent one-step assays is that the kinetics of each binding reaction must be appropriately tuned to occur sequentially in time at the right

moment. To this end, DNA hybridization can also be readily tuned, both thermodynamically and kinetically.[70, 267-269]

We designed our one-step CDC assay by employing a DNA-based signaling reaction that has been shown to be highly robust and selective in whole blood.[132] To do so, we employed a 16 nucleotides redox-labeled "signaling" DNA and a complementary "capturing" DNA strand attached to a gold electrode (see S, C and k_3, Figure 4.2a). The selected double helix length (16 Watson-Crick base pairs interactions) is long enough to drive the hybridization reaction to completion (Figure S4.2). The capturing DNA is attached to a gold electrode at high surface coverage (~$2*10^{12}$ strands/cm^2, see Figure S2.1) using a 3'-C6-thiol group via the formation of a sulfur-gold bond (see electrode fabrication in supporting information). This hybridization "signaling reaction" takes place in a time range of minutes ($t_{1/2}$ of k_3 ≈ 19 min, Figure S4.3) and can be easily monitored through electrochemistry (due to the redox-labeled signaling DNA being brought close to the electrode surface) directly in whole blood. In order to render this signaling reaction sensitive to the presence of a specific ligand molecule, we designed the signaling DNA so that it is complementary to a specific DNA aptamer receptors (note: aptamers are available for numerous human proteins[41, 270] and a variety of clinically important molecules[271]).

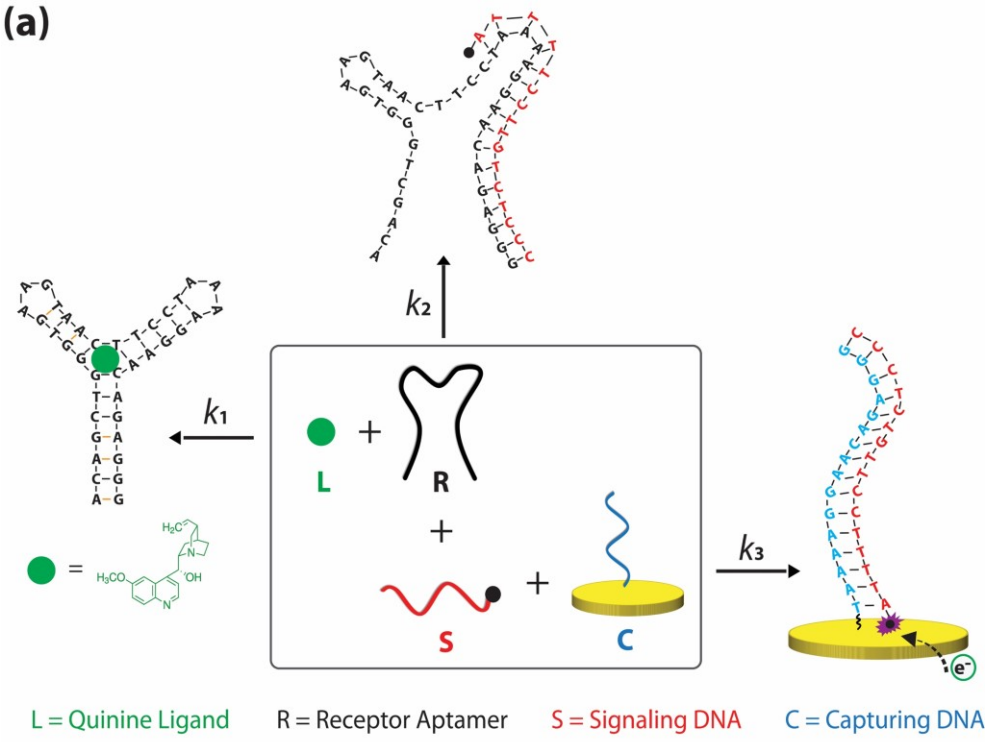
(a)
k2
k1
k3
L
R
S
C
L = Quinine Ligand
R = Receptor Aptamer
S = Signaling DNA
C = Capturing DNA

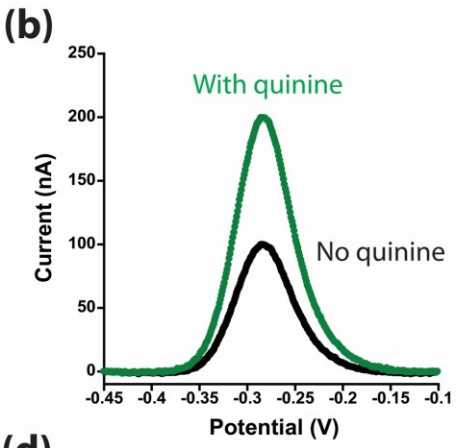
(b)
With quinine
No quinine
Current (nA)
Potential (V)

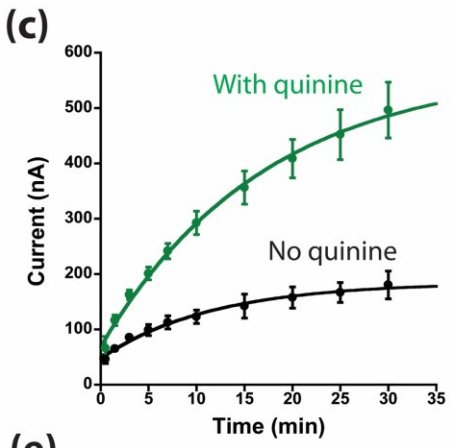
(c)
With quinine
No quinine
Current (nA)
Time (min)

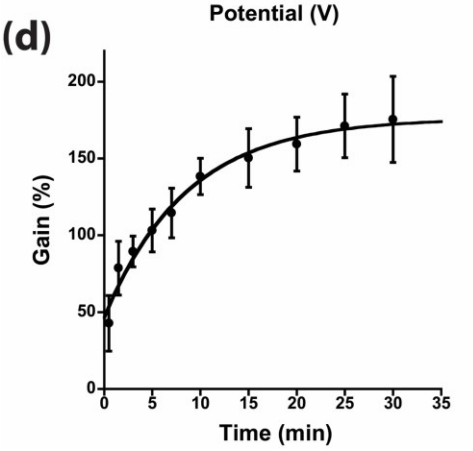
(d)
Gain (%)
Time (min)

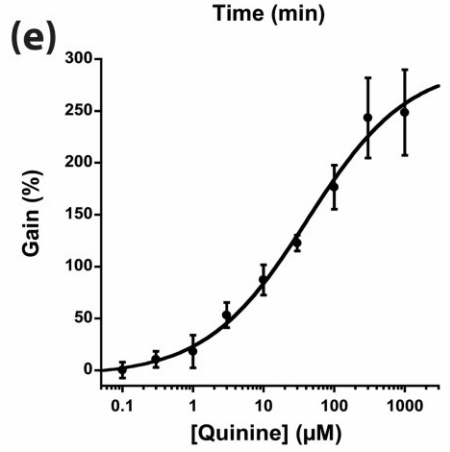
(e)
Gain (%)
[Quinine] (μM)

Figure 4.2 (a) One-step, kinetically programmed CDC assay for the detection of quinine. If unbound to quinine, the receptor aptamer remains relatively unstable and can readily hybridize to the signaling DNA, thus preventing (inhibiting) hybridization of the latter to the capturing DNA on the electrode. When quinine is present, it binds and stabilizes the three-way junction conformation of the aptamer, thus preventing it from binding to the signaling DNA. (b) The electrochemical current (Square wave voltammetry) produced by the signaling-capturing complex increases by two-times (~100% gain) in the presence of 100 μM quinine after 5 min. (c-d) Electrochemical current (c: no quinine: 0.086 min^{-1}; with quinine: 0.058 min^{-1}) and gain (d: 0.12 min^{-1}) of the assay *versus* time). (e) The one-step three-reaction assay responds quantitatively to the concentration of quinine between 1 μM and 300 μM ($C_{50\%}$ = 41 ± 12 μM; 30 min reaction). The concentrations of capturing DNA, signaling DNA, and aptamer used in this assay are 300 nM, 100 nM, and 100 nM, respectively. These experiments were realized in 1 mL phosphate-buffered saline solution. The error bars represent the standard deviation obtained from three electrodes.

As an initial proof-of-principle, we have developed a CDC assay to detect a crucial antimalarial drug, quinine, a natural alkaloid used to treat malaria[272] (Figure 4.2a). Despite being one of the most commonly used antimalarial drugs, quinine remains associated with various dose-related toxicities, including cinchonism, hypoglycemia, and hypotension.[273] Convenient strategies enabling therapeutic drug monitoring of quinine and other antimalarial drugs at home would represent a key breakthrough to improve the efficacy and effectiveness of these treatments.[274] We designed the quinine CDC assay by employing a well-characterized quinine-binding aptamer.[275, 276] We designed the signaling DNA to form 16 Watson-Crick base pairs with the 5' extremity of this aptamer (Figure 4.2a). If unbound to quinine, this aptamer will rapidly unfold (k_{unfold} = 25 s^{-1})[277] in an open conformation that enables rapid hybridization to the signaling DNA (see R, S and k_2, Figure 4.2a) (of note 5% of the aptamer remains unfolded given its small folding energy, ΔG_{fold} = 7.5 kJ/mol).[277] Upon hybridization to the aptamer, the signaling strand becomes "inhibited" and can no longer bind to the capturing DNA on the electrode. When quinine is present, it binds and stabilizes the three-way junction conformation of the aptamer (through stacking interactions with the DNA bases[275, 276]), thus preventing the aptamer from adopting an open conformation with high affinity for the signaling DNA (see L, R and k_1, Figure 4.2a).[278] In such a case, the signaling DNA is now free to hybridize to the capturing DNA, creating

a high electrochemical current within minutes. Interestingly, the rate of complex formation between quinine and its aptamer receptor, k_1, is three orders of magnitude faster than the rate of DNA-DNA hybridization in solution (Figure S4.3), k_2, due to charge repulsion between the DNA strands. Also, DNA hybridization on surface-bound DNA, k_3, is typically slower (Figure S4.3). Having $k_1 > k_2 > k_3$ should ensure that this CDC system displays a high gain and rate (see simulations in Figure S4.1).

Our first CDC assay produced a two-times increase (~100% gain) in electrochemical current in the presence of 100 μM of quinine after only 5 min of reaction (Figures 4.2b-d). To obtain this result, we performed the assay by rapidly (< 10 s) mixing 100 nM of the aptamer and 100 nM of the signaling DNA in a 1 mL phosphate-buffered saline solution (pH 7.0) with or without quinine (green curve and black curve, respectively) and this mixture was then rapidly (< 15 s) transferred on the capturing DNA-functionalized electrode. After only 30 s, the electrochemical current is already ~40% higher in the presence of quinine and keeps increasing up to ~175% after 30 min of reaction time (Figure 4.2d). An independent control in the absence of aptamer demonstrates that this current increase is not attributable to some putative electrochemical activity of quinine (Figure S4.4). We also find that the electrochemical current increases in a quinine concentration-dependent manner with a $C_{50\%}$ of around 41 ± 12 μM (Figure 4.2e: incubation time=30 min). The variation between the $C_{50\%}$ of the assay and the quinine-aptamer affinity (K_{D1} = 0.871 μM; 47 times difference, Figure S4.5) was also predicted by numerical simulations using the experimentally obtained rate constants of each of the reactions (predicted $C_{50\%}$: 13.9 μM; see Figure S4.6c). Of note, longer equilibration times also lead to significant gain reduction as predicted by the numerical simulations (see Figure S4.7).

As suggested by the simulation results (Figures 4.1b-c and Figure S4.6), the performance of our one-step CDC assay is assumed to be kinetically controlled. To demonstrate this experimentally, we proceeded with the same three reaction assay but favored one binding reaction over the two others through pre-incubation of their components, hence promoting the formation of either the quinine-aptamer (k_1), the aptamer-signaling DNA (k_2), or the signaling-capturing DNA (k_3) complexes (Figure 4.3). We first artificially mimicked an increase in the rate

of k_1 relative to k_2 and k_3 by pre-mixing quinine and its aptamer before adding the signaling and capturing DNA. Since k_1 is already much faster than k_2 and k_3 (at least 3 orders of magnitude, see Figure S4.3), no significant difference in electrochemical current is observed, suggesting that signaling-capturing complex formation has already reached its maximum under the conditions tested (Figure 4.3b). In contrast, we observe a significant drop in electrochemical current when pre-incubating the aptamer and signaling DNA for 30 min before adding the quinine and capturing DNA. In this second instance, we mimicked an increase in k_2 to a point where it is faster than k_1 and k_3 (Figure 4.3c). This result suggests that once the aptamer-signaling DNA complex forms, their high affinity or slow dissociation rate (k_{-2}) do not allow quinine to bind to the aptamer during the timeframe of this experiment ($t_{1/2}$ of aptamer-signaling complex is ~630 min, see Figure S4.5b). Finally, a very high signal background is obtained when pre-incubating the signaling-capturing DNA for 30 min before adding the quinine and aptamer (*i.e.,* when mimicking a k_3 increase to a point where it is faster than k_1 and k_2) (Figure 4.3d). In the absence of quinine, the high background current decreases slowly with time as the signaling DNA dissociates from the capturing DNA to bind to the aptamer ($t_{1/2}$ of signaling-detecting complex is ~592 min, Figure S4.5c). In the presence of quinine, the signal remains relatively constant since the aptamer interacts with quinine and is therefore unavailable to sequester any dissociated signaling DNA. Overall, these results demonstrate that our kinetically programmed one-step CDC assay provides much higher gains (~175% at 30 min) when the reactions rates are programmed so that $k_1 > k_2 > k_3$.

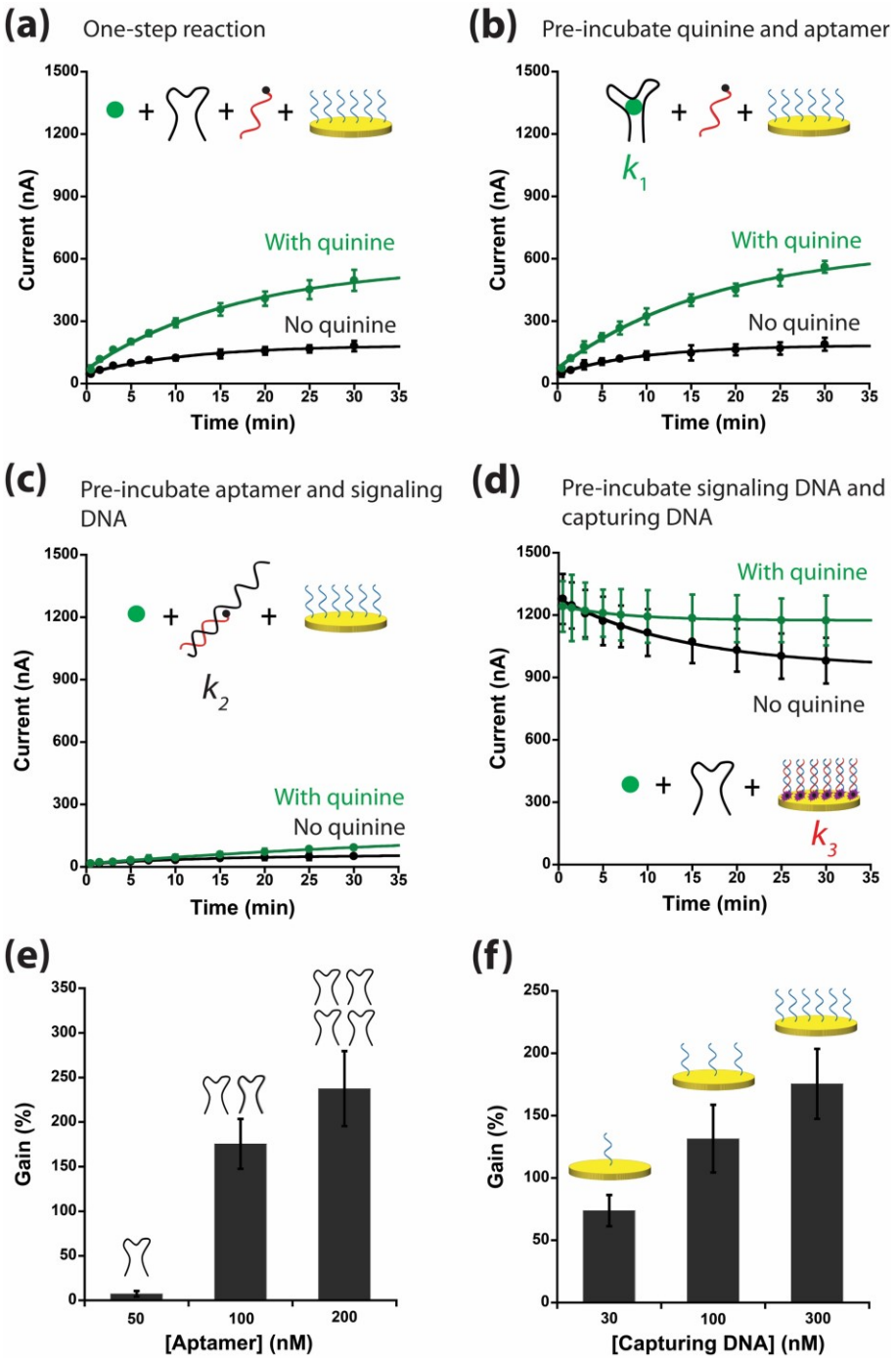

Figure 4.3 The CDC assay is kinetically controlled and requires optimization of its reaction rates (k_1>k_2 >k_3). CDC assay performed: (a) by using a one-step reaction; (b) by pre-incubating quinine with its aptamer for 30 min; (c) by pre-incubating the aptamer and the signaling DNA for 30 min; (d) by pre-incubating the signaling and capturing DNA for 30 min. (e) Improving the gain by increasing k_2 relative to k_3 by increasing aptamer concentration (see also simulation in Figure S4.8a-c). (f) Improving the gain by decreasing k_3 relative to k_2 by increasing the density of the capturing DNA on the surface of the electrode (hybridization

rates decrease with increasing charge density on the surface-see Figure S4.8d-f). Figure e and f were realized using 100 μM quinine, 100 nM aptamer (unless otherwise stated -e.g., panel e), 100 nM signaling DNA, and 300 nM capturing DNA (unless otherwise stated -e.g., panel f). The error bars represent the standard deviation obtained from three electrodes.

In order to improve the gain and thus the performance of our one-step CDC assay, we then explored to which extent varying experimental and design conditions could impact the kinetic difference between k_1, k_2 or k_3, and ultimately the signal gain. Using computer simulations, we previously demonstrated that increasing the rate difference between k_1, k_2, and k_3 increases the signal gain (e.g., smaller background and higher signal, see Figures 4.1c and S4.1). Since the difference of reaction rate between k_2 and k_3 in our assay remains relatively small (~39 times, see Figure S4.3), we modified the experimental conditions of our assay to increase k2 or decrease k3 selectively. To increase k_2, we simply raised the concentration of the aptamer from 50 nM to 200 nM (Figure S4.8a-c). This increases k_2 (and thus the difference between k_2 and k_3) by around 2.4 times (Figure S4.8b), and this optimized CDC assay improved its gain from ~7.4% to ~237% (Figure 4.3e) (see also simulations Figure S4.8c). We also changed the rate difference between k_2 and k_3 by changing k_3 (Figure S4.8d-e). To do so, we simply decreased the density of the capturing DNA at the electrode surface, as this is known to increase the kinetics of hybridization by decreasing charge density and repulsion near the electrode surface (DNA is charged negatively).[212] By reducing the capturing concentration from 300 nM to 30 nM when functionalizing our electrode, we were able to decrease the rate difference between k_2 and k_3 by 6.84-times (Figure S4.8e), which reduced the signal gain of our CDC assay from ~175% to ~73.9% (Figure 4.3f) (see also simulation Figure S4.8f).

A critical advantage of our strategy is its simplicity of design and optimization. For example, numerical simulations highlighted that our kinetically programmed assay is relatively insensitive to variation in thermodynamic parameters (binding affinities) of the inhibition and signaling reactions (see Figure S4.6). To verify this, we varied K_{D2}, the affinity between the aptamer and signaling DNA (inhibition reaction), by changing the duplex lengths from 12 and 18 Watson-Crick base pairs (7.7 kcal/mol variation -see Table S2) (Figure 4.4a). Signaling DNA making 14 to 18

Watson-Crick base pairs with the aptamer all produced signal gains above 100% with the 16 Watson-Crick base pairs producing the maximal gain of ~175% after 30 min in the presence of 100 μM of quinine (Figure 4.4a). Shorter signaling DNA (e.g., the one forming 12 base pairs) simply does not display sufficient affinity to bind the aptamer in the absence of the quinine, therefore producing a high signal background and lower gain (~21.6%). We also explored the effect of varying K_{D3}, the affinity between the signaling and capturing DNA (signaling reaction), by varying the duplex lengths from 10 and 16 Watson-Crick base pairs (9.1 kcal/mol variation - see Table S4.3) (Figure 4.4b). Signaling DNA making 12 to 16 Watson-Crick base pairs with the capturing DNA all produced signal gains above 100%, with the 16 Watson-Crick base pairs having the maximal gain of ~175% in the presence of 100 μM of quinine (Figure 4.4b). Shorter capturing DNA (e.g., the one forming only ten base pairs) simply does not display sufficient affinity to bind to the signaling DNA, therefore, producing low current and low signal gain (~27.3%). The relative insensitivity of this CDC assay to K_{D2} and K_{D3} variation represents an important design advantage over typically equilibrium-based biosensors and suggest that the assay can be rapidly adapted for the detection of other molecule-aptamer pair.

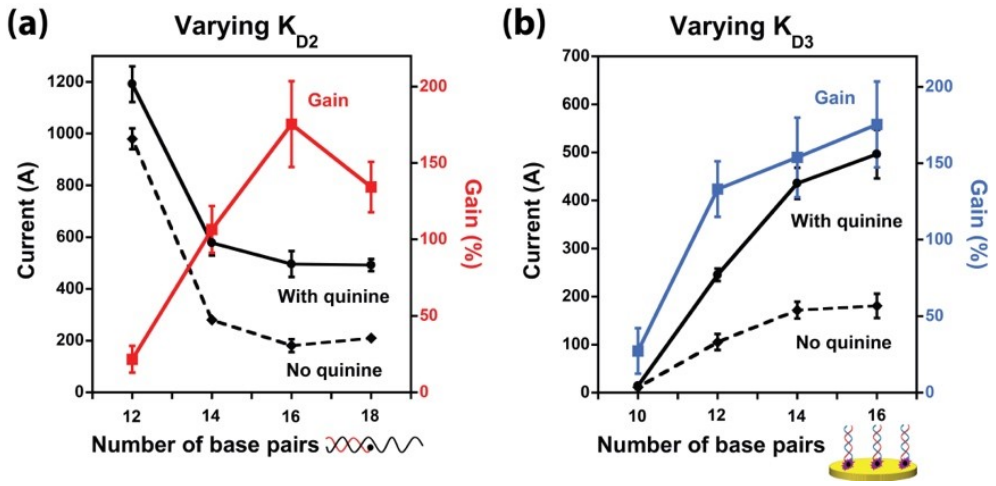

Figure 4.4 The kinetically programmed CDC assay is relatively insensitive to the affinities between the aptamer and the signaling DNA (K_{D2}: inhibition reaction) and between the signaling and detecting DNA (K_{D3}: signaling reaction). (a) Signaling DNA forming more than 14 Watson-Crick base pairs with its aptamer display gains higher than 100%. A smaller duplex length simply leads to a higher signal background in the absence of quinine, thus drastically reducing the gain. (b) Signaling DNA forming more than 12 Watson-Crick base pairs with the capturing DNA display gains higher than 100%. The concentrations of capturing

DNAs, signaling DNAs, aptamer, and quinine used in this assay are 300 nM, 100 nM, 100 nM, and 100 µM, respectively. The error bars represent the standard deviation obtained from three electrodes.

The recognition, inhibition and signaling reactions in our strategy are highly modular and can be easily adapted for the detection of any other ligand molecules for which a receptor exists. To highlight the versatility of our one-step kinetically programmed CDC assay, and its simple design rules, we also developed a sensor for the detection of other molecules (such as adenosine triphosphate (ATP), thrombin, and platelet-derived growth factor (PDGF)). To do so, we simply replaced the quinine-binding aptamer with different aptamers and designed complementary signaling DNA and its corresponding capturing DNA. As shown in Figure S4.9, ATP, thrombin, and PDGF have been successfully detected at 5 min using our one-step kinetically programmed CDC assay. Overall, these results demonstrate how simple and universal the design of this one-step three reaction system is. In the classical electrochemical aptamer-based sensors, the aptamer needs to be modified with redox, which may affect the binding affinity of aptamer-ligand. Also, it is hard to predict the signal-on or signal-off readout for different ligand molecules detection because different aptamers have various folding conformations on the surface. In contrast, our assay is always signal-on when it is applied for other molecules detection. Also, we don't need to modify the aptamer, and it is always unlabeled with the best binding affinity as it is selected.

In order to showcase the simplicity and usefulness of this kinetically programmed assay for health monitoring applications, we adapted our quinine CDC assay into an inexpensive sensor that enables therapeutic drug monitoring directly in a single drop of blood (5 µL). Following optimization of the CDC assay on ED-SE1-AuPt Micrux electrodes (see supporting information, Figure S4.10), we demonstrated that the detection of 100 µM of quinine in a drop of mouse blood (5 µL) provides a 316% gain (Figure 4.5b-c). We also find that the electrochemical current increases in a quinine concentration-dependent manner in whole blood with a $C_{50\%}$ of around 95 $\pm$ 22 µM. We then performed pharmacokinetics in mice by injecting a clinically relevant concentration of quinine (10 mg /kg of body weight) and found that the profile (rate of elimination) varied by up to three folds (Figure 4.5d). Notably, pharmacokinetic profiling

performed on five additional mice using gold standard HPLC measurements revealed similar pharmacokinetic profiles (Figure 4.5e). While our CDC assay could be performed in a simple one-step, 5-minutes procedure using only 5 µL of unprocessed blood, the HPLC procedure required hours of pre-treatment and analysis and required a volume of blood volume larger than 20 µL.

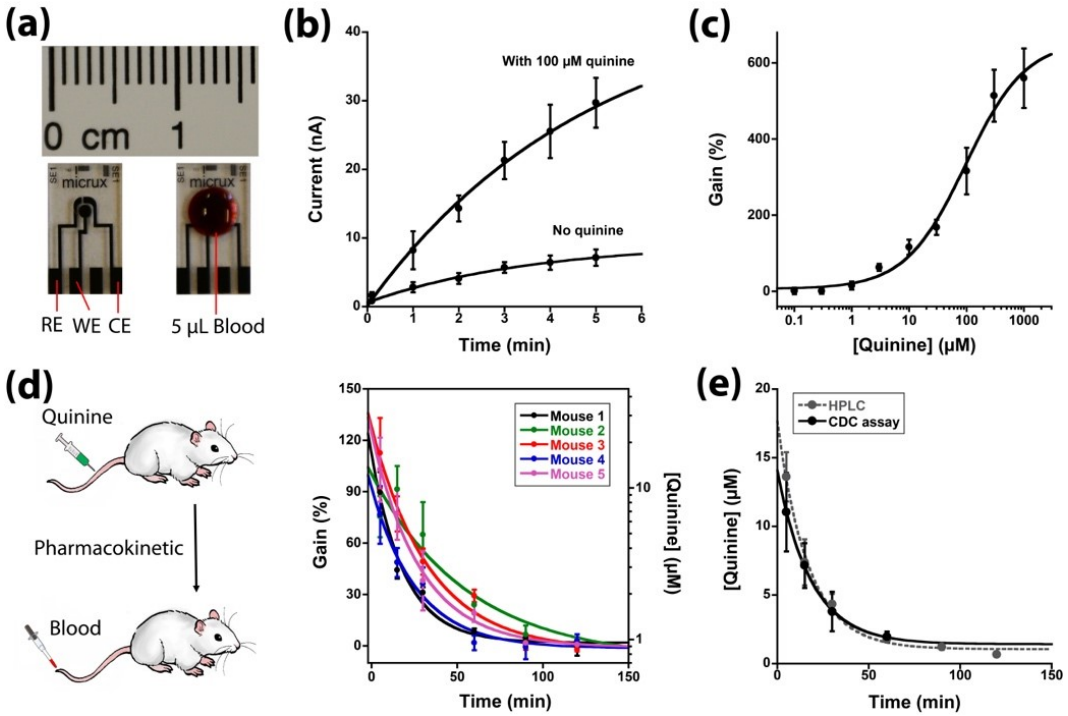

Figure 4.5 Therapeutic drug monitoring using the kinetically programmed CDC assay. (a) The CDC assay can be performed directly in 5 µL of whole blood on an ED-SE1-AuPt Micrux electrode (RE=reference electrode, WE=working electrode, and CE=counter electrode). (b) Electrochemical current kinetics when performing the assay in 5 µL of mice blood with 100 µM or no quinine. (c) Dose-response curve of the quinine CDC assay in whole blood after 5 min reaction time. (d) Pharmacokinetic of quinine (10 mg/kg of body weight) in five mice measured using the CDC assay. (e) Average pharmacokinetic obtained on five mice using the CDC assay and the gold standard HPLC assay. The quinine concentration could only be precisely measured in one mouse after 60 min using the CDC assay (LOD= 2 µM). The individual HPLC results for the other five mice are shown in Figure S4.11. The concentrations of capturing DNA, signaling DNA, and aptamer used in this assay are 300 nM, 200 nM, and 600 nM, respectively. The error bars represent the standard deviation obtained from three electrodes.

The DNA-based CDC assay also performs in a multiplexed format with other

electrochemical DNA-based assays[132] (Figure S4.12). To demonstrated this, we performed the CDC assay (for quinine detection) simultaneously with another DNA-based electrochemical assay that employs steric hindrance to detect large molecules (such as antibodies) in the same blood sample (Figure S4.12b).[132] To do this, we fabricated two rod electrodes, each functionalized with a specific capturing DNA (i.e., for each specific assay) and these "multiplexed assays" provided similar performance when performed simultaneously in the same blood sample.

4.4 Conclusions

In this paper, we have developed a universal, one-step, kinetically-programmed CDC assay that enables the quantitative detection of a wide range of molecules directly in a drop of blood within less than five minutes. We first show that our assay is simple in its design and execution as well as being potentially universal for the detection of any molecule for which we possess a specific nucleotide-based receptor. We also demonstrated that the assay can be kinetically programmed to generate high gains rapidly within five minutes, well before reaching equilibrium. Finally, and perhaps most importantly, this assay can function directly in a drop of unprocessed blood (5 uL) in a multiplexed format, using a simple one-step procedure without the need for time-consuming separation, washing, or additional purification steps typically required by current centralized lab methods.

Our kinetically programmed one-step CDC assay displays several advantages over other electrochemical DNA-based sensors. Firstly, its simple and modular design creates high signal-on gains that can be, in principle, rapidly adapted to detect thousands of molecular markers for which we already possess specific aptamer-binding sequences (e.g., SOMAlogic[41, 260, 261, 270]). In contrast, more conventional electrochemical aptamer-based (E-AB) sensors[76, 279] that require the covalent attachment of the aptamers on the gold electrodes must typically be optimized individually depending on the size, conformation and stability of the aptamer employed (e.g., the location of the redox-element on the aptamer, thermodynamic properties of the aptamer, the density of the aptamer on the surface of the electrode).[153, 280] Secondly, the signaling mechanism of our CDC assay is not affected by the non-specific adsorption of blood proteins on the sensor

surface (biofouling): the redox molecule is attached to the signaling DNA (and not covalently linked to the gold electrode) and its hybridization efficiency is not affected by the complex biological matrix. Thirdly, our CDC assay performs relatively faster than typical duplex-based aptamer sensors that require DNA dissociation before being activated, which is typically orders of magnitude slower.[281] On the other hand, our assay is not exempt from limitations. For example, it may not reach a temporal resolution below 1 min like E-AB sensors do and could hardly be performed in a continuous format to monitor marker concentration in real-time in living organisms.

Aptamer-based recognition elements are still relatively new in the field of medical diagnostics, they nevertheless display several advantages over protein-based assays that employ costly enzymes and antibodies. One such advantage is the simplicity of DNA chemistry (e.g., Watson-Crick base pair) that do not require complex conjugation strategies for building the assay. Overall, our one-step CDC assay, therefore, displays all the characteristics to be readily adapted in a rapid, easy-to-use, point-of-care format for the detection of molecular markers directly in a drop of blood. In this manuscript, we have shown an application for therapeutic drug monitoring in animal models. However, the CDC assay could also be employed for more frequent patient testing at home to enable chronic disease monitoring and proactive clinical interventions.

More broadly, our results also highlight the importance of programming chemical reaction rates in order to design one-step multicomponent reactions with optimal performance and minimum reaction time.[282, 283] This often-overlooked aspect should be of interest to a wide range of scientists, engineers and chemists (organic, inorganic, analytical, material or chemical biology). Finally, our findings also illustrate how kinetically programmed CDC systems enable the development of easy-to-use chemistries that may help democratize chemistry and open the door to numerous technological innovations.

4.5 Acknowledgments

This work was supported by the Natural Sciences and Engineering Research Council of Canada (Grant 2014-06403) and the CREATE continuous-flow chemistry program (NSERC). A.V.-

B. is Canada Research Chair in Bioengineering and Bionanotechnology, Tier II, G.Z. acknowledges a TransMedTech Excellence Scholarship as well as a PROTEO fellowship. The authors thank Ms. Manon Laprise at l'Institut de Recherche Clinique de Montreal for performing the animal experiments (quinine injection and blood collection). The authors also thank Liliana Pedro, Dr. Nancy Schoenbrunner, and Dr. Nagarjun Narayanaswamy for valuable comments on the manuscript and help on the experiment, and the members of the Laboratory of Biosensors & Nanomachines (LBN).

4.6 Supporting information

4.6.1 Materials

Tris (2-carboxyethyl) phosphine hydrochloride (TCEP), 6-Mercaptohexanol (MCH), Quinine, ATP disodium salt hydrate, and platelet-derived growth factor-BB (PDGF-BB) were purchased from Sigma Aldrich (St. Louis, MO). Thrombin was obtained from Cayman Chemical (Ann Arbor, MI). Polyclonal anti-digoxigenin was ordered from Roche Diagnostics (Indianapolis, IN). Whole blood (newborn calf) was purchased from Innovative Research (Novi, MI). Methylene Blue II phosphoramidite (Catalog # is 10-5961-95) was purchased from Glen Research (Sterling, VA). 3'-Thiol modified column (Catalog # is CG1-5003-1) was purchased from Biosearch Technologies (Novato, CA). The standard adenine, guanine, cytosine, and thymine columns and reagents for DNA synthesis were purchased from Biosearch Technologies (Novato, CA) and ChemGenes Corporation (Wilmington, MA), respectively. The buffer used for the quinine and ATP assay is 50 mM NaH_2PO_4, 150 mM NaCl, pH 7.0. The buffer used for thrombin and PDGF-BB assay is 50 mM Tris, 140 mM NaCl, 1 mM $MgCl_2$, pH 7.4.

4.6.2 DNA sequences

The DNAs were synthesized in our laboratory using a DNA/RNA synthesizer (K&A Laborgeraete, Germany). Unlabeled DNAs were purified by reverse-phase cartridge (RPC) while labeled DNAs (methylene blue-labeled or fluorescent-labeled) were purified using high-performance liquid chromatography (HPLC) equipped with a XBridge Oligonucleotide BEH C18

column (130 Å, 2.5 µm, 4.6 mm×50 mm, 1/pkg). The signaling DNA-Dig and capturing DNA-Dig were synthesized by Biosearch Technologies (Novato, CA). The sequences of DNAs are listed in Table S4.1.

Table S4.1 Sequences of aptamer, signaling DNA, and capturing DNA

Notes	Sequence (5'-3')
Quinine aptamer	GGG AGA CAA GGA AAA TCC TTC AAT GAA GTG GGT CGA CA[276]
Signaling DNA-12	*MB**-GAA ATC CTT GTC TCC C
Signaling DNA-14	*MB*-GAT TTC CTT GTC TCC C
Signaling DNA-16	*MB*-ATT TTC CTT GTC TCC C
Signaling DNA-18	*MB*-GGA TTT TCC TTG TCT CCC
Capturing DNA-12	GGG AGA CAA GGA TTT C-*SH*
Capturing DNA-14	GGG AGA CAA GGA AAT C-*SH*
Capturing DNA-16	GGG AGA CAA GGA AAA T-*SH*
Capturing DNA-18	GAG ACA AGG AAA ATC C-*SH*
ATP aptamer	ACC TGG GGG AGT ATT GCG GAG GAA GGT[281]
Signaling DNA-14atp	*MB*-ACC TTC CTC CGC AAA T
Capturing DNA-14atp	ATT TGC GGA GGA AGG T-*SH*
Thrombin aptamer	AGT CCG TGG TAG GGC AGG TTG GGG TGA CT[284]
Signaling DNA-14thr	*MB*-CAC CCT ACC ACG GAC T
Capturing DNA-14thr	AGT CCG TGG TAG GGT G-*SH*
PDGF-BB aptamer	CAG GCT ACG GCA CGT AGA GCA TCA CCA TGA TCC TG[285]
Signaling DNA-14pdgf	*MB*-CAG GAT CAT GGT GAA C
Capturing DNA-14pdgf	GTT CAC CAT GAT CCT G-*SH*
Signaling DNA-dig[#]	*Dig*-CTT CTT CCC TTT CCT T-*MB*
Capturing DNA-dig	*SH*-AAG GAA AGG GAA GAA G

**MB= Methylene blue*

[#]*dig= Digoxigenin*

4.6.3 Electrode fabrication and electrochemical measurement

The gold working electrodes (rod) (0.2 cm diameter, 0.0314 cm^2 surface area, West Lafayette, IN) were cleaned as described in the literature.[121] The gold electrodes were functionalized using the following procedure: 1 μL of 100 μM capturing DNA was mixed with 2 μL of 10 mM TCEP for one hour at room temperature to reduce disulfide bonds. This 3 μL solution is then added to 330 μL of buffer solution (50 mM NaH_2PO_4, 150 mM NaCl, pH 7.0) in order to obtain a 300 nM capturing DNA solution in which the electrode is incubated for 2 hours at room temperature. The gold electrodes are then rinsed with deionized water and transferred into 2 mM MCH solution for 2 hours at room temperature in order to remove physically adsorbed capturing DNA and to passivate the gold electrode. The gold electrodes are then rinsed with deionized water and stored in buffer at 4 °C until use.

The electrochemical measurements were conducted at room temperature using a EmStatMUX potentiostat multiplexer (Palmsens Instruments, Netherland) equipped with a standard three-electrodes cell containing a working electrode (gold rod electrode), a counter electrode (platinum, Sigma-Aldrich), and a reference electrode (Ag/AgCl (1 M KCl), CH Instruments). The electrochemical measurements were initiated immediately after adding the 100 nM signaling DNA and 100 nM aptamer into the sample containing the target molecules. The experimental data were recorded using square wave voltammetry between -0.1 to -0.45 V. The peak currents were collected by using the manual fitting mode in the PSTrace 5.4 (2018) software and the gain (%) represents the difference of peak current in the presence and absence of target molecules. Our functionalized gold electrodes could be re-used by washing them with room temperature-deionized water. Currents or gains versus time (or versus analyte concentration) were fitted using Kaleidagraph, version 4.1 (2009).

4.6.4 Association and dissociation rates of the CDC reactions

Recognition reaction: Association and dissociation rates of the recognition reaction (quinine-aptamer) were acquired using an Applied Photophysics SX18.MV Stopped-Flow Fluorimeter in the buffer of 150 mM NaH_2PO_4 (pH 7.0). The fluorescent data were obtained by

exciting quinine at 330 nm (2.5 nm bandwidth) and monitoring the total fluorescence above 395 nM using a cut-off filter at room temperature. Single-jump experiments for measuring the association kinetic were carried out by rapidly mixing 5 volumes of 120 nM of quinine solution with 1 volume of aptamer (from 3 to 12 μM). The observed rate constants were plotted against the aptamer concentrations and fitted with a linear function. The slope of this graph represents the association rate constant of the recognition reaction. Single-jump experiments for measuring the dissociation kinetic were carried out by rapidly mixing 5 volumes of buffer with 1 volume of the complex of quinine-aptamer (0.6-2.4 μM quinine and 0.6-2.4 μM aptamer). The average observed rate constant was used as the dissociation rate constant for the recognition reaction.

Inhibition reaction: Association and dissociation rates of the inhibition reaction (aptamer-signaling DNA) were acquired using a Cary Eclipse Fluorimeter at room temperature. The fluorescent spectra were recorded at an excitation wavelength of 496 nm and an emission wavelength of 520 nm in 50 mM NaH_2PO_4, 150 mM NaCl, pH 7.0. The association rate constant of the inhibition reaction was determined using 10 nM of signaling DNA-labeled with an internal FAM and 50-300 nM concentration of aptamer. The observed rate constants were plotted against the aptamer concentrations and fitted with a linear function. The slope of this graph represents the association rate constant of the inhibition reaction. The dissociation rate constant of the inhibition reaction was obtained by rapidly adding 100-400 nM of unlabeled signaling strand to a solution containing 10 nM of signaling DNA-labeled with internal FAM in complex with 10 nM aptamer.

Signaling reaction: Association and dissociation rates of the signaling reaction (signaling-capturing DNA) were acquired using EmStatMUX potentiostat multiplexer at room temperature in 50 mM NaH_2PO_4, 150 mM NaCl, pH 7.0. The association rate constant of the signaling reaction was determined by adding 400-1000 nM of signaling DNA strand (MB-labeled) to the electrode functionalized with the capturing strand. The observed rate constants were plotted against the aptamer concentrations and fitted with a linear function. The slope of this graph represents the association rate constant of the signaling reaction. The dissociation rate constant of signaling reaction was determined by rapidly immersing the functionalized electrode complexed to the

signaling strand in different volumes of buffer (50-300 mL). The dissociation rate constant was determined using an average of the different curves.

4.6.5 Kinetic simulations

The kinetic simulations were done by solving the ordinary differential equations (ODE) of the system by using MATLAB and the ODE solver ode15s. The seven equations that represent this kinetic mechanism are the following.

$$\frac{d[L]}{dt} = -k_1[L][R] + k_{-1}[LR] \quad \text{(Eq. 1)}$$

$$\frac{d[R]}{dt} = -k_1[L][R] - k_2[R][S] + k_{-1}[LR] + k_{-2}[RS] \quad \text{(Eq. 2)}$$

$$\frac{d[S]}{dt} = -k_2[R][S] - k_3[S][C] + k_{-2}[RS] + k_{-3}[SC] \quad \text{(Eq. 3)}$$

$$\frac{d[C]}{dt} = -k_3[S][C] + k_{-3}[SC] \quad \text{(Eq. 4)}$$

$$\frac{d[LR]}{dt} = k_1[L][R] - k_{-1}[LR] \quad \text{(Eq. 5)}$$

$$\frac{d[RS]}{dt} = k_2[R][S] - k_{-2}[RS] \quad \text{(Eq. 6)}$$

$$\frac{d[SC]}{dt} = k_3[S][C] - k_{-3}[SC] \quad \text{(Eq. 7)}$$

Here, k_1 and k_{-1} are respectively the associative and dissociative rate constants for the formation of the ligand-receptor complex (LR), k_2 and k_{-2} are respectively the associative and dissociative rate constants for the formation of the receptor-signaling complex (RS) and k_3 and k_{-3} are respectively the associative and dissociative rate constants for the formation of the signaling-capturing complex (SC).

4.6.6 Pharmacokinetics assay

Ten normal CD-1 Elite mice (female, 8-weeks) ordered from Charles River were housed in a pathogen-free environment according to the protocol #19-017 approved by the Institutional Animal Care Committee (CDEA) of University of Montreal. 10 mg/kg of body weight of quinine solution (in 25 mM NaH_2PO_4, 100 mM NaCl, 6.5% DMSO, pH 7.0) was injected in the tail of each mouse, and the blood (typically 25-35 μL) was collected by Minivette POCT (50 μL, K3EDTA) from the end of the tail after 5, 15, 30, 60, 90, 120 and 240 min. Mice sample analyzed using the CDC assay on Micrux electrodes (5 mice) were transferred immediately to freezer (-20°C). Blood sample of the other five mice selected for the HPLC measurement, were centrifuged 10 min at 3000 rpm at 4°C, and their plasma were transferred immediately to freezer (-20°C).

Micrux electrode measurement: The Micrux electrodes (ED-SE1-AuPt) were ordered from MicruX Technologies (Asturias, Spain). These electrodes were cleaned by 0.05 M sulfuric acid with cyclic voltammetry (-1.5 to +1.5 V with scan rate of 0.1 V/s, and the number of scans is 10). After cleaning, the electrodes were functionalized with the capturing DNA using the same procedure as the gold rod electrode. The electrochemical measurements were performed in triplicate by rapidly mixing 1 μL aptamer (12 μM) and 1 μL signaling DNA (4 μM) with 18 μL collected mouse blood. 5 μL of "mixed" blood was then applied on three electrodes (one time point). The experimental data were recorded using square wave voltammetry between -0.15 to -0.60 V.

HPLC measurement: Quinine was extracted from mouse plasma. 1 μL of 1 mM internal standard (ofloxacin) was first added to 10 μL of mouse plasma. After, 100 μL acetonitrile (HPLC grade) was added to the plasma sample containing the internal standard and mixed for 30 s to precipitate the proteins. The mixture was centrifuged at 10 000 g for 10 min (at 4°C), then removed the precipitate but keep the supernatant. This centrifugation procedure was repeated twice. The acetonitrile was then evaporated by using a SpeedVac for 30 min (at 35°C), and 25 μL mobile phase (100 mM triethylamine/acetic acid, pH=7.0) was employed to dissolve the remaining solid. The HPLC measurements were conducted at 40°C using a 1260 Infinity II LC System from Agilent Technologies (Santa Clara, CA) equipped with an XBridge Oligonucleotide

BEH C18 column from Waters (Milford, MA). The fluorescent data were obtained by exciting quinine and ofloxacin at 330 nm and monitoring the multiple emissions at 390, 420, 440 and 460 nm. For every injection, the volume of sample was set as 22.5 µL, and the AUC (area under curve) ratio of quinine and ofloxacin in chromatogram was used to quantify quinine concentration.

4.6.7 Supporting figures

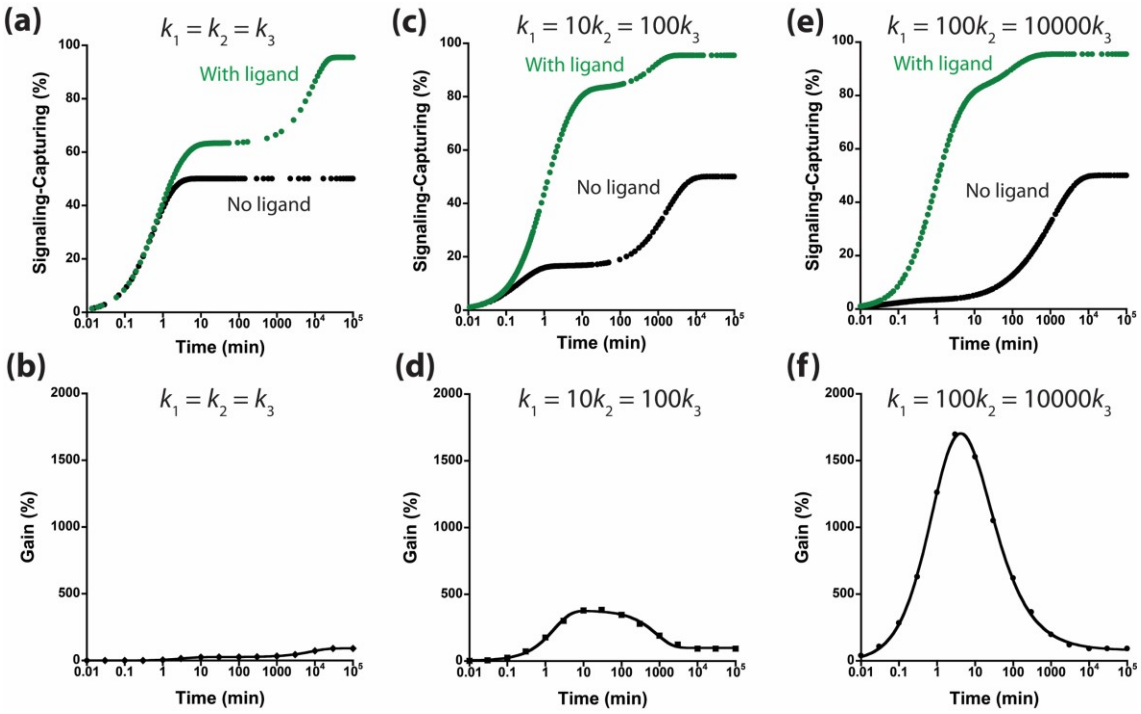

Figure S4.1 Simulation of our one-step, kinetically programmed CDC assay reveals that high gain response can be obtained rapidly when $k_1 > k_2 > k_3$. While varying k_1, k_2, and k_3 in this simulation we decided to keep the dissociation constant of all interacting pairs constant (K_D=0.01 nM) (Ligand-Receptor, Receptor-Signaling, and Signaling-Capturing). For all these simulations, we set k_3 and k_{-3}, the association and dissociation rates of the S-C interacting pair, to values similar to DNA hybridization and dissociation (0.01 nM^{-1} min^{-1} and 0.0001 min^{-1}, respectively). (a, b) For the $k_1=k_2=k_3$ simulation we set all association rates to 0.01 nM^{-1} min^{-1} while we set all dissociation rates to 0.0001 min^{-1}. (c, d) For the $k_1=10k_2=100k_3$ simulation we set the association rates to 1, 0.1 and 0.01 nM^{-1} min^{-1}, respectively while we set the dissociation rates to 0.01 min^{-1}, 0.001 min^{-1}, and 0.0001 min^{-1}, respectively. (e, f) For the $k_1=100k_2=10000k_3$ simulation we set the association rates to 100, 1 and 0.01 nM^{-1} min^{-1}, respectively while we set the dissociation rates to set to 1 min^{-1}, 0.01 min^{-1}, and 0.0001 min^{-1}, respectively.

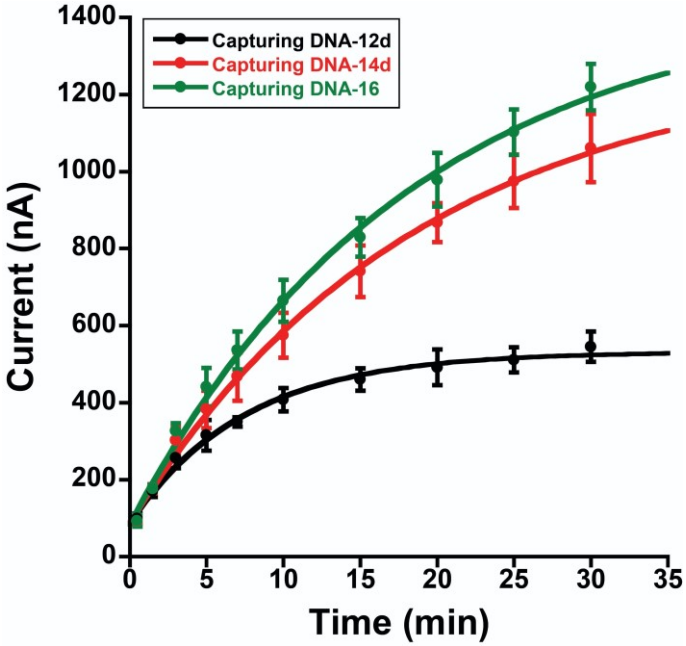

Figure S4.2 Hybridization kinetics between the signaling DNA-16 (100 nM) and surface-attached capturing DNA with different complementary length (12, 14, and 16). 16 Watson-Crick base pair interaction is enough to drive the hybridization reaction to completion. The concentrations of capturing DNAs and signaling DNA used in this assay are 300 nM and 100 nM, respectively.

Here are the DNA sequences:

Signaling DNA-16: MB-5'-ATT TTC CTT GTC TCC C-3'

Capturing DNA-12d: 5'-GAC AAG GAA AAT-3'-SH

Capturing DNA-14d: 5'-GAG ACA AGG AAA AT-3'-SH

Capturing DNA-16: 5'-GGG AGA CAA GGA AAA T-3'-SH

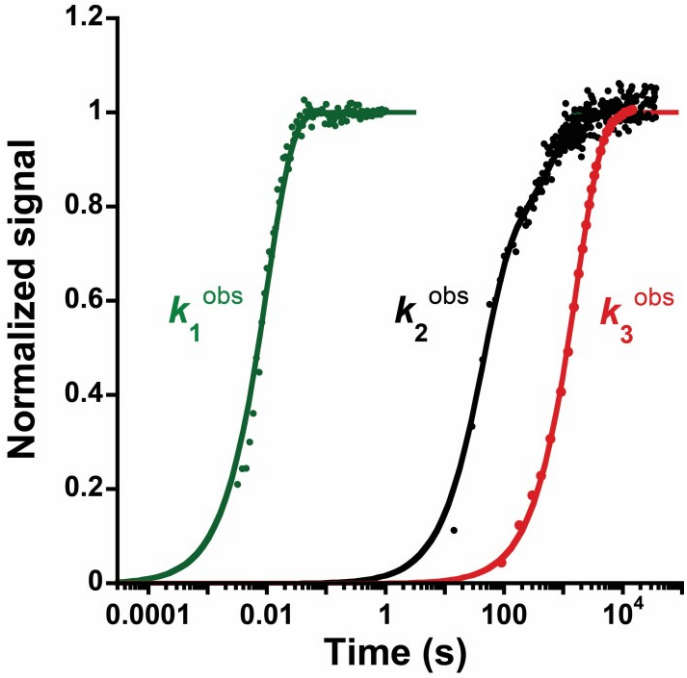

Figure S4.3 Kinetic traces of our three different reactions. k_1: Association kinetic for the quinine-aptamer complex. k_2: Association kinetic for the aptamer-signaling complex. k_3: Association kinetic for the signaling-capturing complex. The observed rate constant k_1^{obs}, k_2^{obs}, and k_3^{obs} are 98.7 s^{-1}, 0.0230 s^{-1}, and 0.000596 s^{-1}, respectively.

k_1: Binding between quinine and its aptamer (5'-GGG AGA CAA GGA AAA TCC TTC AAT GAA GTG GGT CGA CA-3') was monitored using the fluorescence of quinine with an Applied Photophysics SX18.MV stopped-flow fluorimeter by exciting at 330 nm and monitoring the total fluorescence above 395 nM using a cut-off filter.

k_2: Binding between the aptamer (5'-GGG AGA CAA GGA AAA TCC TTC AAT GAA GTG GGT CGA CA-3') and the signaling DNA (5'-ATT TTC CTT GTC TCC C-3') was monitored using a covalently attached FAM on a modified thymine (see underlined nucleotide in the signaling DNA) and a Cary Eclipse Fluorimeter.

k_3: Binding between the signaling DNA (MB-5'-ATT TTC CTT GTC TCC C-3') and the capturing DNA (5'-GGG AGA CAA GGA AAA T-3'-SH) attach on the god electrode surface was obtained by using square wave voltammetry (electrochemistry). The concentrations of capturing DNA and signaling DNA used in this assay are 300 nM and 100 nM, respectively.

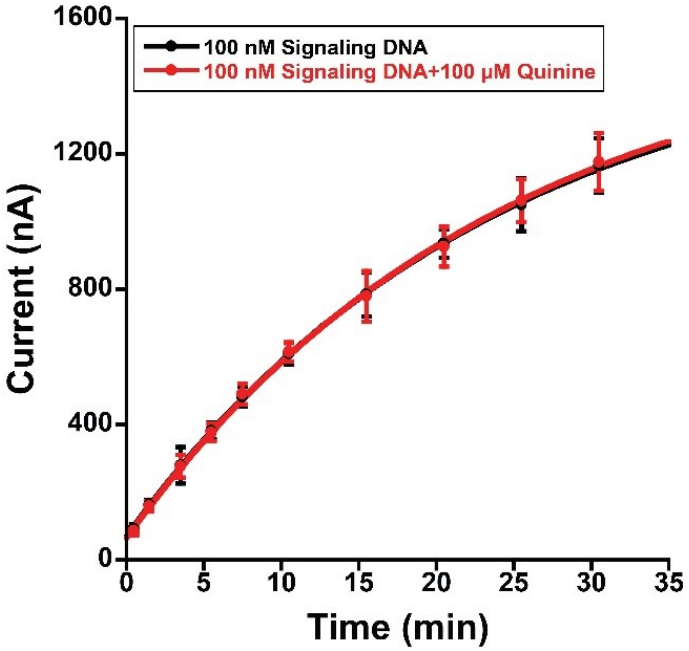

Figure S4.4 Addition of quinine to the signaling reaction (hybridization between the signaling strand and the capturing strand attached on the electrode) does not modify its efficiency. The concentrations of capturing DNA-16 and signaling DNA-16 used in this assay is 300 nM and 100 nM, respectively.

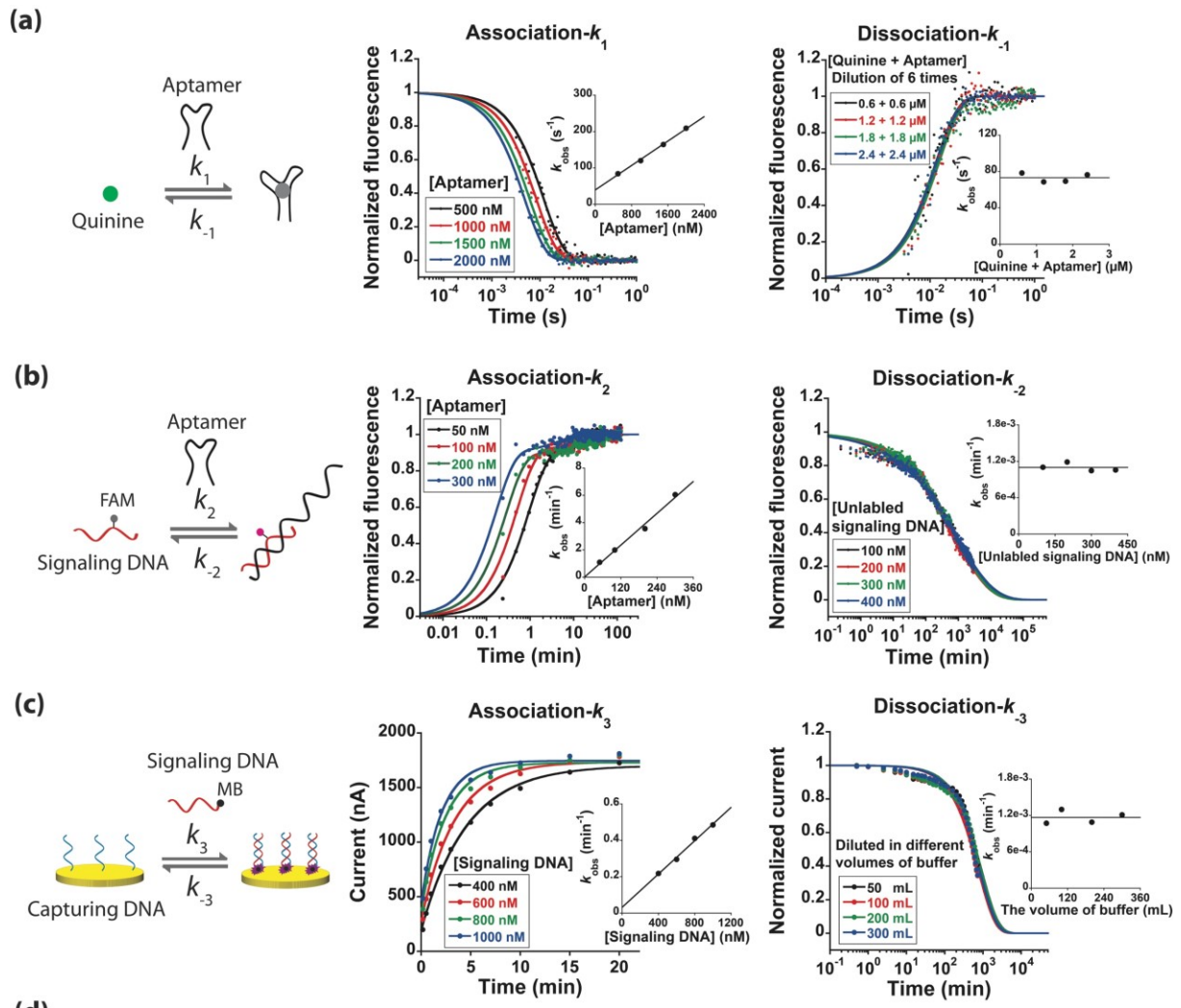

(d)

	k_x (nM^{-1} min^{-1})	k_{-x} (min^{-1})	K_D (nM)*
1. Quinine-Aptamer	5.04	4390	871
2. Aptamer-Signaling DNA	0.0195	0.00110	0.0564
3. Signaling-Capturing DNA	0.000458	0.00117	2.55

*K_D was estimated using k_{-x} / k_x

Figure S4.5 Association and dissociation rate constants of the (a) recognition reaction (quinine-aptamer), the (b) inhibition reaction (aptamer-signaling DNA), and the (c) signaling reaction (signaling-capturing DNA). The association rate constants of all three reactions were obtained from the slope of the k_{obs} versus [DNA] graph. The dissociation rate constants of all three reactions were obtained directly from the average k_{obs} of dissociation kinetic. See section 4 of "Association and dissociation rates of the CDC reactions" for all details. (d) k_{on}, k_{off}, and K_D for the recognition, inhibition and signaling reactions. These analyses have been performed using Kaleidagraph, version 4.1 (2009). The concentrations of capturing DNA used in this assay is 300 nM.

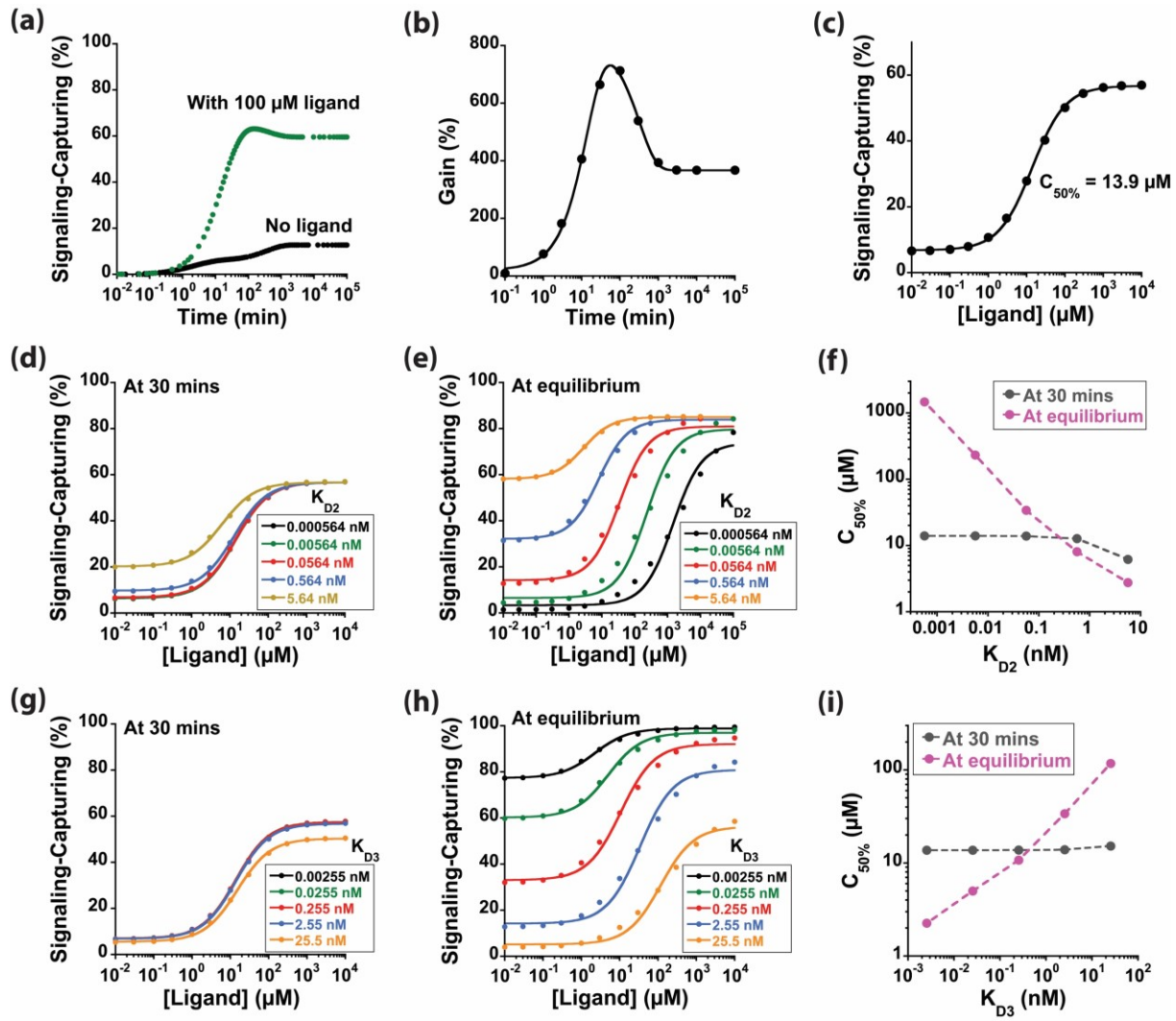

Figure S4.6 (a-b) Numerical simulations of the quinine CDC assay using the experimentally derived rate constants (see Figure S4.5 for all parameters). c) The predicted observed $C_{50\%}$ after 30 min (13.9 µM) increases by 35.9-times compared to the K_D of quinine-aptamer (0.387 µM, see Figure S5). (d-f) The CDC "kinetic" assay is relatively insensitive to variation in affinity between the aptamer and signaling DNA (K_{D2}). When changing K_{D2} by up to 4 orders of magnitude, the $C_{50\%}$ of the CDC assay obtained after 30 min only varies between 6.15 and 14.0 µM. In contrast, when performed at equilibrium (>100 h) the same K_{D2} variation displaces the $C_{50\%}$ from 2.75 to 1468 µM for the most stable aptamer-signaling pair. (g-i) The CDC "kinetic" assay is also relatively insensitive to variation in affinity between the signaling and capturing DNA (K_{D3}). When changing K_{D3} by up to 4 orders of magnitude, the $C_{50\%}$ of the CDC assay obtained after 30 min only varies between 15.2 and 13.8 µM. In contrast, when performed at equilibrium (>100 h) the same K_{D3} variation displaces the $C_{50\%}$ from 117 to 2.25 µM for the most stable signaling-capturing pair.

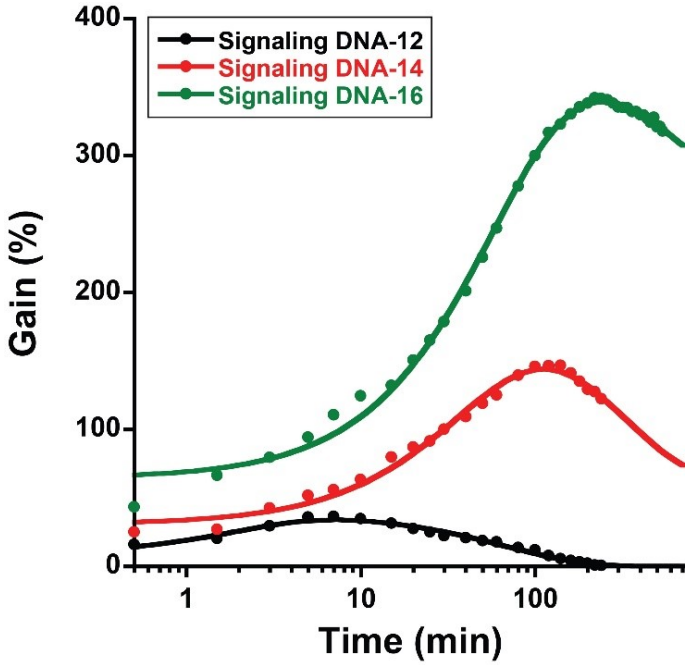

Figure S4.7 The optimal gain of our kinetically programmed CDC assay is reached before equilibrium. Numerical simulations of the quinine assay (Figure S6a-c) predict that the maximum gain of the assay should take place at around 100 min and that this gain should reduce significantly with longer equilibration time. This is due to the fact that in absence of quinine, the kinetically trapped signaling DNA (trapped with aptamer) will undergo slow spontaneous dissociation (k_{-2} = 0.00110 min^{-1}, see Figure S4.5d) enabling more signaling DNA to hybridize to the capturing DNA (creating a higher current background in absence of quinine and therefore a lower gain). When testing a much longer reaction time (9 hours) we find indeed that the gain of the assay starts decreasing after 4 hours. Numerical simulations predicted that k_{-2} might be even slower than the value measured using a competition experiment. To validate that this is due to the slow spontaneous dissociation of the signaling DNA from the aptamer (k_{-2}) we also tested signaling DNA with faster k_{-2}, making 14 and 12 Watson-Crick base pairs with the aptamer. These signaling strands generated assays with faster equilibration rates and saw their maximum gain reached at 2 hours (signaling DNA-14) and 5 min (signaling DNA-12). These kinetics were fitted using a double exponential function. The concentrations of capturing DNA, signaling DNAs, aptamer, and quinine used in this assay are 300 nM, 100 nM, 100 nM, and 100 µM, respectively.

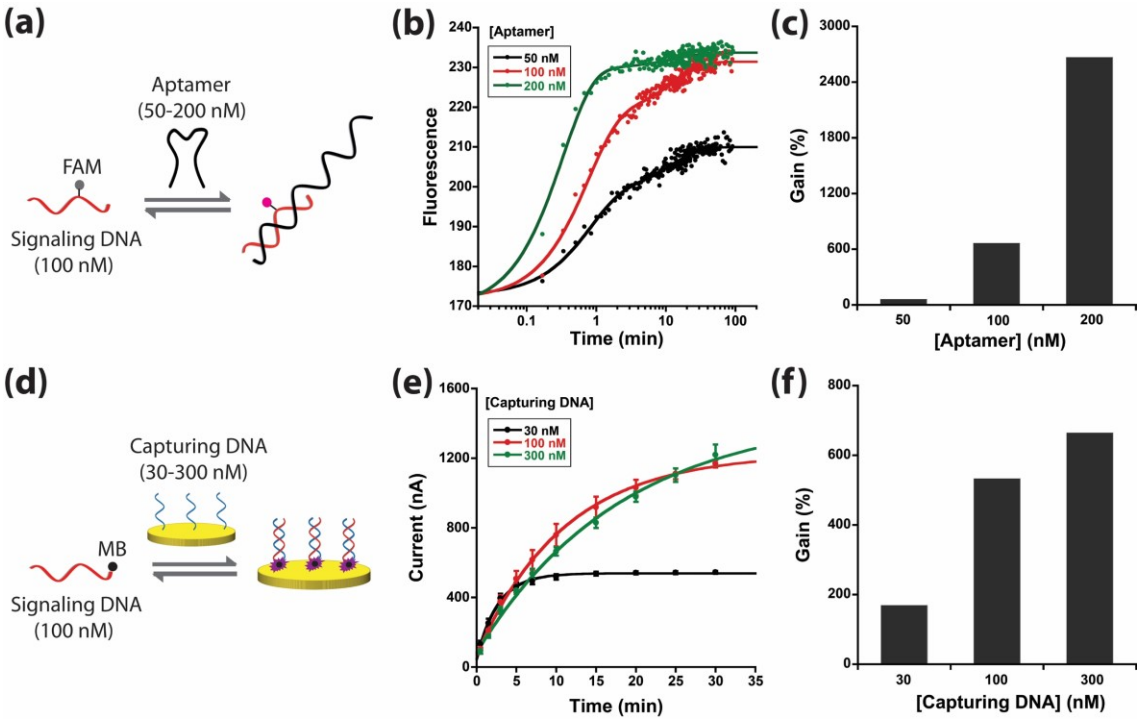

Figure S4.8 (a, b) Kinetic binding curves between signaling DNA (100 nM) and aptamer (50-200 nM). The observed rate constants are 1.28 min^{-1}, 1.34 min^{-1} and 3.03 min^{-1}, respectively. The fluorescence data was obtained by using a Cary Eclipse Fluorimeter. (c) Simulated gains obtained by using the experimentally derived rate constants. (d, e) Kinetic binding curves between signaling DNA (100 nM) and capturing DNA (30-300 nM). The observed rate constants for 30 nM, 100 nM, 300 nM capturing DNA are 0.376 min^{-1}, 0.0913 min^{-1}, and 0.0550 min^{-1}, respectively. (f) Simulated gains obtained by using the experimentally derived rate constants.

Table S4.2 The theoretical calculation of K_D between aptamer and signaling DNA 12-18.

	ΔG (kcal/mol) *	Theoretical K_D #
Signaling DNA-12	-15.3	6.08 pM
Signaling DNA-14	-17.5	0.148 pM
Signaling DNA-16	-19.0	0.0118 pM
Signaling DNA-18	-23.0	0.0000138 pM

*The ΔG values were estimated using *mfold* at 25 °C with 200 mM Na^+ concentration (experimental conditions). #The theoretical K_D was calculated by the equation of $\Delta G = RT \ln K_D$, in which R is the ideal gas constant, T is thermodynamic temperature. The following are the DNA sequences,

Aptamer: 5'- GGG AGA CAA GGA AAA TCC TTC AAT GAA GTG GGT CGA CA-3'

Signaling DNA-12: *MB*-5'-GAA ATC CTT GTC TCC C-3'

Signaling DNA-14: *MB*-5'-GAT TTC CTT GTC TCC C-3'

Signaling DNA-16: *MB*-5'-ATT TTC CTT GTC TCC C-3'

Signaling DNA-18: *MB*-5'-GGA TTT TCC TTG TCT CCC-3'

Table S4.3 The theoretical calculation of K_D between signaling DNA-16 and capturing DNA 10d-16d.

	ΔG (kcal/mol) *	Theoretical K_D #
Capturing DNA-10d	-9.9	55 nM
Capturing DNA-12d	-13.0	0.295 nM
Capturing DNA-14d	-15.5	0.00434 nM
Capturing DNA-16	-19.0	0.0000118 nM

*The ΔG values were estimated using *mfold* at 25 °C with 200 mM Na^+ concentration (experimental conditions). #The theoretical K_D was calculated by the equation of $\Delta G = RT \ln K_D$, in which R is the ideal gas constant, T is thermodynamic temperature. The following are the DNA sequences,

Signaling DNA-16: *MB*-5'-ATT TTC CTT GTC TCC C-3'

Capturing DNA-10d: 5'-CAA GGA AAA T-3'-SH

Capturing DNA-12d: 5'-GAC AAG GAA AAT-3'-SH

Capturing DNA-14d: 5'-GAG ACA AGG AAA AT-3'-SH

Capturing DNA-16: 5'-GGG AGA CAA GGA AAA T-3'-SH

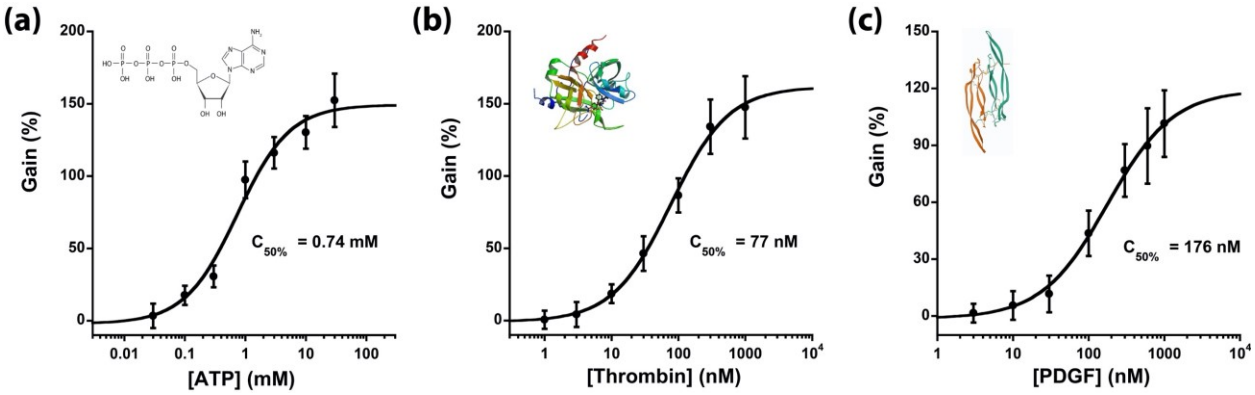

Figure S4.9 One-step kinetically programmed CDC assay for the detection of other ligand molecules. (a) The binding curve of ATP detection with a $C_{50\%}$ of 0.74 mM. (b) The binding curve of thrombin detection with a $C_{50\%}$ of 77 nM. (c) The binding curve of PDGF detection with a $C_{50\%}$ of 176 nM. The incubation time in these assays is 5 min. The concentrations of capturing DNAs, signaling DNAs, and aptamers used in this assay are 300 nM, 100 nM, and 100 nM, respectively. The error bars represent the standard deviation obtained from three electrodes.

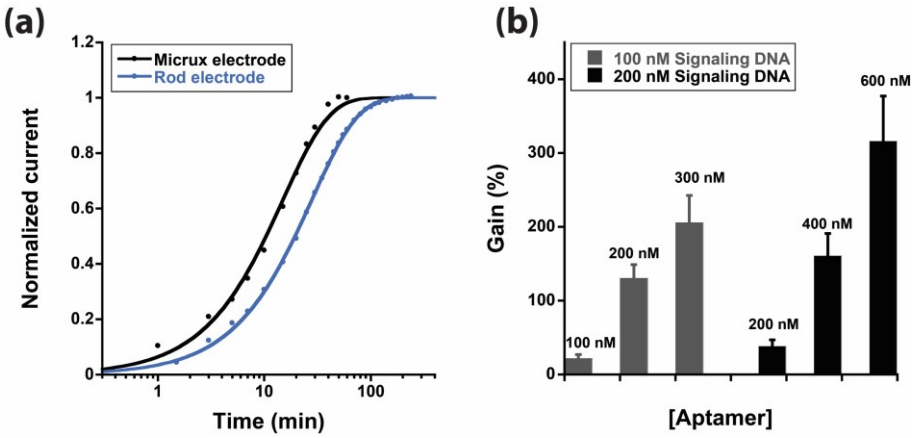

Figure S4.10 Optimization of the CDC assay on ED-SE1-AuPt Micrux electrodes. (a) Kinetics of hybridization of the signaling DNA to the capturing DNA (k_3) on Micrux (black) are around two times faster than on the rod (blue) electrodes (the observed rate constants are 0.0667 min^{-1} and 0.0357 min^{-1}, respectively). (b) Optimizing the gain of the CDC assay on Micrux electrodes by tuning the concentration of signaling DNA and aptamer (programming k_2 and k_3). The gain of the assay can be improved by increasing k_2 with a higher concentration of aptamer: 100 to 300 nM provides gains from 21.5% to 205.6%. We also tested the assay at higher concentration of signaling DNA (200 nM), which increased k_3 and require higher concentration of aptamer (200 to 600 nM) to reach similar gains (38.2% to 316%). We selected concentrations of signaling DNA of 200 nM and aptamer of 600 nM for performing the pharmacokinetics analysis. These optimization experiments were performed in fresh mouse blood by spiking 100 µM of quinine and the gain was determined after 5 min of reaction time. The concentration of capturing DNA used in this assay is 300 nM. The error bars represent the standard deviation obtained from three electrodes.

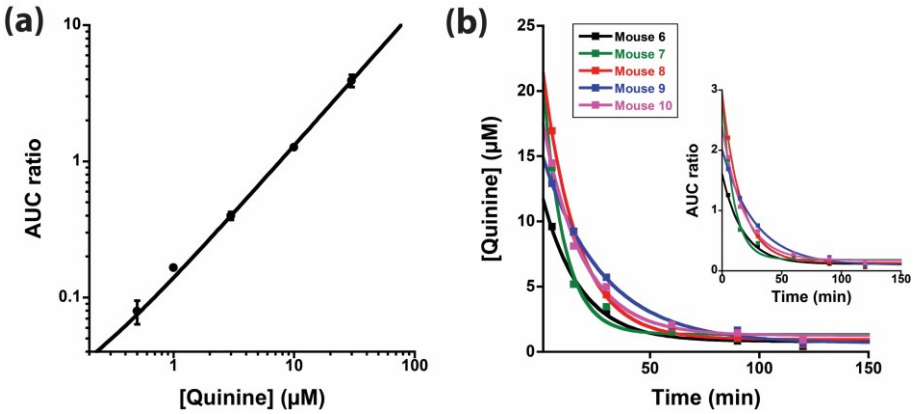

Figure S4.11 Quinine pharmacokinetic profile on five mice determined using HPLC. (a) The standard curve obtained for HPLC measurements. The fluorescence ratio indicates the AUC (area under curve) ratio of the quinine and the ofloxacin in the HPLC chromatogram. (b) Individual pharmacokinetic results obtained on five mice using HPLC. Insert: Raw AUC ratio for five mice.

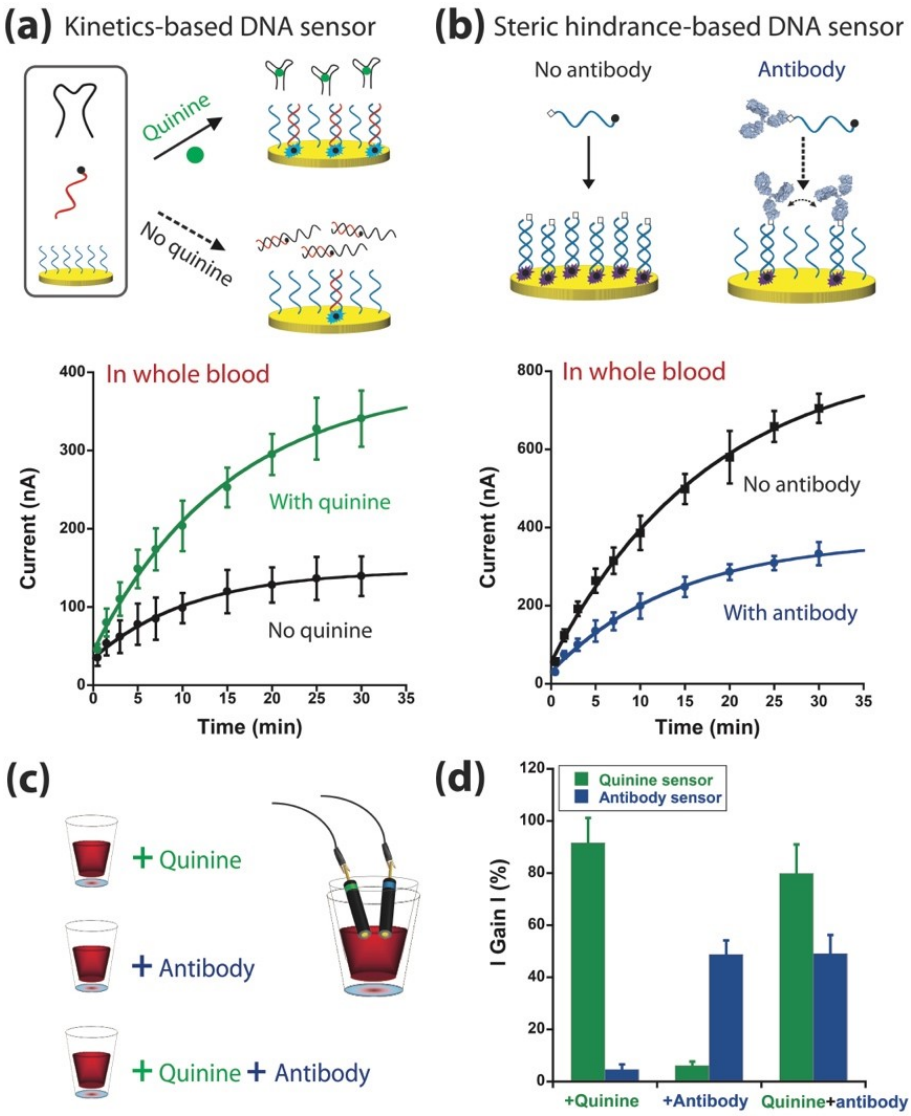

Figure S4.12 The one-step, kinetically programmed CDC assay works directly in whole blood and can be performed simultaneously (*i.e.,* in a multiplexed format) with another DNA-based assay. (a) The one-step quinine assay performs with similar efficiency and rate directly in whole blood (100 μM quinine is used in these experiments); (b) Electrochemical steric-hindrance hybridization assay (eSHHA) for antibody detection (100 nM antibody is used in this signal-off assay). (c, d) Two electrodes, each functionalized with a specific capturing DNA, are used to detect quinine (100 μM) and an antibody (100 nM) simultaneously in whole blood; (d) Signal gain in the absolute value obtained after 5 min when whole blood is spiked with quinine alone, with antibody alone or with a mixture of quinine and antibody. The concentrations of capturing DNA, signaling DNA, and aptamer used for quinine assay are 300 nM, 100 nM, and 100 nM, respectively. The concentrations of capturing DNA and signaling DNA used for antibody assay are 300 nM and 100 nM, respectively. The error bars represent the standard deviation obtained from three electrodes.

Chapter 5: Summary and Perspectives

5.1 Summary

The overarching aim of this Ph.D. work was to develop the next generation of eDNA sensing mechanisms that possess outstanding features to enable rapid and efficient commercialization. More specifically, the main focus of this work addressed the main limitations of current eDNA sensor technologies, which include: (i) the reproducibility issue of the electrodes linked to fabrication challenges and limited storage half-life; (ii) the complexity (and elevated cost) of dual-labeled DNA strands; (iii) the time-consuming procedures to develop sensors with optimal gain and dynamic range and; (iv) the typical signal baseline drift observed upon sensor immersion in the complex biological matrix (e.g., whole blood). Although we haven't developed one ideal, universal sensing mechanism that overcomes all these limitations, we have successfully proposed three novel sensor families that solve most of these issues.

We first developed eSHRI, a signaling mechanism that combines three steric hindrance effects and a novel redox inhibition mechanism that is insensitive to surface density variation. This specific signaling mechanism displays low or no variation to significant change in electrode fabrication (*e.g.,* DNA density on sensor surface) and storage time (*e.g*., sensor degradation). We have also developed a molecular barrier assay that does not require dual labeling of DNA strands, which remains expensive and time-consuming to synthesize. This assay works by attaching the recognition element and redox molecule on two separate DNA strands that hybridize to each other. The novelty of this strategy is that it enables to create high signal gain for the detection of any large protein analytes. Finally, we also took advantage of the high recognition ability of aptamers, an emerging class of antibody-like DNA molecules, and developed a kinetically programmed molecular system that enables the one-step detection of any molecular markers in a drop of blood in less than five minutes. This strategy also solves numerous challenges of current aptamer-based eDNA sensors by: (1) simplifying the design and optimization strategy to obtain high "signal-on" gain; (2) employing the more stable high-density sensors.[156] All the above-mentioned signaling mechanisms are also exempted from the typical signal drift observed when

deploying the sensor in complex biological samples. This is due to the fact that the redox molecules in these assays are not being attached directly on the surface of the sensor but are rather conjugated to a signaling DNA that can hybridize to an electrode-attached complementary DNA in any type of biological sample (e.g., see also eSHHA[132]).

One of the main advantages of the eSHRI signaling mechanism is that it solves one of the most significant limitations of current eDNA sensors, which is their high sensitivity to variation in DNA density linked to fabrication or ageing processes (Table 5.1). This signaling mechanism also allows creating sensors displaying among the highest gain obtained to date (-93%, Table 5.1) while still displaying low detection limits (low nM). Three types of steric hindrance mechanisms have been exploited to develop eSHRI: (1) analyte-analyte steric hindrance, (2) analyte-DNA layer steric hindrance, (3) analyte-electrode steric hindrance. The first mechanism is also exploited in eSHHA, and the second mechanism only works efficiently with sensors fabricated at high surface density. On the other hand, the third mechanism (analyte-electrode steric hindrance) performs similarly at high and low surface densities. In addition to those three steric hindrance mechanisms, we have also integrated a novel redox inhibition mechanism that is relatively insensitive to sensor density. This mechanism works by having the protein analyte move in close proximity (< 5 nm) to the redox molecule, which can then be inhibited through a binding-induced mechanism on the analyte surface. More specifically, the electrochemical activity of the redox molecule may be inhibited through direct contact with a protein analyte, thus resulting in an efficient signal-off mechanism. This unique redox inhibition mechanism is able to display a high signal gain of -83% even when employing sensors fabricated at low surface density (compared to -7% for the traditional eSHHA). In addition, eSHRI could also be used in a competition format[134] to detect any small antigen molecules for which we have a protein recognition element (*e.g.* antibodies) (Figure 5.1). We are currently testing and validating the usefulness of this assay format, which would drastically improve the universality of this class of sensors.

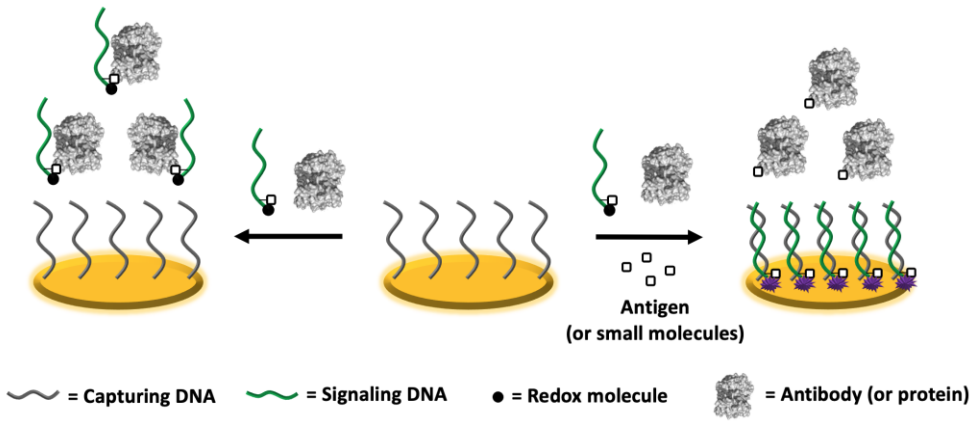

Figure 5.1 eSHRI can also be adapted into a competition format to detect antigens or small molecules. In the absence of antigen (or small molecules), a reagent antibody (or specific protein) is available to bind a signaling DNA that contains a copy of the antigen, resulting in a very low hybridization efficiency and thus low electrochemical signal due to the steric hindrances and redox inhibition. In the presence of antigen, the antibody preferentially binds the free antigen molecules instead of the antigen conjugated to the signaling DNA, thus leaving the signaling DNA unbound and free to efficiently hybridize to the capturing DNA on the surface of the electrode, generating a high electrochemical signal.

The main advantage of the molecular barrier signaling mechanism is that it does not require complicated and time-consuming dual-labelling conjugation strategies to DNA. In this assay, the recognition element of a target protein is attached to the capturing DNA that is immobilized on the surface of the electrode, whereas the redox molecule is attached to the signaling DNA. Upon binding to its recognition element, the target protein creates a molecular barrier that prevents the signaling DNA from reaching the capturing DNA on the surface of the electrode. We found that short capturing DNAs create more efficient molecular barriers and produce a higher signal gain (*e.g.,* -89% for an 8-nt capturing DNA *versus* -40% for a 16-nt capturing DNA). This is likely because short ssDNA is less flexible and can create a smoother, more compact surface in which a more compact molecular barrier can assemble. Using this sensing architecture, we have also characterized a new high gain "kick-out" sensing mechanism where the target protein can also trigger the dissociation of the signaling DNA from a preformed capturing-signaling DNA duplex. Like the eSHRI assay, the molecular barrier assay can likely be

adapted in a competition format to detect small antigens using specific antibodies (see Figure 5.2).

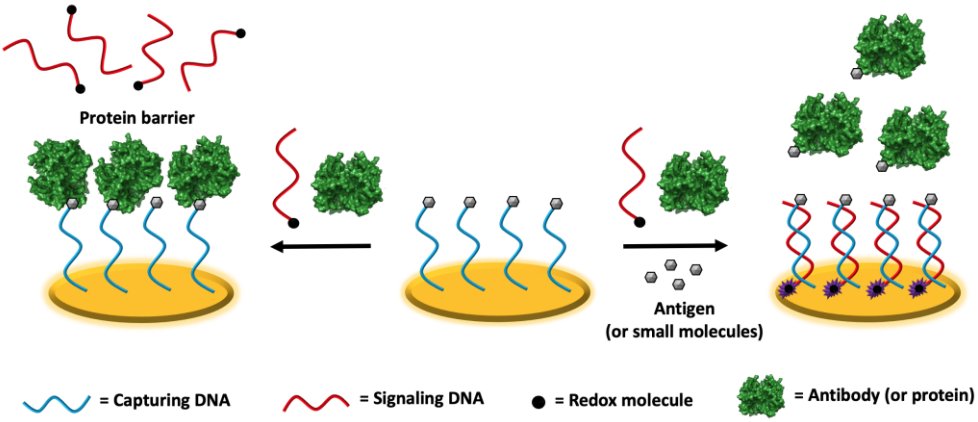

Figure 5.2 The molecular barrier assay can also be adapted into a competition format to detect antigens or small molecules. In the absence of antigen (or small molecules), a reagent antibody (or specific protein) is available to bind to capturing DNAs containing a copy of the antigen, resulting in a compact molecular barrier and low electrochemical signal. In the presence of antigen, the antibody preferentially binds the free antigen molecules instead of the antigen conjugated to the capturing DNA, thus leaving the signaling DNA unbound and free to efficiently hybridize to the capturing DNA on the surface of the electrode, generating a high electrochemical signal.

Finally, our kinetically programmed electrochemical assay provides a simple modular and predictable strategy to adapt any aptamer into high gain signal-on sensors (~248%) that work on stable "high density" electrodes. For example, in contrast to other traditional aptamer-based eDNA sensors,[123, 124, 286] our method does not require any chemical modification of the aptamer and tuning its stability, which often affects the performance (specificity, selectivity, affinity…) of the aptamer. Moreover, this specific sensing architecture does not require a case-by-case optimization of the surface probe density for each novel sensor.[153] It reaches an optimal signal gain at a high surface density, thus providing a high electrochemical current that can be detected using inexpensive potentiostats. This strategy is modular and can be rapidly adapted for most aptamers, as demonstrated in my thesis for the detection of quinine, ATP, thrombin, and PDGF. Importantly, we also showed that this sensing architecture can be adapted in an easy-to-use,

point-of-care format that enabled us to perform various drug monitoring applications (see e.g., our pharmacokinetics study of quinine in mice blood by using a drop of blood -Figure 4.5).

Table 5.1 summarizes the characteristics of our three novel sensing mechanisms and their competitive advantage over other eDNA sensing technologies. Importantly, these three methods have eliminated the problem of baseline drift in blood samples that have plagued other popular eDNA sensors. To our knowledge, eSHRI is the only eDNA sensor that is insensitive to variation in surface density. However, it still requires a complex and expensive dual-labeling strategy. Another main advantage of our three novel methods is that they all provide high or moderate signal gain with few optimizations required. In contrast, other methods, such as eSHHA, E-AB sensors, and collision dynamic-based sensors usually display highly variable gains and require time-consuming and complex optimization strategies. It is worth mentioning that two recently developed approaches from the lab of Kelley (University of Toronto) and Li and Soleymani (McMaster University), namely molecular pendulum[130] and e-RCDs[287], display very high signal-on gain. However, the pendulum approach likely suffers from signal drift when performed in blood, while the e-RCD approach remains long to perform (>30 min).

Table 5.1. Advantages and limitations of most popular eDNA sensors architectures

	Analytes	Detection time	The limit of detection	Baseline drift[@]	Surface density	Dual labeling	Maximum signal gain*
eSHRI *(2022)*	all[#]	< 5 min	up to nM	no	independent	yes	signal-off: -93.6%
Molecular barrier *(2022)*	all[#]	< 5 min	up to nM	no	dependent	no	signal-off: -90%
Kinetically programmed *(2020)*	all	< 5 min	up to nM	no	dependent	no	signal-on: 248%
eSHHA (2015)[132]	all[#]	< 5 min	up to nM	no	dependent	yes	signal-off: -60%
E-AB sensors (2005)[61, 124]	all	s	up to nM	yes	dependent	no	signal-off: -35% signal-on: 270%
Collision dynamic sensors (2009)[125, 129]	all[#]	s	up to nM	yes	dependent	no	signal-off: -45% signal-on: 100%[‡]

Molecular pendulum (2021)[130]	proteins + virus	ms	pg/ml or 4000 copies/mL	likely	dependent	no	signal-on: >900%‡
e-RCDs (2021)[287]	all	>30 min	10CFU	not sure	dependent	no	signal-off: -88%‡ signal-on: >4000%‡

#The small molecules detection can be achieved by using a competition format.

@The baseline drift indicates the electrochemical signal is unstable in the blood or serum samples at the beginning of the measurement.

*The gain of signal-off: **High**: -80% to -100%; **Moderate**: -50% to -80%; **Low**: below -50%. For example, upon adding analytes, an assay that reduces the signal from 100 nA to 30 nA has a gain of (30 nA-100 nA)/100 nA = -70%.

The gain of signal-on: **High**: above 400%; **Moderate**: 100% to 400%; **Low**: below 100%. For example, upon adding analytes, an assay that increases the signal from 30 nA to 100 nA has a gain of (100 nA-30 nA)/30 nM = 233%.

‡The signal gain is estimated from the references.

Our novel eDNA sensors also compares advantageously with other currently commercial point-of-care testing (POCT) technologies including the glucose meter, lateral flow assays, and microfluidic-based platforms. Glucose meter is one of the most successful POCT technologies in the world, and it has greatly alleviated the suffering of millions of people with diabetes. However, the glucose meter for continuous monitoring applications still suffers from biofouling and enzyme degradation. Furthermore, the signaling mechanism of glucose meter cannot be adapted for the (ideally multiplexed) detection of other molecular markers for diabetes (e.g., insulin, ketone bodies, and glucagon).[13] Lateral flow assay is a dominant rapid diagnostic technology in the field of POCT, especially useful in resource-limited areas. It can measure a variety of biomarkers including hormones, nucleic acids, antibodies, bacteria, and viruses by the naked eye.[288] However, lateral flow assays can typically only detect biomarkers qualitatively, which is not sufficient for many applications that require quantitative analysis of biomarkers (e.g., to accurately assess the stage of disease, possible complications, and subsequent treatment options).[289] Finally, microfluidic platforms are emerging widely adopted POCT technology, which enable the precise control of fluids, thereby greatly reducing the volume of sample required. In addition, it can easily integrate with various signal transduction methods, such as optics,[290] electrochemistry,[291] surface plasmon resonance (SPR),[292] magnetism,[293] and even acoustics.[294-296] However, these approaches are still too expensive and complex for most POCT settings (e.g., at home). Although our three novel methods display many advantages, the extent to which they

are universally applicable remains to be demonstrated. For example, it is possible that some target proteins may not bind the redox molecules in the eSHRI assay. This may depend on whether the structure and chemical composition of the proteins will produce a sufficient high-affinity site to bind methylene blue or other redox molecules. For the molecular barrier assay, one can imagine those specific recognition elements attached to the surface of the electrode may create more or less non-specific adsorption of certain contaminant proteins in a complex biological sample. These non-specific binding events may create non-specific molecular barriers that lead to false positive. Even though our kinetically programmed-CDC assay was able to rapidly detect quinine in mouse blood in small sample volumes (5 min, 5 µL), its unsatisfactory sensitivity (~2 µM) prevented it from providing a complete pharmacokinetics kinetic result (especially after 60 min), so further improving the sensitivity is one of future research work. Moreover, the kinetically programmed CDC assay may require more efforts to commercialize due to the existence of multiple reaction components that must be integrated into an easy-to-use prototype.

5.2 Perspectives

Three novel sensing mechanisms displaying many advantages over currently available eDNA sensors have been developed in this Ph.D. thesis. However, much work remains to be done to ensure their successful commercialization. One critical step towards commercialization consists of adapting these sensing mechanisms into sensors that enable clinical and business-relevant markers and validate their usefulness via correlation studies using human blood samples. To this end, we are currently adapting the eSHRI signaling mechanism into a Covid-19 antibody sensor while we are employing the molecular barrier signaling mechanism to develop a sensor for the detection of various illicit drugs (using the competition format presented in Figure 5.2). One of the main challenges in achieving this goal remains the development of scalable chemistry to attach the various recognition elements (*i.e.*, Covid peptide epitopes and/or drugs) to the DNA strands. Another challenge is to develop a prototype that could be employed and adapted for monitoring all three assays introduced in this thesis. As demonstrated in chapter 4, we have made significant progress towards this goal by achieving the detection of quinine, an antimalaria drug, in a drop of blood of living mice using an integrated electrode (from the Micrux company) that

requires less than 10 µL blood sample. However, the workflow of this assay is still complicated for the untrained user as it involves the use of a pipette. In collaboration with a Montreal-based start-up called Anasens, we are currently in the process of developing an easy-to-use consumable that would allow untrained users to easily perform analyte detection in a drop of blood in the comfort of their home. But this is another story that will be told in the near future.

Publications

List of journal articles:

1. **Guichi Zhu**, Alexis Vallée-Bélisle*, Density independent electrochemical DNA sensors that use steric hindrance and redox inhibition mechanisms, *will be submitted in 2022.*
2. **Guichi Zhu,** Alexis Vallée-Bélisle*, An electrochemical molecular barrier assay for the rapid detection of proteins directly in whole blood, *will be submitted in 2022.*
3. **Guichi Zhu**, Dominic Lauzon, Carl Prévost-Tremblay, Arnaud Desrosiers, Bal-Ram Adhikari, Alexis Vallée-Bélisle*, Rapid, one-step molecular detection in a drop of blood using kinetically programmed constitutional dynamic chemistry, *under review by Nature Chemistry*, 2020.

List of books:

1. Dominic Lauzon, **Guichi Zhu**, Alexis Vallée-Bélisle*, Chapter 7: Engineering DNA Switches for DNA Computing Applications, DNA- and RNA-Based Computing Systems, Edited by Evgeny Katz, Wiley, 2020.

List of patents:

1. Alexis Vallée-Bélisle, **Guichi Zhu**, Kinetically programmed systems and reactions for molecular detection, WO2019232618A1, June 2018.
2. Alexis Vallée-Bélisle, **Guichi Zhu**, New signaling mechanism that employs steric hindrance/redox inhibition and molecular barrier assay for molecular detection, *Submitting*, 2021.

List of conference presentations:

1. The 19th Edition of PROTEO Annual Symposium, Québec, May 9-10, 2019. (Poster)
2. Gordon Research Seminar (GRS)---Bioanalytical Sensors, Newport, June 23-24, 2018. (Poster)
3. The Third Functional DNA Nanotechnology (FDN) Workshop, Rome, June 6-8, 2018. (Poster)
4. The 18th Edition of PROTEO Annual Symposium, Québec, May 17-18, 2018. (Poster)
5. The 3rd CREATE-CFS Annual Symposium, Montréal, September 8, 2017. (Poster)
6. CREATE-CFS Summer School, Orford, June 28-29, 2017. (Oral)
7. GRSTB Symposium/TransMedTech Institute of Montreal, Biomedical Nanotechnologies, Montréal, June 5, 2017. (Poster)
8. The 17th Edition of PROTEO Annual Symposium, Québec, May 11-12, 2017. (Poster)
9. The 2nd CREATE-CFS Annual Symposium, Montréal, September 16, 2016. (Poster)
10. CREATE-CFS Summer School, Montréal, June 16-17, 2016. (Oral)
11. The 7th CGCC Annual Meeting, Montréal, June 3, 2016. (Poster)
12. The 16th Edition of PROTEO Annual Symposium, Québec, May 12-13, 2016. (Poster)
13. The 98th Canadian Chemistry Conference and Exhibition, Ottawa, June 13-17, 2015. (Poster)

References

1. Giljohann, D.A. & Mirkin, C.A. Drivers of biodiagnostic development. *Nature* **462**, 461-464 (2009).
2. Yager, P., Domingo, G.J. & Gerdes, J. Point-of-care diagnostics for global health. *Annu Rev Biomed Eng* **10**, 107-144 (2008).
3. Andreas, H., Carsten, R. & Martina, Z. *From Smart Health to Smart Hospitals*, Vol. 8700. (Springer, Cham, 2015).
4. Füzéry, A.K., Levin, J., Chan, M.M. & Chan, D.W. Translation of proteomic biomarkers into FDA approved cancer diagnostics: issues and challenges. *Clin Proteomics* **10**, 13 (2013).
5. Heid, C.A., Stevens, J., Livak, K.J. & Williams, P.M. Real time quantitative PCR. *Genome Res* **6**, 986-994 (1996).
6. Engvall, E. & Perlmann, P. Enzyme-linked immunosorbent assay (ELISA). Quantitative assay of immunoglobulin G. *Immunochemistry* **8**, 871-874 (1971).
7. Kang, J.S. & Lee, M.H. Overview of therapeutic drug monitoring. *Korean J Intern Med* **24**, 1-10 (2009).
8. Balant-Gorgia, A.E., Gex-Fabry, M., Genet, C. & Balant, L.P. Therapeutic drug monitoring of risperidone using a new, rapid HPLC method: reappraisal of interindividual variability factors. *Ther Drug Monit* **21**, 105-115 (1999).
9. Drummond, T.G., Hill, M.G. & Barton, J.K. Electrochemical DNA sensors. *Nat Biotechnol* **21**, 1192-1199 (2003).
10. Turner, A. Biosensors: then and now. *Trends Biotechnol* **31**, 119-120 (2013).
11. Kim, J., Campbell, A.S., de Ávila, B.E. & Wang, J. Wearable biosensors for healthcare monitoring. *Nat Biotechnol* **37**, 389-406 (2019).
12. Ronkainen, N.J., Halsall, H.B. & Heineman, W.R. Electrochemical biosensors. *Chem Soc Rev* **39**, 1747-1763 (2010).
13. Teymourian, H., Barfidokht, A. & Wang, J. Electrochemical glucose sensors in diabetes management: an updated review (2010-2020). *Chem Soc Rev* **49**, 7671-7709 (2020).
14. Wang, J. Electrochemical glucose biosensors. *Chem Rev* **108**, 814-825 (2008).

15. Zaidi, S.A. & Shin, J.H. Recent developments in nanostructure based electrochemical glucose sensors. *Talanta* **149**, 30-42 (2016).
16. Dahm, R. Friedrich Miescher and the discovery of DNA. *Dev Biol* **278**, 274-288 (2005).
17. Pray, L.A. Discovery of DNA structure and function: Watson and Crick. *Nature Education* **1** (2008).
18. WATSON, J.D. & CRICK, F.H. Molecular structure of nucleic acids; a structure for deoxyribose nucleic acid. *Nature* **171**, 737-738 (1953).
19. Beaucage, S.L. & Caruthers, M.H. Deoxynucleoside phosphoramidites-A new class of key intermediates for deoxypolynucleotide synthesis. *Tetrahedron Lett* **22**, 1859-1862 (1981).
20. Kosuri, S. & Church, G.M. Large-scale de novo DNA synthesis: technologies and applications. *Nat Methods* **11**, 499-507 (2014).
21. Idili, A., Vallée-Bélisle, A. & Ricci, F. Programmable pH-triggered DNA nanoswitches. *J Am Chem Soc* **136**, 5836-5839 (2014).
22. Idili, A. *et al.* Folding-upon-binding and signal-on electrochemical DNA sensor with high affinity and specificity. *Anal Chem* **86**, 9013-9019 (2014).
23. Radi, A.E. & O'Sullivan, C.K. Aptamer conformational switch as sensitive electrochemical biosensor for potassium ion recognition. *Chem Commun*, 3432-3434 (2006).
24. Ono, A. & Togashi, H. Highly selective oligonucleotide-based sensor for mercury(II) in aqueous solutions. *Angew Chem Int Ed Engl* **43**, 4300-4302 (2004).
25. Ono, A. *et al.* Specific interactions between silver(I) ions and cytosine-cytosine pairs in DNA duplexes. *Chem Commun* 4825-4827 (2008).
26. McConnell, E.M. *et al.* Biosensing with DNAzymes. *Chem Soc Rev* **50**, 8954-8994 (2021).
27. Breaker, R.R. & Joyce, G.F. A DNA enzyme with Mg(2+)-dependent RNA phosphoesterase activity. *Chem Biol* **2**, 655-660 (1995).
28. Liu, J. & Lu, Y. A colorimetric lead biosensor using DNAzyme-directed assembly of gold nanoparticles. *J Am Chem Soc* **125**, 6642-6643 (2003).
29. Liu, J. *et al.* A catalytic beacon sensor for uranium with parts-per-trillion sensitivity and millionfold selectivity. *Proc Natl Acad Sci USA* **104**, 2056-2061 (2007).

30. Ellington, A.D. & Szostak, J.W. In vitro selection of RNA molecules that bind specific ligands. *Nature* **346**, 818-822 (1990).
31. Tuerk, C. & Gold, L. Systematic evolution of ligands by exponential enrichment: RNA ligands to bacteriophage T4 DNA polymerase. *Science* **249**, 505-510 (1990).
32. Jayasena, S.D. Aptamers: an emerging class of molecules that rival antibodies in diagnostics. *Clin Chem* **45**, 1628-1650 (1999).
33. Fang, X. & Tan, W. Aptamers generated from cell-SELEX for molecular medicine: a chemical biology approach. *Acc Chem Res* **43**, 48-57 (2010).
34. Gopinath, S.C., Hayashi, K. & Kumar, P.K. Aptamer that binds to the gD protein of herpes simplex virus 1 and efficiently inhibits viral entry. *J Virol* **86**, 6732-6744 (2012).
35. Hamula, C.L., Zhang, H., Guan, L.L., Li, X.F. & Le, X.C. Selection of aptamers against live bacterial cells. *Anal Chem* **80**, 7812-7819 (2008).
36. Shangguan, D. *et al.* Aptamers evolved from live cells as effective molecular probes for cancer study. *Proc Natl Acad Sci USA* **103**, 11838-11843 (2006).
37. Sun, H. *et al.* Oligonucleotide aptamers: new tools for targeted cancer therapy. *Mol Ther Nucleic Acids* **3**, e182 (2014).
38. Willner, I. & Zayats, M. Electronic aptamer-based sensors. *Angew Chem Int Ed Engl* **46**, 6408-6418 (2007).
39. Gupta, S. *et al.* Chemically modified DNA aptamers bind interleukin-6 with high affinity and inhibit signaling by blocking its interaction with interleukin-6 receptor. *J Biol Chem* **289**, 8706-8719 (2014).
40. Drolet, D.W., Green, L.S., Gold, L. & Janjic, N. Fit for the Eye: Aptamers in Ocular Disorders. *Nucleic Acid Ther* **26**, 127-146 (2016).
41. Gold, L. *et al.* Aptamer-based multiplexed proteomic technology for biomarker discovery. *PLoS One* **5**, e15004 (2010).
42. Deutsch, E.W. *et al.* Advances and Utility of the Human Plasma Proteome. *J Proteome Res* **20**, 5241-5263 (2021).

43. Rashid, J.I.A. & Yusof, N.A. The strategies of DNA immobilization and hybridization detection mechanism in the construction of electrochemical DNA sensor: A review. *Sens Bio-Sens Res* **17**, 19-31 (2017).
44. Su, L., Sankar, C.G., Sen, D. & Yu, H.Z. Kinetics of ion-exchange binding of redox metal cations to thiolate-DNA monolayers on gold. *Anal Chem* **76**, 5953-5959 (2004).
45. Liu, S., Liu, J., Wang, L. & Zhao, F. Development of electrochemical DNA biosensor based on gold nanoparticle modified electrode by electroless deposition. *Bioelectrochemistry* **79**, 37-42 (2010).
46. Ahmed, M.U., Nahar, S., Safavieh, M. & Zourob, M. Real-time electrochemical detection of pathogen DNA using electrostatic interaction of a redox probe. *Analyst* **138**, 907-915 (2013).
47. Hynek, D. *et al.* Electrochemical Study of Doxorubicin Interaction with Different Sequences of Single Stranded Oligonucleotides, Part I. *Int J Electrochem Sci* **7**, 13-33 (2012).
48. Yang, Y. *et al.* Electrical detection of deoxyribonucleic acid hybridization based on carbon-nanotubes/nano zirconium dioxide/chitosan-modified electrodes. *Anal Chim Acta* **584**, 268-274 (2007).
49. Castro, A.C.H. *et al.* Preparation of genosensor for detection of specific DNA sequence of the hepatitis B virus. *Appl Surf Sci* **314**, 273-279 (2014).
50. Liu, S., Liu, J., Han, X., Cui, Y. & Wang, W. Electrochemical DNA biosensor fabrication with hollow gold nanospheres modified electrode and its enhancement in DNA immobilization and hybridization. *Biosens Bioelectron* **25**, 1640-1645 (2010).
51. Jawad, B., Poudel, L., Podgornik, R., Steinmetz, N.F. & Ching, W.Y. Molecular mechanism and binding free energy of doxorubicin intercalation in DNA. *Phys Chem Chem Phys* **21**, 3877-3893 (2019).
52. Barone, G. *et al.* Intercalation of daunomycin into stacked DNA base pairs. DFT study of an anticancer drug. *J Biomol Struct Dyn* **26**, 115-130 (2008).
53. Wilson, W.D. *DNA Intercalators*, Vol. 7. (Pergamon Press, London; 1999).

54. Ahmed, M.U. *et al.* Electrochemical genosensor for the rapid detection of GMO using loop-mediated isothermal amplification. *Analyst* **134**, 966-972 (2009).

55. Ihara, T., Maruo, Y., Takenaka, S. & Takagi, M. Ferrocene-oligonucleotide conjugates for electrochemical probing of DNA. *Nucleic Acids Res* **24**, 4273-4280 (1996).

56. Squire, C.J., Baker, L.J., Clark, G.R., Martin, R.F. & White, J. Structures of m-iodo Hoechst-DNA complexes in crystals with reduced solvent content: implications for minor groove binder drug design. *Nucleic Acids Res* **28**, 1252-1258 (2000).

57. Ju, H., Ye, B. & Gu, J. Supermolecular Interaction of Ferrocenium with Yeast DNA and Application in Electrochemical Sensing for Hybridization Recognition of Yeast DNA. *Sensors* **4**, 71-83 (2004).

58. Paleček, E. & Bartošík, M. Electrochemistry of nucleic acids. *Chem Rev* **112**, 3427-3481 (2012).

59. Odenthal, K.J. & Gooding, J.J. An introduction to electrochemical DNA biosensors. *Analyst* **132**, 603-610 (2007).

60. Kang, D. *et al.* Comparing the properties of electrochemical-based DNA sensors employing different redox tags. *Anal Chem* **81**, 9109-9113 (2009).

61. Xiao, Y., Piorek, B.D., Plaxco, K.W. & Heeger, A.J. A reagentless signal-on architecture for electronic, aptamer-based sensors via target-induced strand displacement. *J Am Chem Soc* **127**, 17990-17991 (2005).

62. Xiao, Y., Lubin, A.A., Baker, B.R., Plaxco, K.W. & Heeger, A.J. Single-step electronic detection of femtomolar DNA by target-induced strand displacement in an electrode-bound duplex. *Proc Natl Acad Sci USA* **103**, 16677-16680 (2006).

63. Lai, R.Y. *et al.* Rapid, sequence-specific detection of unpurified PCR amplicons via a reusable, electrochemical sensor. *Proc Natl Acad Sci USA* **103**, 4017-4021 (2006).

64. Dauphin-Ducharme, P. *et al.* Chain Dynamics Limit Electron Transfer from Electrode-Bound, Single-Stranded Oligonucleotides. *J Phys Chem C* **122**, 21441-21448 (2018).

65. Du, Y. *et al.* Reagentless, ratiometric electrochemical DNA sensors with improved robustness and reproducibility. *Anal Chem* **86**, 8010-8016 (2014).

66. Harroun, S.G. *et al.* Programmable DNA switches and their applications. *Nanoscale* **10**, 4607-4641 (2018).

67. Vallée-Bélisle, A., Ricci, F. & Plaxco, K.W. Thermodynamic basis for the optimization of binding-induced biomolecular switches and structure-switching biosensors. *Proc Natl Acad Sci USA* **106**, 13802-13807 (2009).

68. Ricci, F., Vallée-Bélisle, A., Simon, A.J., Porchetta, A. & Plaxco, K.W. Using Nature's "Tricks" To Rationally Tune the Binding Properties of Biomolecular Receptors. *Acc Chem Res* **49**, 1884-1892 (2016).

69. Vallée-Bélisle, A. & Plaxco, K.W. Structure-switching biosensors: inspired by Nature. *Curr Opin Struct Biol* **20**, 518-526 (2010).

70. Zhang, D.Y. & Winfree, E. Control of DNA strand displacement kinetics using toehold exchange. *J Am Chem Soc* **131**, 17303-17314 (2009).

71. Ricci, F., Vallée-Bélisle, A., Porchetta, A. & Plaxco, K.W. Rational design of allosteric inhibitors and activators using the population-shift model: in vitro validation and application to an artificial biosensor. *J Am Chem Soc* **134**, 15177-15180 (2012).

72. Pei, H., Zuo, X., Zhu, D., Huang, Q. & Fan, C. Functional DNA nanostructures for theranostic applications. *Acc Chem Res* **47**, 550-559 (2014).

73. Liu, S., Su, W., Li, Z. & Ding, X. Electrochemical detection of lung cancer specific microRNAs using 3D DNA origami nanostructures. *Biosens Bioelectron* **71**, 57-61 (2015).

74. Xu, S. *et al.* One DNA circle capture probe with multiple target recognition domains for simultaneous electrochemical detection of miRNA-21 and miRNA-155. *Biosens Bioelectron* **149**, 111848 (2020).

75. Palecek, E. Oscillographic polarography of highly polymerized deoxyribonucleic acid. *Nature* **188**, 656-657 (1960).

76. Lubin, A.A. & Plaxco, K.W. Folding-based electrochemical biosensors: the case for responsive nucleic acid architectures. *Acc Chem Res* **43**, 496-505 (2010).

77. Labib, M., Sargent, E.H. & Kelley, S.O. Electrochemical Methods for the Analysis of Clinically Relevant Biomolecules. *Chem Rev* **116**, 9001-9090 (2016).

78. Palecek, E. Past, present and future of nucleic acids electrochemistry. *Talanta* **56**, 809-819 (2002).

79. Oliveira-Brett, A.M., Piedade, J.A., Silva, L.A. & Diculescu, V.C. Voltammetric determination of all DNA nucleotides. *Anal Biochem* **332**, 321-329 (2004).

80. Wang, J. *et al.* Indicator-free electrochemical DNA hybridization biosensor. *Anal. Chim. Acta* **375**, 197-203 (1998).

81. Pividori, M.I., Merkoçi, A. & Alegret, S. Electrochemical genosensor design: immobilisation of oligonucleotides onto transducer surfaces and detection methods. *Biosens Bioelectron* **15**, 291-303 (2000).

82. Wang, J. & Kawde, A.-N. Pencil-based renewable biosensor for label-free electrochemical detection of DNA hybridization *Anal. Chim. Acta* **431**, 219-224 (2001).

83. Kerman, K. *et al.* Label-Free Bioelectronic Detection of Point Mutation by Using Peptide Nucleic Acid Probes *Electroanalysis* **15**, 667-670 (2003).

84. Akhavan, O., Ghaderi, E. & Rahighi, R. Toward single-DNA electrochemical biosensing by graphene nanowalls. *ACS Nano* **6**, 2904-2916 (2012).

85. Johnston, D.H., Glasgow, K.C. & Thorp, H.H. Electrochemical Measurement of the Solvent Accessibility of Nucleobases Using Electron Transfer between DNA and Metal Complexes *J Am Chem Soc* **117**, 8933-8938 (1995).

86. Armistead, P.M. & Thorp, H.H. Modification of indium tin oxide electrodes with nucleic acids: detection of attomole quantities of immobilized DNA by electrocatalysis. *Anal Chem* **72**, 3764-3770 (2000).

87. Armistead, P.M. & Thorp, H.H. Oxidation kinetics of guanine in DNA molecules adsorbed onto indium tin oxide electrodes. *Anal Chem* **73**, 558-564 (2001).

88. Yang, I.V. & Thorp, H.H. Modification of indium tin oxide electrodes with repeat polynucleotides: electrochemical detection of trinucleotide repeat expansion. *Anal Chem* **73**, 5316-5322 (2001).

89. Armistead, P.M. & Thorp, H.H. Electrochemical detection of gene expression in tumor samples: overexpression of Rak nuclear tyrosine kinase. *Bioconjug Chem* **13**, 172-176 (2002).

90. Lapierre, M.A., O'Keefe, M., Taft, B.J. & Kelley, S.O. Electrocatalytic detection of pathogenic DNA sequences and antibiotic resistance markers. *Anal Chem* **75**, 6327-6333 (2003).

91. Lapierre-Devlin, M.A. *et al.* Amplified electrocatalysis at DNA-modified nanowires. *Nano Lett* **5**, 1051-1055 (2005).

92. Fang, Z. & Kelley, S.O. Direct electrocatalytic mRNA detection using PNA-nanowire sensors. *Anal Chem* **81**, 612-617 (2009).

93. Das, J. *et al.* An electrochemical clamp assay for direct, rapid analysis of circulating nucleic acids in serum. *Nat Chem* **7**, 569-575 (2015).

94. Das, J. *et al.* An ultrasensitive universal detector based on neutralizer displacement. *Nat Chem* **4**, 642-648 (2012).

95. Katz, E. & Willner, I. Probing Biomolecular Interactions at Conductive and Semiconductive Surfaces by Impedance Spectroscopy: Routes to Impedimetric Immunosensors, DNA‐Sensors, and Enzyme. *Electroanalysis* **15**, 913-947 (2003).

96. Bardea, A., Patolsky, F., Dagan, A. & Willner, I. Sensing and amplification of oligonucleotide-DNA interactions by means of impedance spectroscopy: a route to a Tay–Sachs sensor. *Chem Commun* 21-22 (1999).

97. Zayats, M., Huang, Y., Gill, R., Ma, C.A. & Willner, I. Label-free and reagentless aptamer-based sensors for small molecules. *J Am Chem Soc* **128**, 13666-13667 (2006).

98. Li, W. *et al.* A sensitive, label free electrochemical aptasensor for ATP detection. *Talanta* **78**, 954-958 (2009).

99. Lin, Z., Chen, Y., Li, X. & Fang, W. Pb2+ induced DNA conformational switch from hairpin to G-quadruplex: electrochemical detection of Pb2+. *Analyst* **136**, 2367-2372 (2011).

100. Cai, H., Lee, T.M.-H. & Hsing, I.-M. Label-free protein recognition using an aptamer-based impedance measurement assay. *Sens. Actuators B* **114**, 433-437 (2006).

101. Zhai, Q., Zhang, X., Xia, Y., Li, J. & Wang, E. Electrochromic sensing platform based on steric hindrance effects for CEA detection. *Analyst* **141**, 3985-3988 (2016).

102. Fan, D., Fan, Y., Wang, E. & Dong, S. A simple, label-free, electrochemical DNA parity generator/checker for error detection during data transmission based on "aptamer-nanoclaw"-modulated protein steric hindrance. *Chem Sci* **9**, 6981-6987 (2018).

103. Erdem, A. & Ozsoz, M. Electrochemical DNA Biosensors Based on DNA ‐ Drug Interactions. *Electroanalysis* **14**, 965-974 (2002).

104. Brett, A.M.O., Serrano, S.H.P., Gutz, I. & La-Scalea, M.A. Electrochemical reduction of metronidazole at a DNA-modified glassy carbon electrode. *Bioelectrochem. Bioenerg.* **42**, 175-178 (1997).

105. Xu, J., Zhu, J.-J., Zhu, Y., Gu, K. & Chen, H.-Y. A novel biosensor of DNA immobilization on nano-gold modified ITO for the determination of mifepristone. *Anal Lett* **34**, 503-512 (2001).

106. Jelen, F., Erdem, A. & Palecek, E. Cyclic voltammetry of echinomycin and its interaction with double-stranded and single-stranded DNA adsorbed at the electrode. *Bioelectrochemistry* **55**, 165-167 (2002).

107. Wang, J. *et al.* Accumulation and trace measurements of phenothiazine drugs at DNA-modified electrodes. *Anal Chim Acta* **332**, 139-144 (1996).

108. Kelley, S.O., Barton, J.K., Jackson, N.M. & Hill, M.G. Electrochemistry of methylene blue bound to a DNA-modified electrode. *Bioconjug Chem* **8**, 31-37 (1997).

109. Kelley, S.O., Jackson, N.M., Hill, M.G. & Barton, J.K. Long-Range Electron Transfer through DNA Films. *Angew Chem Int Ed Engl* **38**, 941-945 (1999).

110. Kelley, S.O., Boon, E.M., Barton, J.K., Jackson, N.M. & Hill, M.G. Single-base mismatch detection based on charge transduction through DNA. *Nucleic Acids Res* **27**, 4830-4837 (1999).

111. Shen, J., Li, Y., Gu, H., Xia, F. & Zuo, X. Recent development of sandwich assay based on the nanobiotechnologies for proteins, nucleic acids, small molecules, and ions. *Chem Rev* **114**, 7631-7677 (2014).

112. Ihara, T., Nakayama, M., Murata, M., Nakano, K. & Maeda, M. Gene sensor using ferrocenyl oligonucleotide. *Chem Commun* 1609-1610 (1997).

113. Umek, R.M. *et al.* Electronic detection of nucleic acids: a versatile platform for molecular diagnostics. *J Mol Diagn* **3**, 74-84 (2001).

114. Xia, F. *et al.* An electrochemical supersandwich assay for sensitive and selective DNA detection in complex matrices. *J Am Chem Soc* **132**, 14346-14348 (2010).

115. Chen, X. *et al.* A simple and ultrasensitive electrochemical DNA biosensor based on DNA concatamers. *Chem Commun* **47**, 12116-12118 (2011).

116. Wang, J., Shi, A., Fang, X., Han, X. & Zhang, Y. An ultrasensitive supersandwich electrochemical DNA biosensor based on gold nanoparticles decorated reduced graphene oxide. *Anal Biochem* **469**, 71-75 (2015).

117. Swindells, M.B. & Ikura, M. Pre-formation of the semi-open conformation by the apo-calmodulin C-terminal domain and implications for binding IQ-motifs. *Nat Struct Biol* **3**, 501-504 (1996).

118. Roth, A. & Breaker, R.R. The structural and functional diversity of metabolite-binding riboswitches. *Annu Rev Biochem* **78**, 305-334 (2009).

119. Fan, C., Plaxco, K.W. & Heeger, A.J. Electrochemical interrogation of conformational changes as a reagentless method for the sequence-specific detection of DNA. *Proc Natl Acad Sci USA* **100**, 9134-9137 (2003).

120. Mao, Y., Luo, C. & Ouyang, Q. Studies of temperature-dependent electronic transduction on DNA hairpin loop sensor. *Nucleic Acids Res* **31**, e108 (2003).

121. Xiao, Y., Lai, R.Y. & Plaxco, K.W. Preparation of electrode-immobilized, redox-modified oligonucleotides for electrochemical DNA and aptamer-based sensing. *Nat Protoc* **2**, 2875-2880 (2007).

122. Tyagi, S. & Kramer, F.R. Molecular beacons: probes that fluoresce upon hybridization. *Nat Biotechnol* **14**, 303-308 (1996).

123. Baker, B.R. *et al.* An electronic, aptamer-based small-molecule sensor for the rapid, label-free detection of cocaine in adulterated samples and biological fluids. *J Am Chem Soc* **128**, 3138-3139 (2006).

124. Xiao, Y., Lubin, A.A., Heeger, A.J. & Plaxco, K.W. Label-free electronic detection of thrombin in blood serum by using an aptamer-based sensor. *Angew Chem Int Ed Engl* **44**, 5456-5459 (2005).

125. Cash, K.J., Ricci, F. & Plaxco, K.W. An electrochemical sensor for the detection of protein-small molecule interactions directly in serum and other complex matrices. *J Am Chem Soc* **131**, 6955-6957 (2009).

126. White, R.J. *et al.* Wash-free, electrochemical platform for the quantitative, multiplexed detection of specific antibodies. *Anal Chem* **84**, 1098-1103 (2012).

127. Kang, D. *et al.* Expanding the Scope of Protein-Detecting Electrochemical DNA "Scaffold" Sensors. *ACS Sens* **3**, 1271-1275 (2018).

128. Ogden, N.E., Kurnik, M., Parolo, C. & Plaxco, K.W. An electrochemical scaffold sensor for rapid syphilis diagnosis. *Analyst* **144**, 5277-5283 (2019).

129. Cash, K.J., Ricci, F. & Plaxco, K.W. A general electrochemical method for label-free screening of protein-small molecule interactions. *Chem Commun* 6222-6224 (2009).

130. Yousefi, H. *et al.* Detection of SARS-CoV-2 Viral Particles Using Direct, Reagent-Free Electrochemical Sensing. *J Am Chem Soc* **143**, 1722-1727 (2021).

131. Das, J. *et al.* Reagentless biomolecular analysis using a molecular pendulum. *Nat Chem* **13**, 428-434 (2021).

132. Mahshid, S.S., Camiré, S., Ricci, F. & Vallée-Bélisle, A. A Highly Selective Electrochemical DNA-Based Sensor That Employs Steric Hindrance Effects to Detect Proteins Directly in Whole Blood. *J Am Chem Soc* **137**, 15596-15599 (2015).

133. Taft, R.W. *Steric Effects in Organic Chemistry*. (Wiley, New York; 1956).

134. Mahshid, S.S., Ricci, F., Kelley, S.O. & Vallée-Bélisle, A. Electrochemical DNA-Based Immunoassay That Employs Steric Hindrance To Detect Small Molecules Directly in Whole Blood. *ACS Sens* **2**, 718-723 (2017).

135. Mahshid, S.S., Mahshid, S., Vallée-Bélisle, A. & Kelley, S.O. Peptide-Mediated Electrochemical Steric Hindrance Assay for One-Step Detection of HIV Antibodies. *Anal Chem* **91**, 4943-4947 (2019).

136. Wu, L., Xiong, E., Zhang, X., Zhang, X. & Chen, J. Nanomaterials as signal amplification elements in DNA-based electrochemical sensing. *Nano Today* **9**, 197-211 (2014).

137. Sage, A.T., Besant, J.D., Lam, B., Sargent, E.H. & Kelley, S.O. Ultrasensitive electrochemical biomolecular detection using nanostructured microelectrodes. *Acc Chem Res* **47**, 2417-2425 (2014).

138. Zhu, C., Yang, G., Li, H., Du, D. & Lin, Y. Electrochemical sensors and biosensors based on nanomaterials and nanostructures. *Anal Chem* **87**, 230-249 (2015).

139. Pei, H. *et al.* A DNA nanostructure-based biomolecular probe carrier platform for electrochemical biosensing. *Adv Mater* **22**, 4754-4758 (2010).

140. Wen, Y. *et al.* DNA nanostructure-decorated surfaces for enhanced aptamer-target binding and electrochemical cocaine sensors. *Anal Chem* **83**, 7418-7423 (2011).

141. Pei, H. *et al.* Regenerable electrochemical immunological sensing at DNA nanostructure-decorated gold surfaces. *Chem Commun* **47**, 6254-6256 (2011).

142. Liu, G. *et al.* An enzyme-based E-DNA sensor for sequence-specific detection of femtomolar DNA targets. *J Am Chem Soc* **130**, 6820-6825 (2008).

143. Patterson, A.S., Hsieh, K., Soh, H.T. & Plaxco, K.W. Electrochemical real-time nucleic acid amplification: towards point-of-care quantification of pathogens. *Trends Biotechnol* **31**, 704-712 (2013).

144. Goda, T., Tabata, M. & Miyahara, Y. Electrical and electrochemical monitoring of nucleic Acid amplification. *Front Bioeng Biotechnol* **3**, 29 (2015).

145. Qi, H., Yue, S., Bi, S., Ding, C. & Song, W. Isothermal exponential amplification techniques: From basic principles to applications in electrochemical biosensors. *Biosens Bioelectron* **110**, 207-217 (2018).

146. Dutta, G. & Lillehoj, P.B. An ultrasensitive enzyme-free electrochemical immunosensor based on redox cycling amplification using methylene blue. *Analyst* **142**, 3492-3499 (2017).

147. Ferguson, B.S. *et al.* Real-time, aptamer-based tracking of circulating therapeutic agents in living animals. *Sci Transl Med* **5**, 213ra165 (2013).

148. Arroyo-Currás, N., Scida, K., Ploense, K.L., Kippin, T.E. & Plaxco, K.W. High Surface Area Electrodes Generated via Electrochemical Roughening Improve the Signaling of Electrochemical Aptamer-Based Biosensors. *Anal Chem* **89**, 12185-12191 (2017).

149. Arroyo-Currás, N. *et al.* Real-time measurement of small molecules directly in awake, ambulatory animals. *Proc Natl Acad Sci USA* **114**, 645-650 (2017).

150. Dauphin-Ducharme, P. *et al.* Electrochemical Aptamer-Based Sensors for Improved Therapeutic Drug Monitoring and High-Precision, Feedback-Controlled Drug Delivery. *ACS Sens* (2019).

151. Li, H., Arroyo-Currás, N., Kang, D., Ricci, F. & Plaxco, K.W. Dual-Reporter Drift Correction To Enhance the Performance of Electrochemical Aptamer-Based Sensors in Whole Blood. *J Am Chem Soc* **138**, 15809-15812 (2016).

152. Li, H., Dauphin-Ducharme, P., Ortega, G. & Plaxco, K.W. Calibration-Free Electrochemical Biosensors Supporting Accurate Molecular Measurements Directly in Undiluted Whole Blood. *J Am Chem Soc* **139**, 11207-11213 (2017).

153. White, R.J., Phares, N., Lubin, A.A., Xiao, Y. & Plaxco, K.W. Optimization of electrochemical aptamer-based sensors via optimization of probe packing density and surface chemistry. *Langmuir* **24**, 10513-10518 (2008).

154. Phares, N., White, R.J. & Plaxco, K.W. Improving the stability and sensing of electrochemical biosensors by employing trithiol-anchoring groups in a six-carbon self-assembled monolayer. *Anal Chem* **81**, 1095-1100 (2009).

155. Ricci, F. *et al.* Surface chemistry effects on the performance of an electrochemical DNA sensor. *Bioelectrochemistry* **76**, 208-213 (2009).

156. Ma, T., Martens, I. & Bizzotto, D. Thermal Stability of Thiolated DNA SAMs in Buffer: Revealing the Influence of Surface Crystallography and DNA Coverage via In Situ Combinatorial Surface Analysis. *Langmuir* **36**, 14495-14506 (2020).

157. Li, H. *et al.* High frequency, calibration-free molecular measurements. *Chem Sci* **10**, 10843-10848 (2019).

158. Li, H. *et al.* A Biomimetic Phosphatidylcholine-Terminated Monolayer Greatly Improves the In Vivo Performance of Electrochemical Aptamer-Based Sensors. *Angew Chem Int Ed Engl* **56**, 7492-7495 (2017).

159. Wang, G. *et al.* Zwitterionic peptide anchored to conducting polymer PEDOT for the development of antifouling and ultrasensitive electrochemical DNA sensor. *Biosens Bioelectron* **92**, 396-401 (2017).

160. Hui, N., Sun, X., Niu, S. & Luo, X. PEGylated Polyaniline Nanofibers: Antifouling and Conducting Biomaterial for Electrochemical DNA Sensing. *ACS Appl Mater Interfaces* **9**, 2914-2923 (2017).

161. Jin, H., Gui, R., Yu, J., Lv, W. & Wang, Z. Fabrication strategies, sensing modes and analytical applications of ratiometric electrochemical biosensors. *Biosens Bioelectron* **91**, 523-537 (2017).

162. Zhang, J. *et al.* A ratiometric electrochemical biosensor for the exosomal microRNAs detection based on bipedal DNA walkers propelled by locked nucleic acid modified toehold mediate strand displacement reaction. *Biosens Bioelectron* **102**, 33-40 (2018).

163. An, Y., Li, R., Zhang, F. & He, P. A ratiometric electrochemical sensor for the determination of exosomal glycoproteins. *Talanta* **235**, 122790 (2021).

164. Sheng, Q., Cheng, N., Bai, W. & Zheng, J. Ultrasensitive electrochemical detection of breast cancer cells based on DNA-rolling-circle-amplification-directed enzyme-catalyzed polymerization. *Chem Commun* **51**, 2114-2117 (2015).

165. Liu, S., Wang, C., Zhang, C., Wang, Y. & Tang, B. Label-free and ultrasensitive electrochemical detection of nucleic acids based on autocatalytic and exonuclease III-assisted target recycling strategy. *Anal Chem* **85**, 2282-2288 (2013).

166. Wang, C. *et al.* Ultrasensitive electrochemical DNA detection based on dual amplification of circular strand-displacement polymerase reaction and hybridization chain reaction. *Biosens Bioelectron* **47**, 324-328 (2013).

167. Shivalingam, A. & Brown, T. Synthesis of chemically modified DNA. *Biochem Soc Trans* **44**, 709-715 (2016).

168. Chen, J. *et al.* An ultrahighly sensitive and selective electrochemical DNA sensor via nicking endonuclease assisted current change amplification. *Chem Commun* **46**, 5939-5941 (2010).

169. Zhu, D. *et al.* A novel electrochemical sensing strategy for rapid and ultrasensitive detection of Salmonella by rolling circle amplification and DNA-AuNPs probe. *Anal Chim Acta* **846**, 44-50 (2014).

170. Yin, B.C., Guan, Y.M. & Ye, B.C. An ultrasensitive electrochemical DNA sensor based on the ssDNA-assisted cascade of hybridization reaction. *Chem Commun* **48**, 4208-4210 (2012).

171. Mahshid, S.S., Vallée-Bélisle, A. & Kelley, S.O. Biomolecular Steric Hindrance Effects Are Enhanced on Nanostructured Microelectrodes. *Anal Chem* **89**, 9751-9757 (2017).

172. Zhou, W. *et al.* Steric Hindrance Assay for Secreted Factors in Stem Cell Culture. *ACS Sens* **2**, 495-500 (2017).

173. Wei, Y.P. *et al.* Highly sensitive electrochemical biosensor for streptavidin detection based on CdSe quantum dots. *Biosens Bioelectron* **103**, 99-103 (2018).

174. Liu, Q. *et al.* Electrochemiluminescent biosensor with DNA link for selective detection of human IgG based on steric hindrance. *Talanta* **194**, 745-751 (2019).

175. Liao, N., Liu, J.L., Chai, Y.Q., Yuan, R. & Zhuo, Y. DNA Structure Transition-Induced Affinity Switch for Biosensing Based on the Strong Electrochemiluminescence Platform from Organic Microcrystals. *Anal Chem* **92**, 3940-3948 (2020).

176. Trasatti, S. & Petrii, O.A. Real surface area measurements in electrochemistry. *Pure and Appl Chem* **63**, 711-734 (1991).

177. Makaraviciute, A., Xu, X., Nyholm, L. & Zhang, Z. Systematic Approach to the Development of Microfabricated Biosensors: Relationship between Gold Surface Pretreatment and Thiolated Molecule Binding. *ACS Appl Mater Interfaces* **9**, 26610-26621 (2017).

178. Hallek, M., Wanders, L., Strohmeyer, S. & Emmerich, B. Thymidine kinase: a tumor marker with prognostic value for non-Hodgkin's lymphoma and a broad range of potential clinical applications. *Ann Hematol* **65**, 1-5 (1992).

179. Topolcan, O. & Holubec, L. The role of thymidine kinase in cancer diseases. *Expert Opin Med Diagn* **2**, 129-141 (2008).

180. Sato, Y. *et al.* Early Recognition of Hepatocellular Carcinoma Based on Altered Profiles of Alpha-Fetoprotein. *N Engl J Med* **328**, 1802-1806 (1993).

181. Riaz, A. *et al.* Alpha-fetoprotein response after locoregional therapy for hepatocellular carcinoma: oncologic marker of radiologic response, progression, and survival. *J Clin Oncol* **27**, 5734-5742 (2009).

182. Reynoso, G. *et al.* Carcinoembryonic Antigen in Patients With Different Cancers. *JAMA* **220**, 361-365 (1972).

183. Benchimol, S. *et al.* Carcinoembryonic antigen, a human tumor marker, functions as an intercellular adhesion molecule. *Cell* **57**, 327-334 (1989).

184. Grunnet, M. & Sorensen, J.B. Carcinoembryonic antigen (CEA) as tumor marker in lung cancer. *Lung Cancer* **76**, 138-143 (2012).

185. Anderson, L. Candidate-based proteomics in the search for biomarkers of cardiovascular disease. *J Physiol* **563**, 23-60 (2005).

186. Dhingra, R. *et al.* C-reactive protein, inflammatory conditions, and cardiovascular disease risk. *Am J Med* **120**, 1054-1062 (2007).

187. Harris, E.N. *et al.* Anticardiolipin antibodies: detection by radioimmunoassay and association with thrombosis in systemic lupus erythematosus. *Lancet* **2**, 1211-1214 (1983).

188. Lindstrom, J.M., Seybold, M.E., Lennon, V.A., Whittingham, S. & Duane, D.D. Antibody to acetylcholine receptor in myasthenia gravis. Prevalence, clinical correlates, and diagnostic value. *Neurology* **26**, 1054-1059 (1976).

189. Costagliola, S. *et al.* Second generation assay for thyrotropin receptor antibodies has superior diagnostic sensitivity for Graves' disease. *J Clin Endocrinol Metab* **84**, 90-97 (1999).

190. Herold, K.C. *et al.* An Anti-CD3 Antibody, Teplizumab, in Relatives at Risk for Type 1 Diabetes. *N Engl J Med* **381**, 603-613 (2019).

191. Ray, S. *et al.* Classification and prediction of clinical Alzheimer's diagnosis based on plasma signaling proteins. *Nat Med* **13**, 1359-1362 (2007).

192. Doecke, J.D. *et al.* Blood-based protein biomarkers for diagnosis of Alzheimer disease. *Arch Neurol* **69**, 1318-1325 (2012).

193. Long, Q.X. *et al.* Antibody responses to SARS-CoV-2 in patients with COVID-19. *Nat Med* **26**, 845-848 (2020).

194. Ibarrondo, F.J. *et al.* Rapid Decay of Anti-SARS-CoV-2 Antibodies in Persons with Mild Covid-19. *N Engl J Med* **383**, 1085-1087 (2020).

195. Fiebig, E.W. *et al.* Dynamics of HIV viremia and antibody seroconversion in plasma donors: implications for diagnosis and staging of primary HIV infection. *AIDS* **17**, 1871-1879 (2003).

196. Weiblen, B.J. *et al.* Early diagnosis of HIV infection in infants by detection of IgA HIV antibodies. *Lancet* **335**, 988-990 (1990).

197. Terrault, N.A. *et al.* Update on prevention, diagnosis, and treatment of chronic hepatitis B: AASLD 2018 hepatitis B guidance. *Hepatology* **67**, 1560-1599 (2018).

198. Gitlin, N. Hepatitis B: diagnosis, prevention, and treatment. *Clin Chem* **43**, 1500-1506 (1997).

199. Gosling, J.P. A decade of development in immunoassay methodology. *Clin Chem* **36**, 1408-1427 (1990).

200. Mohammed, M.I. & Desmulliez, M.P. Lab-on-a-chip based immunosensor principles and technologies for the detection of cardiac biomarkers: a review. *Lab Chip* **11**, 569-595 (2011).

201. Diercks, A.H. *et al.* A microfluidic device for multiplexed protein detection in nano-liter volumes. *Anal Biochem* **386**, 30-35 (2009).

202. Mok, J., Mindrinos, M.N., Davis, R.W. & Javanmard, M. Digital microfluidic assay for protein detection. *Proc Natl Acad Sci USA* **111**, 2110-2115 (2014).

203. Tekin, H.C. & Gijs, M.A. Ultrasensitive protein detection: a case for microfluidic magnetic bead-based assays. *Lab Chip* **13**, 4711-4739 (2013).

204. Vallée-Bélisle, A., Ricci, F., Uzawa, T., Xia, F. & Plaxco, K.W. Bioelectrochemical switches for the quantitative detection of antibodies directly in whole blood. *J Am Chem Soc* **134**, 15197-15200 (2012).

205. Bayer, E.A., Ben-Hur, H., Hiller, Y. & Wilchek, M. Postsecretory modifications of streptavidin. *Biochem J* **259**, 369-376 (1989).

206. Duan, X. *et al.* Quantification of the affinities and kinetics of protein interactions using silicon nanowire biosensors. *Nat Nanotechnol* **7**, 401-407 (2012).

207. Weisenhorn, A.L., Schmitt, F.J., Knoll, W. & Hansma, P.K. Streptavidin binding observed with an atomic force microscope. *Ultramicroscopy* **42-44 (Pt B)**, 1125-1132 (1992).

208. Srisa-Art, M., Dyson, E.C., deMello, A.J. & Edel, J.B. Monitoring of real-time streptavidin-biotin binding kinetics using droplet microfluidics. *Anal Chem* **80**, 7063-7067 (2008).

209. Tawa, K., Yao, D. & Knoll, W. Matching base-pair number dependence of the kinetics of DNA-DNA hybridization studied by surface plasmon fluorescence spectroscopy. *Biosens Bioelectron* **21**, 322-329 (2005).

210. Li, D., Zou, X., Shen, Q. & Dong, S. Kinetic study of DNA/DNA hybridization with electrochemical impedance spectroscopy. *Electrochem Commun* **9**, 191-196 (2007).

211. De Crozals, G. *et al.* Methylene blue phosphoramidite for DNA labelling. *Chem Commun* **51**, 4458-4461 (2015).

212. Peterson, A.W., Heaton, R.J. & Georgiadis, R.M. The effect of surface probe density on DNA hybridization. *Nucleic Acids Res* **29**, 5163-5168 (2001).

213. Steel, A.B., Levicky, R.L., Herne, T.M. & Tarlov, M.J. Immobilization of nucleic acids at solid surfaces: effect of oligonucleotide length on layer assembly. *Biophys J* **79**, 975-981 (2000).

214. Bustamante, C., Marko, J.F., Siggia, E.D. & Smith, S. Entropic elasticity of lambda-phage DNA. *Science* **265**, 1599-1600 (1994).

215. Bustamante, C., Smith, S.B., Liphardt, J. & Smith, D. Single-molecule studies of DNA mechanics. *Curr Opin Struct Biol* **10**, 279-285 (2000).

216. Esteban Fernández de Ávila, B. *et al.* Determinants of the detection limit and specificity of surface-based biosensors. *Anal Chem* **85**, 6593-6597 (2013).

217. Ranallo, S., Rossetti, M., Plaxco, K.W., Vallée-Bélisle, A. & Ricci, F. A Modular, DNA-Based Beacon for Single-Step Fluorescence Detection of Antibodies and Other Proteins. *Angew Chem Int Ed Engl* **54**, 13214-13218 (2015).
218. Vallée-Bélisle, A., Ricci, F. & Plaxco, K.W. Engineering biosensors with extended, narrowed, or arbitrarily edited dynamic range. *J Am Chem Soc* **134**, 2876-2879 (2012).
219. Ranallo, S., Prévost-Tremblay, C., Idili, A., Vallée-Bélisle, A. & Ricci, F. Antibody-powered nucleic acid release using a DNA-based nanomachine. *Nat Commun* **8**, 15150 (2017).
220. Bilgiçer, B., Moustakas, D.T. & Whitesides, G.M. A synthetic trivalent hapten that aggregates anti-2,4-DNP IgG into bicyclic trimers. *J Am Chem Soc* **129**, 3722-3728 (2007).
221. James, L.C. & Tawfik, D.S. The specificity of cross-reactivity: promiscuous antibody binding involves specific hydrogen bonds rather than nonspecific hydrophobic stickiness. *Protein Sci* **12**, 2183-2193 (2003).
222. Mallika, B., Yin, N.H.Y. & Ali, J. Wearable sweat sensors. *Nature Electronics* **1**, 160-171 (2018).
223. Steinmetz, L.M. & Jones, A. Sensing a revolution. *Mol Syst Biol* **12**, 867 (2016).
224. Snyder, L.R. HPLC: past and present. *Anal Chem* **72**, 412A-420A (2000).
225. Jameson, D.M. & Ross, J.A. Fluorescence polarization/anisotropy in diagnostics and imaging. *Chem Rev* **110**, 2685-2708 (2010).
226. Yager, P. *et al.* Microfluidic diagnostic technologies for global public health. *Nature* **442**, 412-418 (2006).
227. Sackmann, E.K., Fulton, A.L. & Beebe, D.J. The present and future role of microfluidics in biomedical research. *Nature* **507**, 181-189 (2014).
228. Wooseok, J., Jungyoup, H., Jin-Woo, C. & H., A.C. Point-of-care testing (POCT) diagnostic systems using microfluidic lab-on-a-chip technologies. *Microelectron Eng* **132**, 46-57 (2015).
229. Vashist, S.K., Luppa, P.B., Yeo, L.Y., Ozcan, A. & Luong, J.H.T. Emerging Technologies for Next-Generation Point-of-Care Testing. *Trends Biotechnol* **33**, 692-705 (2015).
230. Wang, Y.P. & Lei, Q.Y. Metabolite sensing and signaling in cell metabolism. *Signal Transduct Target Ther* **3**, 30 (2018).

231. Yu, Z. & Fischer, R. Light sensing and responses in fungi. *Nat Rev Microbiol* **17**, 25-36 (2019).

232. Chantranupong, L., Wolfson, R.L. & Sabatini, D.M. Nutrient-sensing mechanisms across evolution. *Cell* **161**, 67-83 (2015).

233. Rolland, F., Baena-Gonzalez, E. & Sheen, J. Sugar sensing and signaling in plants: conserved and novel mechanisms. *Annu Rev Plant Biol* **57**, 675-709 (2006).

234. Golynskiy, M.V., Koay, M.S., Vinkenborg, J.L. & Merkx, M. Engineering protein switches: sensors, regulators, and spare parts for biology and biotechnology. *Chembiochem* **12**, 353-361 (2011).

235. Bayley, H. & Cremer, P.S. Stochastic sensors inspired by biology. *Nature* **413**, 226-230 (2001).

236. Scognamiglio, V., Antonacci, A., Lambreva, M.D., Litescu, S.C. & Rea, G. Synthetic biology and biomimetic chemistry as converging technologies fostering a new generation of smart biosensors. *Biosens Bioelectron* **74**, 1076-1086 (2015).

237. Mulvaney, S.P. & Sheehan, P.E. Nature inspires sensors to do more with less. *ACS Nano* **8**, 9729-9732 (2014).

238. Lehn, J.M. Toward self-organization and complex matter. *Science* **295**, 2400-2403 (2002).

239. Lehn, J.M. Toward complex matter: supramolecular chemistry and self-organization. *Proc Natl Acad Sci USA* **99**, 4763-4768 (2002).

240. Lehn, J.M. From supramolecular chemistry towards constitutional dynamic chemistry and adaptive chemistry. *Chem Soc Rev* **36**, 151-160 (2007).

241. Lehn, J.M. Perspectives in chemistry--steps towards complex matter. *Angew Chem Int Ed Engl* **52**, 2836-2850 (2013).

242. Ramström, O. & Lehn, J.M. Drug discovery by dynamic combinatorial libraries. *Nat Rev Drug Discov* **1**, 26-36 (2002).

243. Herrmann, A. Dynamic combinatorial/covalent chemistry: a tool to read, generate and modulate the bioactivity of compounds and compound mixtures. *Chem Soc Rev* **43**, 1899-1933 (2014).

244. Zhang, Y. & Barboiu, M. Constitutional Dynamic Materials--Toward Natural Selection of Function. *Chem Rev* **116**, 809-834 (2016).

245. Roche, C. & Percec, V. Complex adaptable systems based on self-assembling dendrimers and dendrons: toward dynamic materials. *Isr J Chem* **53**, 30-44 (2013).

246. Nasr, G., Macron, T., Gilles, A., Mouline, Z. & Barboiu, M. Metallodynameric membranes--toward the constitutional transport of gases. *Chem Commun* **48**, 6827-6829 (2012).

247. Wei, Z. *et al.* Self-healing gels based on constitutional dynamic chemistry and their potential applications. *Chem Soc Rev* **43**, 8114-8131 (2014).

248. Wang, S. *et al.* Controlling the Catalytic Functions of DNAzymes within Constitutional Dynamic Networks of DNA Nanostructures. *J Am Chem Soc* **139**, 9662-9671 (2017).

249. Yue, L. *et al.* Intercommunication of DNA-Based Constitutional Dynamic Networks. *J Am Chem Soc* **140**, 8721-8731 (2018).

250. Zhou, Z., Yue, L., Wang, S., Lehn, J.M. & Willner, I. DNA-Based Multiconstituent Dynamic Networks: Hierarchical Adaptive Control over the Composition and Cooperative Catalytic Functions of the Systems. *J Am Chem Soc* **140**, 12077-12089 (2018).

251. Yin, B.C., Liu, Y.Q. & Ye, B.C. One-step, multiplexed fluorescence detection of microRNAs based on duplex-specific nuclease signal amplification. *J Am Chem Soc* **134**, 5064-5067 (2012).

252. Elghanian, R., Storhoff, J.J., Mucic, R.C., Letsinger, R.L. & Mirkin, C.A. Selective colorimetric detection of polynucleotides based on the distance-dependent optical properties of gold nanoparticles. *Science* **277**, 1078-1081 (1997).

253. Xue, X., Wang, F. & Liu, X. One-step, room temperature, colorimetric detection of mercury (Hg2+) using DNA/nanoparticle conjugates. *J Am Chem Soc* **130**, 3244-3245 (2008).

254. Cao, Y.C., Jin, R. & Mirkin, C.A. Nanoparticles with Raman spectroscopic fingerprints for DNA and RNA detection. *Science* **297**, 1536-1540 (2002).

255. Ma, W. *et al.* A SERS active gold nanostar dimer for mercury ion detection. *Chem Commun* **49**, 4989-4991 (2013).

256. Homola, J. Surface plasmon resonance sensors for detection of chemical and biological species. *Chem Rev* **108**, 462-493 (2008).

257. Masson, J.F. Surface Plasmon Resonance Clinical Biosensors for Medical Diagnostics. *ACS Sens* **2**, 16-30 (2017).

258. Charbonneau, D.M. *et al.* Development of Escherichia coli asparaginase II for immunosensing: a trade-off between receptor density and sensing efficiency. *ACS Omega* **2**, 2114-2125 (2017).

259. Aubé, A., Charbonneau, D.M., Pelletier, J.N. & Masson, J.-F. Response monitoring of acute lymphoblastic leukemia patients undergoing L-asparaginase therapy: successes and challenges associated with clinical sample analysis in plasmonic sensing. *ACS Sens* **11**, 1358-1365 (2016).

260. Gold, L. *et al.* Aptamers and the RNA world, past and present. *Cold Spring Harb Perspect Biol* **4** (2012).

261. Joshi, A. & Mayr, M. In Aptamers They Trust: The Caveats of the SOMAscan Biomarker Discovery Platform from SomaLogic. *Circulation* **138**, 2482-2485 (2018).

262. Wang, F., Liu, X. & Willner, I. DNA switches: from principles to applications. *Angew Chem Int Ed Engl* **54**, 1098-1129 (2015).

263. Yurke, B., Turberfield, A.J., Mills, A.P., Simmel, F.C. & Neumann, J.L. A DNA-fuelled molecular machine made of DNA. *Nature* **406**, 605-608 (2000).

264. Qian, L. & Winfree, E. Scaling up digital circuit computation with DNA strand displacement cascades. *Science* **332**, 1196-1201 (2011).

265. Seeman, N.C. & Sleiman, H.F. DNA nanotechnology. *Nat Rev Mater* **3**, 17068 (2018).

266. Liu, J., Cao, Z. & Lu, Y. Functional nucleic acid sensors. *Chem Rev* **109**, 1948-1998 (2009).

267. Genot, A.J., Zhang, D.Y., Bath, J. & Turberfield, A.J. Remote toehold: a mechanism for flexible control of DNA hybridization kinetics. *J Am Chem Soc* **133**, 2177-2182 (2011).

268. Gareau, D., Desrosiers, A. & Vallée-Bélisle, A. Programmable Quantitative DNA Nanothermometers. *Nano Lett* **16**, 3976-3981 (2016).

269. Zhang, D.Y. & Seelig, G. Dynamic DNA nanotechnology using strand-displacement reactions. *Nat Chem* **3**, 103-113 (2011).

270. Ostroff, R. *et al.* The stability of the circulating human proteome to variations in sample collection and handling procedures measured with an aptamer-based proteomics array. *J Proteomics* **73**, 649-666 (2010).
271. Ruscito, A. & DeRosa, M.C. Small-Molecule Binding Aptamers: Selection Strategies, Characterization, and Applications. *Front Chem* **4**, 14 (2016).
272. Achan, J. *et al.* Quinine, an old anti-malarial drug in a modern world: role in the treatment of malaria. *Malar J* **10**, 144 (2011).
273. AlKadi, H.O. Antimalarial drug toxicity: a review. *Chemotherapy* **53**, 385-391 (2007).
274. White, N.J., Stepniewska, K., Barnes, K., Price, R.N. & Simpson, J. Simplified antimalarial therapeutic monitoring: using the day-7 drug level? *Trends Parasitol* **24**, 159-163 (2008).
275. Reinstein, O. *et al.* Quinine binding by the cocaine-binding aptamer. Thermodynamic and hydrodynamic analysis of high-affinity binding of an off-target ligand. *Biochemistry* **52**, 8652-8662 (2013).
276. Stojanovic, M.N., de Prada, P. & Landry, D.W. Aptamer-based folding fluorescent sensor for cocaine. *J Am Chem Soc* **123**, 4928-4931 (2001).
277. Lawrence, C. *et al.* A comparison of the folding kinetics of a small, artificially selected DNA aptamer with those of equivalently simple naturally occurring proteins. *Protein Sci* **23**, 56-66 (2014).
278. Porchetta, A., Vallée-Bélisle, A., Plaxco, K.W. & Ricci, F. Using distal-site mutations and allosteric inhibition to tune, extend, and narrow the useful dynamic range of aptamer-based sensors. *J Am Chem Soc* **134**, 20601-20604 (2012).
279. Schoukroun-Barnes, L.R. *et al.* Reagentless, Structure-Switching, Electrochemical Aptamer-Based Sensors. *Annu Rev Anal Chem* **9**, 163-181 (2016).
280. Hsieh, K. *et al.* Polarity-switching electrochemical sensor for specific detection of single-nucleotide mismatches. *Angew Chem Int Ed Engl* **50**, 11176-11180 (2011).
281. Nutiu, R. & Li, Y. Structure-switching signaling aptamers. *J Am Chem Soc* **125**, 4771-4778 (2003).
282. Ganem, B. Strategies for innovation in multicomponent reaction design. *Acc Chem Res* **42**, 463-472 (2009).

283. Dömling, A., Wang, W. & Wang, K. Chemistry and biology of multicomponent reactions. *Chem Rev* **112**, 3083-3135 (2012).

284. Centi, S., Tombelli, S., Minunni, M. & Mascini, M. Aptamer-based detection of plasma proteins by an electrochemical assay coupled to magnetic beads. *Anal Chem* **79**, 1466-1473 (2007).

285. Fang, X., Sen, A., Vicens, M. & Tan, W. Synthetic DNA aptamers to detect protein molecular variants in a high-throughput fluorescence quenching assay. *Chembiochem* **4**, 829-834 (2003).

286. Lai, R.Y., Plaxco, K.W. & Heeger, A.J. Aptamer-based electrochemical detection of picomolar platelet-derived growth factor directly in blood serum. *Anal Chem* **79**, 229-233 (2007).

287. Pandey, R. *et al.* Integrating programmable DNAzymes with electrical readout for rapid and culture-free bacterial detection using a handheld platform. *Nat Chem* **13**, 895-901 (2021).

288. Mak, W.C., Beni, V. & Turner, A.P.F. Lateral-flow technology: From visual to instrumental. *TrAC, Trends Anal Chem* **79**, 297-305 (2016).

289. Shrivastava, S., Trung, T.Q. & Lee, N.E. Recent progress, challenges, and prospects of fully integrated mobile and wearable point-of-care testing systems for self-testing. *Chem Soc Rev* **49**, 1812-1866 (2020).

290. Myers, F.B. & Lee, L.P. Innovations in optical microfluidic technologies for point-of-care diagnostics. *Lab Chip* **8**, 2015-2031 (2008).

291. Rackus, D.G., Shamsi, M.H. & Wheeler, A.R. Electrochemistry, biosensors and microfluidics: a convergence of fields. *Chem Soc Rev* **44**, 5320-5340 (2015).

292. Wang, D.S. & Fan, S.K. Microfluidic Surface Plasmon Resonance Sensors: From Principles to Point-of-Care Applications. *Sensors* **16** (2016).

293. Lim, C.T. & Zhang, Y. Bead-based microfluidic immunoassays: the next generation. *Biosens Bioelectron* **22**, 1197-1204 (2007).

294. Dow, P., Kotz, K., Gruszka, S., Holder, J. & Fiering, J. Acoustic separation in plastic microfluidics for rapid detection of bacteria in blood using engineered bacteriophage. *Lab Chip* **18**, 923-932 (2018).

295. Mitsakakis, K. & Gizeli, E. Detection of multiple cardiac markers with an integrated acoustic platform for cardiovascular risk assessment. *Anal Chim Acta* **699**, 1-5 (2011).

296. Ding, X. *et al.* Surface acoustic wave microfluidics. *Lab Chip* **13**, 3626-3649 (2013).